AMERICAN SOCIETY OF CIVIL ENGINEERS

Founded November 5, 1852

PAPERS

HIGH-VELOCITY FLOW IN OPEN CHANNELS

A SYMPOSIUM

NOTE.—Written comments are invited for immediate publication; to insure publication the last discussion should be submitted by **April 1, 1950.**

FOREWORD

Although specific problems of high-velocity flow arising from changes in open-channel cross section or alinement had frequently been solved by model tests, not until the early 1930's did the broad applicability of elastic-wave analysis to such gravity-wave phenomena become evident. The resulting principles of wave mechanics were first applied at the California Institute of Technology at Pasadena in 1935, during the study of flow around the curves of the Los Angeles County flood-relief channels in California; shortly thereafter similar applications were made to channel contractions at Lehigh University in Bethlehem, Pa., and the Massachusetts Institute of Technology in Cambridge, and to channel expansions at the State University of Iowa in Iowa City.

In distinction to the empirical solution of particular design problems, these investigations involved the use of general principles whereby simple designs could be completed without recourse to experiment and complex designs could be approximated understandingly prior to experimental refinement. Several papers describing certain phases of the investigations were eventually published, but the major part of the material remained in the form of graduate theses and reports to various public and private organizations. Therefore, much of the essential information did not become readily available to the profession, and in no way could the engineer secure a unified treatment of the subject as a whole.

Because of this deficiency in the technical literature, in 1946 the newly formed Fluid Mechanics Committee of the ASCE Hydraulics Division undertook as one of its initial projects the sponsorship of a comprehensive symposium on the design of curves and transitions for high-velocity flow. This was arranged as a series of correlated papers, prepared by those who were responsible for the original investigations and so organized as to include the underlying principles of wave analysis as well as their application to the primary types of transition structure. The high lights of the Symposium were presented to the 1948 Annual Meeting of the Society, and the papers themselves are reproduced for discussion in the following pages. It is hoped both by the authors and by the Committee on Fluid Mechanics that the ultimate result will be a compact yet inclusive treatise on the subject which will prove of practical value to design engineers.

Notation.—The following letter symbols, adopted for the Symposium and for the guidance of discussers, conform substantially with American Standard Letter Symbols for Hydraulics (ASA—Z10.21942), prepared by a committee of the American Standards Association, with ASCE participation, and adopted by the Association in January, 1942:

b = width of channel;
c = celerity of small waves = $\sqrt{g\,h}$;
d = height of a sill;
$\mathbf{F}$ = Froude number;
g = gravitational acceleration;

H = specific head;
h = depth; h_c = critical depth;
K = a correction factor = $\frac{\text{actual sin } \beta_1}{\text{theoretical sin } \beta_1}$;
L = distance along a channel;
Q = rate of flow;
r = radius, mean; r_i = radius of a counterdisturbance section;
S = slope; S_c = cross slope;
V = mean velocity = Q/A:
V_c = critical velocity;
$\bar{V}$ = dimensionless velocity;
x = longitudinal distance from beginning of expansion;
y = lateral distance from center line;
z = depth of channel drop;
α = angle of a sill in a flume or channel;
β = wave angle;
γ = specific weight;
θ = deflection angle:
$\Delta\theta$ = small but finite deflection angle;
θ' = angle of curve of the entire flow;
θ_o = central angle of the half wave length in the main curve; and
ρ = mass density.

MECHANICS OF SUPERCRITICAL FLOW

BY ARTHUR T. IPPEN,[1] M. ASCE

SYNOPSIS

The theory of high-velocity flow—flow defined as shooting, rapid, or supercritical—is presented comprehensively. The principles discussed find practical application in the design of all open-channel structures in which surface disturbances and standing waves appear as a consequence of the geometry of the lateral boundaries. These surface disturbances are subject to systematic analysis on the basis of two distinct methods of approach:

1. Gradual surface changes may be analyzed on the basis of constant specific head; and
2. Standing wave fronts of appreciable height (so-called oblique or slanting hydraulic jumps) can be computed, considering the energy dissipation involved.

Graphical aids for the solution of both types of problems are given in detail, and the characteristic disturbance patterns are developed to illustrate a number of basic cases. Specific verification of the theory by experiment is left to subsequent papers of the Symposium.

INTRODUCTION

In recent years the hydraulic designer has been increasingly confronted with problems of high-velocity flow in steep flood channels and spillway chutes. The specific character of such flow results from the fact that the velocities exceed considerably the critical velocity and therefore the velocity at which surface disturbances and waves are transmitted in free surface flow. It was found that similar problems of design are encountered in the field of high-velocity gas dynamics and that, by analogy, a hydraulic theory could be deduced from the concepts and analytic developments already available in that science. Definite findings have resulted from intermittent research conducted since 1934, and the accumulated experimental evidence confirmed essentially the soundness of the theoretical approach. Within the limitations imposed by the fundamental premises of the theory, consistent qualitative and good quantitative results were obtained which justify the comprehensive presentation of the work at this time.

The historical development of research in this field may be summarized briefly. In the United States the first impulse toward work in this field came in the early nineteen thirties when the engineers of the Los Angeles County Flood Control District found the conventional methods of designing flood channels not applicable to the steep gradients employed in their area of service. They therefore approached the Hydraulic Structures Laboratory at the California Institute of Technology, under the direction of R. T. Knapp, M. ASCE, with a proposal to study the flow at supercritical velocities through curved

[1] Prof. of Hydraulics, Dept. of Civ. and San. Eng., Mass. Inst. of Technology, Cambridge, Mass.

sections of rectangular channels in the laboratory. Extensive tests were then performed by the writer from 1935 to 1938, under a variety of conditions as far as radii, slope, and channel forms were concerned. The test results[2,3,4,5] pointed toward characteristics of such flow, which according to Theodor von Kármán,[6] M. ASCE, had their counterpart in the supersonic flow of gases and to which the previous findings for such flow could be adapted. The application of these principles resulted in a remarkable correlation of the test data. It also became clear that a general method of analysis for supercritical flow had been found which could be applied to the study of the design characteristics of hydraulic structures.

The analogy of supercritical flow of water to supersonic gas flow had been pointed out also by D. Riabouchinsky[7] and L. Prandtl[8] without experimental evidence. Ernst Preiswerk[9] worked on the extension of the theory and conducted a number of systematic experiments on a so-called Laval nozzle at Zürich, Switzerland. Although these writers were primarily interested in applications to supersonic flow of gases, work was continued more along hydraulic lines at the California Institute of Technology under Mr. Knapp's direction, at Lehigh University, at the Massachusetts Institute of Technology under the direction of the writer, and at the Iowa Institute of Hydraulic Research in Iowa City under the direction of Hunter Rouse, M. ASCE. The findings made in these investigations have been embodied in Symposium papers Nos. 2 to 4 in a form adapted to the specific problem of design under discussion. By contrast the task of this paper is an outline of the general principles of supercritical flow and a complete development of the fundamental train of ideas for those interested in the general physical aspects of the various problems.

General Physical Background

The theory of nonuniform supercritical flow as reflected by its treatment in conventional texts has been concerned mainly with the changes taking place in only two dimensions, length and height. Depth and velocity changes are related in general to the slope and roughness factors by the backwater equation and its basic solutions, giving surface points as a function of distance. Lateral changes of cross section are absorbed into an average depth and the cross slope is always assumed to be zero. Although this method is justified for subcritical flow, it must be rejected for supercritical flow because of the appearance of

[2] "A Study of High Velocity Flow in Curved Channels of Rectangular Cross Section," by A. T. Ippen and R. T. Knapp, *Transactions*, Am. Geophysical Union, Vol. 17, 1936, p. 516.

[3] "An Analytical and Experimental Study of High Velocity Flow in Curved Sections of Open Channels," by A. T. Ippen, thesis presented to the California Inst. of Technology at Pasadena, in 1936, in partial fulfilment of the requirements for the degree of Doctor of Philosophy.

[4] "Experimental Investigations of Flow in Curved Channels" (abstract of results and recommendations), by A. T. Ippen and R. T. Knapp, U. S. Engr. Office, Los Angeles, Calif., 1938.

[5] "Curvilinear Flow of Liquids with Free Surfaces at Velocities Above That of Wave Propagation," by R. T. Knapp and A. T. Ippen, *Proceedings*, 5th International Cong. of Applied Mechanics, Cambridge, Mass., 1938, p. 531.

[6] "Eine praktische Anwendung der Analogie zwischen Überschallströmung in Gasen und über kritischer Strömung in Offenen Gerinnen," by Theodor von Kármán, *Zeitschrift für Angewandte Mathematik und Mechanik*, February, 1938, pp. 49–56.

[7] "Sur l'Analogie Hydraulique des Mouvements d'un Fluide Compressible," by D. Riabouchinsky, *Comptes Rendus de l'Académie des Sciences*, Vol. 195, 1932, p. 998, and Vol. 199, 1934, p. 632.

[8] "Abriss der Strömungslehre," by L. Prandtl, Braunschweig, Vieweg, 1931.

[9] "Application of the Methods of Gas Dynamics to Water Flows with Free Surface," by Ernst Preiswerk, *Technical Memoranda Nos. 934 and 935*, National Advisory Committee for Aeronautics, Washington, D. C., March, 1940.

standing waves as the result of lateral boundary changes for such flow. The different types of backwater curves discussed by the classical theory can be conceived as valid only for rectilinear supercritical flow between parallel walls and for zero cross slope of the bottom. If these conditions are not fulfilled, considerable errors are to be expected from computations in accordance with this theory, although computations for subcritical flow are acceptable.

The physical difference between subcritical and supercritical flow is best revealed by the specific-head diagram (see Fig. 1). A few remarks may summarize its significance with respect to this paper.

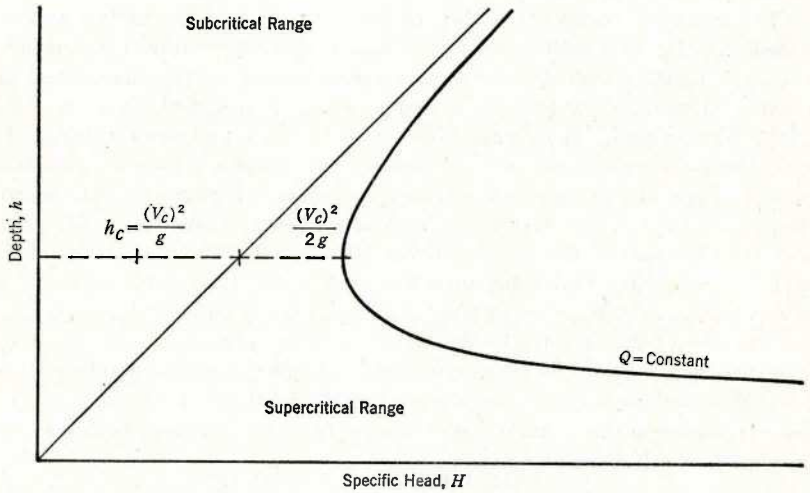

FIG. 1.—PLOT OF SPECIFIC HEAD VERSUS DEPTH OF FLOW

1. In subcritical flow the velocity head $V^2/(2g)$ is usually a small percentage of the specific head H; considerable changes in boundary alinement cause dynamic pressures which may be large percentages of the velocity head, but they remain small when expressed in terms of depth. It is therefore normally safe to assume hydrostatic pressure distribution for gradual boundary curvatures, whether on the bottom or along the walls. Also, large variations in H are synonymous with large variations of depth.

2. In supercritical flow the velocity head not only is comparable to depth h in order of magnitude but, in most cases of practical interest, exceeds the depth considerably. In this instance, large variations in specific head H are equivalent to large changes in velocity head. Slight curvatures of the boundaries may cause relatively small dynamic pressures in terms of velocity head, but the changes in depth or surface elevation will be relatively large. Hydrostatic pressure distribution may be altered radically, while the velocity head is changed only a small percentage.

3. Flow near the so-called critical depth, when $V = \sqrt{g\,h}$, results in values of h and $V^2/(2g)$ of practically the same order of magnitude. While H remains almost constant, changes in h or $V^2/(2g)$ are reflected in mutual changes.

Slight variations of H cause large changes in $V^2/(2\,g)$ and h. Since slight changes in boundary alinement, because of their influence on the hydrostatic pressure distribution, correspond in effect to slight variations in H, large disturbances result as far as the depth and velocity head are concerned for flow near critical velocity, as evidenced by high undulations. Since the ratio $V/\sqrt{g\,h}$ is generally recognized as the Froude number, **F**, it is used subsequently to characterize these flow conditions. The flow described in item 1 therefore corresponds to Froude numbers smaller than unity, whereas for the flow described in item 2 the Froude number is always larger than unity. For flow at critical depth **F** equals one.

The critical velocity $V = \sqrt{g\,h}$ also has significance as the velocity with which very small disturbances or gravity waves travel in shallow water. However, it must be remembered, that waves of large height travel faster than those of small height and consequently are able to travel upstream even in supercritical flow, whenever the wave velocity exceeds the velocity of flow. If the velocity of flow changes along the line of travel of such a high wave, a position is eventually reached where the velocity of flow equals the wave velocity. Such a stationary surge or wave is well known as the hydraulic jump, the theory of which is assumed to be familiar to the reader.

Gradual changes in supercritical flow can be treated by conventional methods only as long as the flow is confined between parallel, rectilinear walls with zero cross slope of the bottom. Only then will the theoretical surface curves apply as computed for cases of accelerated or decelerated motion in long channels and vertical transitions. The same restrictions hold for the transition from supercritical to subcritical flow in the hydraulic jump, conceived as a standing surge at right angles to the flow.

The theory of nonuniform flow at supercritical velocities is extended in the following text by the additional variants of curvilinear walls and by the abrupt changes of wall alinement considered under specific assumptions, which are outlined as the treatment proceeds. In addition to velocity changes in the original direction of flow, changes in the direction perpendicular to the original one are computed in connection with transverse changes of depth. The surface, therefore, is no longer considered horizontal crosswise or of a definite cross slope; but its classification may become quite arbitrary. The only restriction remaining is that vertical changes in velocity be neglected, which requires in turn that the pressure distribution remain hydrostatic. It will be shown that satisfactory solutions can be derived for flow through curved sections of open channels and through converging and diverging channels as long as the basic assumptions are fulfilled. The limitations imposed by these shapes are clearly shown in connection with individual applications. The physical features of such flow are characterized by oblique standing wave fronts, originating at the walls of the channels at the points of changing alinement. These waves cross the channel to the opposite wall, where they are reflected, and in this fashion they continue almost undiminished in the downstream direction. Of course this visible evidence of boundary disturbance is made up of a multitude of small disturbances, the characteristics of which may now be taken up in detail.

Mechanics of Wave Propagation in Supercritical Flow

A uniform, rectilinear flow is assumed for depth h_1 with a velocity V_1 in a wide rectangular channel. The streamlines are parallel throughout. If the flow is now disturbed at any point by placing an obstacle in the stream, the surface of the stream will show deformations whose characteristics are dependent on the value of the velocity V_1 with respect to the critical velocity $\sqrt{g\,h_1}$, which is equal to the celerity c of small waves. If the velocity V_1 is smaller than $\sqrt{g\,h_1}$ (that is, if $\mathbf{F}_1 = V_1/\sqrt{g\,h_1} < 1$), the flow upstream from the obstruction will be affected by the presence of the obstacle. The backwater will extend a long distance upstream considering the dimensions of the obstacle, and a typical wake will appear in the rear of the obstacle. The streamlines will be deflected in all directions over a considerable area in conformance with the shape of the body. If the local velocities are expressed as percentages of the initial velocity V_1, a dimensionless streamline pattern may be drawn which remains geometrically similar for a wide range of variation in V_1 and h_1, or better, for values $\mathbf{F}_1 < 1$. Surface depressions or superelevations are not very marked. If the flow conditions are changed, however, so that V_1 approaches the value of $\sqrt{g\,h_1}$ or $\mathbf{F}_1$ approaches unity, a marked change in the flow pattern becomes apparent. Flow conditions at critical velocity would nevertheless still cause a backwater, since in such a more or less hypothetical case the slightest obstruction would cause a wave of sufficient height to travel upstream and the obstruction would remain surrounded by subcritical flow.

Only if the velocity V_1 increases sufficiently above the value of $\sqrt{g\,h_1}$ is it possible to have a sizable obstruction which will not exert any influence upstream, as will be shown in detail subsequently. It may suffice to state that for $\mathbf{F}_1 > 1$, in general, typical standing wave patterns appear as a consequence of any obstacle placed in the stream. These patterns will change with $\mathbf{F}_1$ and therefore the resistance created by flow obstructions will also change as a function of $\mathbf{F}_1$. For supercritical flow, in contrast to subcritical flow, it is no longer possible to describe the streamline patterns independently of $\mathbf{F}_1$, since these patterns do not remain geometrically similar as before in subcritical flow, where they are subject only to Reynolds number distortions or to frictional distortions. Any attempt, therefore, to express head losses due to flow obstructions in terms of the Reynolds number only is impossible unless similarity exists with respect to the Froude number.

Basic Properties of Standing Waves.—If the discussion is confined at first to relatively small disturbances, a very useful analysis may be made which will aid greatly in anticipating the performance of numerous hydraulic structures in supercritical flow, whenever the changes in boundary alinement along a body within the flow or along the side walls are gradual. In such cases angular deflections are considered small, resulting therefore in small changes of depth. For this reason vertical accelerations can be neglected entirely, and consequently hydrostatic pressure distribution will be assumed to exist over the depth of flow at every point. The flow field shown in Fig. 2 conforms with these assumptions. In addition, the velocities are taken as constant over the depth, and the energy dissipation is disregarded along the bottom and within

the zone of change from depth h_1 to depth h_2. The assumption of zero shear along the bottom may be modified by stating that the bottom shear equals the component of the gravity force, so that accelerations from this source may be disregarded. This procedure is common in the derivation of the

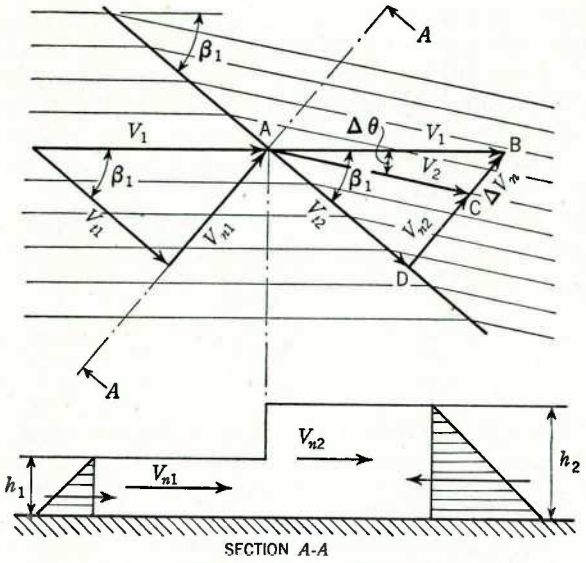

FIG. 2.—PLAN OF WAVE FRONT CROSSING FIELD OF FLOW WITH VECTOR DIAGRAM OF VELOCITIES

hydraulic jump equation. Thus, one may write the continuity equation and the momentum equation for a unit length of wave front crossing a flow of depth h_1 and velocity V_1 at an angle β_1 as follows:

$$h_1 V_{n1} = h_2 V_{n2} \quad \ldots\ldots\ldots\ldots\ldots\ldots\ldots\ldots\ldots\ldots (1)$$

and

$$\frac{\gamma (h_1)^2}{2} + \frac{\gamma}{g} h_1 (V_{n1})^2 = \frac{\gamma (h_2)^2}{2} + \frac{\gamma}{g} h_2 (V_{n2})^2 \quad \ldots\ldots\ldots\ldots (2)$$

It is clear that the net pressure force acting to decelerate the flow can affect only the momentum of the stream normal to the wave front; and, since no force component exists parallel to the front, the tangential components V_{t1} and V_{t2} of the velocity must remain unaltered as the flow passes under the wave front.

From Eqs. 1 and 2, the expression for the normal component V_{n1} is obtained in terms of the depths h_1 and h_2:

$$V_{n1} = \sqrt{g h_1} \sqrt{\frac{h_2}{h_1} \frac{1}{2} \left(1 + \frac{h_2}{h_1} \right)} \quad \ldots\ldots\ldots\ldots\ldots\ldots\ldots\ldots (3)$$

In applying the momentum equation, V_{n1} has been automatically defined as the wave velocity, since the wave front was assumed stationary. In turn

any wave of a certain height, $h_2 - h_1$, will assume in supercritical flow such a position that the normal component of V_1 with respect to the front will equal V_{n1} as defined by Eq. 3. The wave front will not be stationary otherwise. It may also be stated that in agreement with the equation there must always be a stationary position for any wave in supercritical flow, until V_{n1} as defined by Eq. 3 exceeds the value of V_1. If $V_{n1} = V_1$, the wave front assumes a position at a right angle to the flow, and becomes the familiar hydraulic jump. For $V_{n1} > V_1$ the jump will start moving upstream, detaching itself from the source of the disturbance, which then remains surrounded by subcritical flow.

Wave Angle.—The relation between V_1 and V_{n1} may best be given by the ratio V_{n1}/V_1 from the vector diagram as $\sin \beta_1 = V_{n1}/V_1$ (in which β_1 is defined as the wave angle).

Substituting for V_{n1} in Eq. 3 the equivalent $V_1 \sin \beta_1$ and solving for $\sin \beta_1$ the expression—

$$\sin \beta_1 = \frac{\sqrt{g\,h_1}}{V_1} \sqrt{\frac{h_2}{h_1} \frac{1}{2} \left(1 + \frac{h_2}{h_1} \right)} \quad \ldots\ldots\ldots\ldots\ldots\ldots (4)$$

—is obtained, which holds for any ratio of h_2/h_1. For small wave heights with $h_2 \approx h_1$, the expression under the square root approaches unity and the angle β_1 tends toward a minimum value for any given Froude number $\mathbf{F}_1 = V_1/\sqrt{g\,h_1}$. A continuous small disturbance in a supercritical flow defined by $\mathbf{F}_1 > 1$ will therefore always proceed to an angular position with respect to the oncoming flow which is given by

$$\sin \beta_1 = \frac{1}{\mathbf{F}_1} \quad \ldots\ldots\ldots\ldots\ldots\ldots\ldots\ldots (5)$$

The disturbance cannot travel beyond the line defined by this wave angle β_1 unless the wave height increases materially. It will always assume this position ultimately after a disturbance has been established, since it is the only possible stationary position for it.

Some additional deductions are possible from the geometry of the velocity vectors which are shown in Fig. 2. The law of sines applied to triangle ABC gives: $\dfrac{\Delta V_n}{V_1} = \dfrac{\sin \Delta\theta}{\sin (90° - \beta_1 + \Delta\theta)}$ and, for infinitesimal changes of θ,

$$dV_n = \frac{V\,d\theta}{\cos \beta} \quad \ldots\ldots\ldots\ldots\ldots\ldots\ldots\ldots (6)$$

in which the subscripts may now be omitted. Rewriting the momentum equation for infinitesimal changes in depth and velocity, a second differential expression for dV_n is obtained: $\gamma\,h\,dh = \dfrac{\gamma}{g} h\,V_n\,dV_n$; or

$$dV_n = \frac{dh}{V_n}\,g \quad \ldots\ldots\ldots\ldots\ldots\ldots\ldots\ldots (7)$$

Since V_n may be replaced by $V \sin \beta$, Eqs. 6 and 7 may be combined into $\frac{V\, d\theta}{\cos \beta} = \frac{g\, dh}{V \sin \beta}$; or

$$dh = \frac{V^2}{g} \tan \beta \, d\theta \quad \ldots\ldots\ldots\ldots\ldots\ldots\ldots\ldots (8)$$

Assumption of Constant Specific Head.—Eq. 8 may be integrated to obtain the gradual change of depth with gradual angular deflections of the stream if the basic assumption made in the beginning of this section is next introduced to relate β and V to h—namely, that energy dissipation may be disregarded for such flow in accordance with the Bernoulli theorem. Therefore: $H = h + \frac{V^2}{2g}$ = constant; and, thus, $V = \sqrt{2\, g(H - h)}$. Since $\tan \beta = \frac{V_n}{V_t}$ $= \frac{\sin \beta}{\sqrt{1 - \sin^2 \beta}} = \frac{\sqrt{g\, h}}{\sqrt{V^2 - g\, h}} = \frac{\sqrt{h}}{\sqrt{2\, H - 3\, h}}$. Eq. 8 can be transformed finally into

$$\frac{dh}{d\theta} = \frac{2\,(H - h)\,\sqrt{h}}{\sqrt{2\, H - 3\, h}} = \frac{\sqrt{\frac{2\, h}{H}}\left(1 - \frac{h}{H}\right) H}{\sqrt{1 - \frac{3}{2}\frac{h}{H}}} \quad \ldots\ldots\ldots\ldots (9)$$

which was first established by Mr. von Kármán in 1935–1936. The exact integration of Eq. 9 gives

$$\theta = \sqrt{3} \tan^{-1} \sqrt{\frac{\frac{h}{2\, H/3}}{1 - \frac{h}{2\, H/3}}} - \tan^{-1} \frac{1}{\sqrt{3}} \sqrt{\frac{\frac{h}{2\, H/3}}{1 - \frac{h}{2\, H/3}}} - \theta_1 \ldots (10a)$$

in which θ_1 constitutes the constant of integration defined by the condition that for $\theta = 0$ the depth h is the initial depth h_1.

Eq. 10*a* may also be written in an alternate form employing the Froude number to express $\frac{h}{2\, H/3} = \frac{3}{2 + \mathbf{F}^2}$. Substitution of this equivalent results in

$$\theta = \sqrt{3} \tan^{-1} \frac{\sqrt{3}}{\sqrt{\mathbf{F}^2 - 1}} - \tan^{-1} \frac{1}{\sqrt{\mathbf{F}^2 - 1}} - \theta_1 \ldots\ldots\ldots (10b)$$

Summary.—Before discussing Eqs. 10 and their implications any further, it is well to summarize the accomplishments of the theory developed up to this point:

1. Assuming an initial flow defined by a definite value of $\mathbf{F}_1 > 1$ and characterized by the assumption that H remains constant, it has been shown that a change in depth Δh due to any disturbance of the stream must in general always occur along lines or wave fronts crossing the flow at a characteristic angle β, and cannot exist for steady conditions at any other angle.

2. This wave angle β and the depth change Δh determine in turn a change in the velocity normal to the wave front. Therefore, a definite change $\Delta\theta$ in the direction of flow must take place under each wave front.

3. As the flow crosses successive wave fronts at arbitrary distances (the only requirement being that they be not too closely arranged to keep vertical

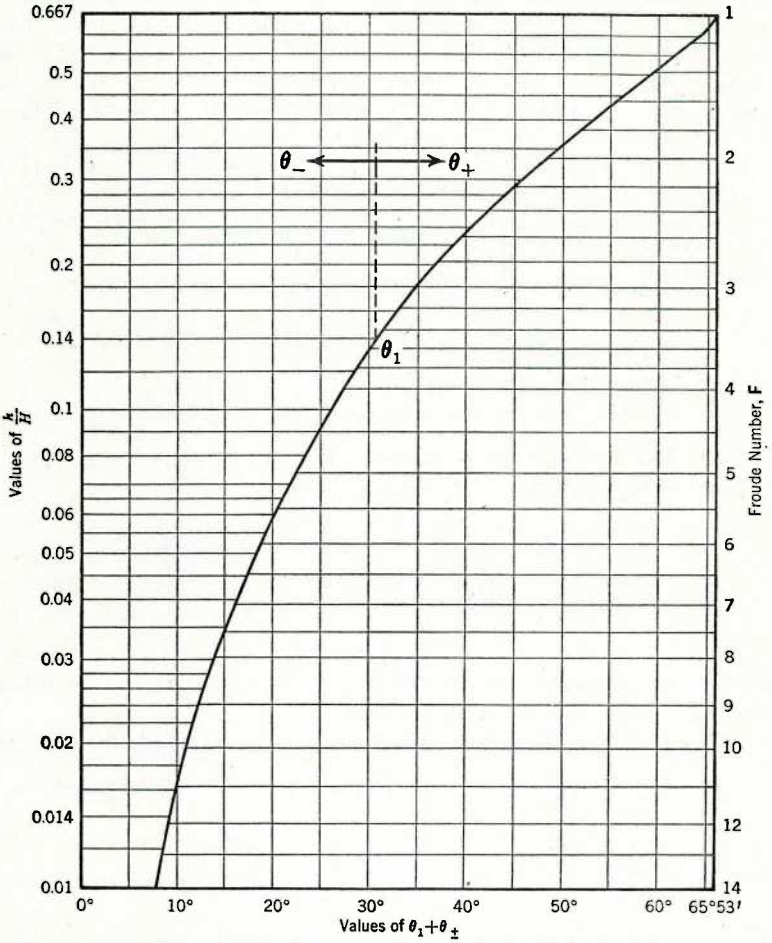

FIG. 3.—PLOT OF EQS. 10

accelerations small), the total change in direction may be related directly to the total change in velocity and depth between any two points along any streamline. Since any boundary of arbitrary curvature represents a streamline, the change of depth along such a boundary can be computed. Conversely, for any desirable changes in depth along a boundary the corresponding curvature may be determined.

4. Since a curved lateral boundary contains the origins of all disturbance lines, the characteristics of which are given by Eqs. 1 to 10, the entire surface configuration of the supercritical flow is determined by the family of disturbance lines emanating from that boundary or any combination of boundaries. The tools by which such contour surfaces may be determined will be developed subsequently, and a number of applications are given in Symposium papers Nos. 2 to 4.

Graphical Aids.—Returning now to Eq. 10, it is clear that a curve for the maximum range of θ for all values of h/H in the supercritical range of flow will be useful. This range extends from $\theta = 0°$ to $\theta_{max} = 65° 53'$, if θ_1 is zero and if h/H is varied from a value of two thirds for critical flow to zero. Neither extreme is of practical interest. The curve is plotted in Fig. 3. Since in a specific case the value of θ_1 constitutes the starting point from which the deflection angle θ is measured, it is only necessary to compute the initial value of h_1/H to determine the value of θ_1 from the curve. The values of h/H are then read from the curve as the angles θ, of a boundary or streamline, are added to or subtracted from θ_1. It is important to note that the change in h may be positive or negative, depending on whether the boundary is curving into the stream or away from it. In the first case the surface will rise and in the second case the surface will be lowered along the disturbance lines originating at the boundary. Both possibilities are indicated in Fig. 3 by the arrows pointing to the left and right from an assumed initial value of θ_1. In addition to the $\frac{h}{H}$-scale, a scale of the corresponding Froude numbers is given for convenience.

The general trend of Eq. 10 may easily be recognized from an approximation based on the first term of the series for $\tan^{-1}$ only. The approximate solution, which naturally becomes incorrect for large values of h/H is given algebraically by

$$\theta = \left(\sqrt{3} - \frac{1}{\sqrt{3}}\right)\sqrt{\frac{\frac{h}{2H/3}}{1 - \frac{h}{2H/3}}} - \theta_1 \approx \sqrt{2}\sqrt{\frac{h}{H}} - \theta_1 \quad \ldots\ldots (11a)$$

Since the ratio h/H may be replaced in terms of the Froude number $\mathbf{F}$, the equation may also be written for small values of h/H (that is, for large values of $\mathbf{F}$) in the form:

$$\theta = 2\sqrt{\frac{1}{\mathbf{F}^2 - 1}} - \theta_1 \approx \frac{2}{\mathbf{F}} - \theta_1 \quad \ldots\ldots\ldots\ldots\ldots (11b)$$

It is obvious that Eqs. 11 could also be solved for h/H or for $\mathbf{F}$ in terms of θ and θ_1. The results given under Eq. 11*a* for small values of h/H could have been obtained directly by neglecting h as compared to H in Eq. 9, thus simplifying the differential expression to

$$\frac{dh}{d\theta} = \sqrt{2\,h\,H} \quad \ldots\ldots\ldots\ldots\ldots\ldots\ldots (12a)$$

which is integrated easily into

$$\theta = \sqrt{2}\sqrt{\frac{h}{H}} - \theta_1 \quad \text{.....(12b)}$$

For small changes in θ the approximations to Eqs. 10 are usually very close.

If the streamlines are given, the changes in h/H or **F** along a streamline can be readily determined. Conversely, the angular changes necessary to accomplish desired changes in h/H or **F** are also easily obtained. Thus, the application of the equations in this form is restricted to determining the changes taking place along boundaries which are streamlines, as long as the flow process along such boundaries is not subject to disturbances propagated from other boundaries. In the case of most hydraulic structures this latter possibility necessitates the study of the interrelations of various boundaries as sources of disturbance lines and of the corresponding system of wave fronts.

Characteristics of Disturbance Lines.—Any curved boundary can be represented as a series of tangents or chords with small but finite angular changes taking place successively. Every angular change $\Delta\theta$ thus becomes the origin of a line of small finite disturbance or a wave front, which will cause a change in depth as indicated by Eq. 9. These wave fronts will traverse the flow at a typical angle β, which is fixed by the Froude number **F** of the flow as given by Eq. 5 for every section of the field of flow. As long as the Froude number remains constant in the undisturbed flow, there cannot be any break or curvature in the line of disturbance and the disturbance itself is constant along its line of propagation.

It has already been mentioned that disturbance lines may indicate positive or negative disturbances. Henceforth, positive disturbances or positive wave or surge fronts will be defined as those which deflect the flow toward the line of disturbance and cause a rise in the water surface. A wall curved into the flow and displacing fluid would be the source of such positive wave fronts. Negative disturbances or depression fronts are caused by boundaries curving away from the flow, providing larger cross sections of flow and therefore producing a lowering of the surface and a deflection of the flow away from the wave front. It is clear that fixed boundaries alone can be the sources of disturbance lines, and that a disturbance line cannot appear or disappear unless by action of a boundary or of another disturbance line. Disturbances once created must be propagated undiminished from one boundary to the other and the effect of the wave front on the flow traversed will be the same as the effect of the boundary itself, the same deflection and the same change in surface elevation being transmitted. This process may now be illustrated schematically in Fig. 4 by a flow between two parallel walls with an initial depth h_1 and a velocity V_1, which at points A and B is subjected to a change in direction through a small angle $\Delta\theta$—exaggerated in the sketch for the sake of clearness.

In agreement with the theory, the disturbances to which the flow is exposed at A and B are communicated along only the fronts BC and AC without effect on the flow in the sector ABC. Along BC and along AC the flow is deflected through an angle $\Delta\theta$. The flow passing under BC is parallel to the

wall beyond point B, and its depth has decreased and its velocity has increased in accordance with the equations developed; in other words, it was affected by the negative or depression front BC. Point C, Fig. 4, is also the intersection with a positive or surge front, which deflects the flow passing between points A and C through the same angle $\Delta\theta$. This positive front in continuing beyond C enters a field of flow already turned through $\Delta\theta$, of smaller depth and with a higher value of $\mathbf{F}_{-2}$. It will therefore proceed with respect to the new direction, but at a new angle β smaller than before. As a positive wave, it will produce a further deflection of the stream toward the front and bring the lower value of h in field $\mathbf{F}_{-2}$ back to h_1, thus reestablishing the original value of $\mathbf{F}_1$ beyond CD. In turn, the negative wave front BC enters a field with $\mathbf{F}_{+2}$ as its hydraulic characteristic. Since the deflection $\Delta\theta$ for a negative front is away from the front, it tends to aline the streamlines beyond CE parallel to those beyond CD, so that also beyond CE the normal value of $\mathbf{F}_1$ is restored. Along AE and beyond, the normal depth is raised to a higher value, whereas between points E and G it drops back to below normal under the influence of wave BCE and its reflection. Therefore, it will alternate between values higher than h_1 and lower than h_1 all along this wall. At the

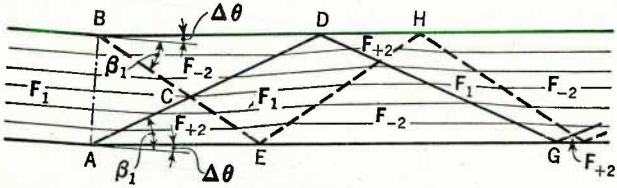

FIG. 4.—SMALL SIDE-WALL DEFLECTIONS IN A RECTANGULAR CHANNEL

reflection points of the positive wave originating first at point A, the depth will be raised; at the reflection points of the negative wave emanating from point B, the depth will always be lowered. In analogy to this, along the wall through points B and D the flow will alternate between zones of lower than normal and higher than normal depth. In zones of normal depth, in the center of the stream, the flow is always at an angle $\Delta\theta$ to the walls. In the other zones adjacent to the walls the flow is always parallel to the walls; but it is also seen that the flow beyond points B and A will always remain disturbed unless further wall-angle changes follow, which may augment the disturbances or may be effective in canceling them.

Wave Interference.—Of course, by proper alinement of walls, methods of wave interference may be utilized to remove the undesired disturbances. This very possibility will be a challenge to the designer and has already led to certain rules in the design of various structures for high-velocity flow, as shown by subsequent papers in this Symposium.

The fact that a negative wave may be canceled by a positive wave, and vice versa, would lead to the design of a bend as illustrated in Fig. 5. In the first case (Fig. 5(*a*)) the positive wave produced by a wall-angle change at A

is not immediately matched by a negative wave opposite A, but the break on the other wall is purposely delayed until the front starting at A arrives at B. Since the flow beyond AB is already deflected through an angle $\Delta\theta$, the wall may be turned through $\Delta\theta$ at B without causing any disturbance at B. This condition may be expressed also by saying that the positive front originating at A is canceled at B by a negative wave, since the latter would coincide with the reflection of AB in B.

The second possibility is shown by Fig. 5(*b*), which indicates that the same turn through an angle $\Delta\theta$ may be accomplished by starting a negative wave first at B and by delaying the break at A until this negative wave has crossed the channel. The possibilities of combining both methods to obtain flow turns with controlled disturbances which will not exceed specified magnitudes are easily recognized. Symposium paper No. 2 is concerned more specifically

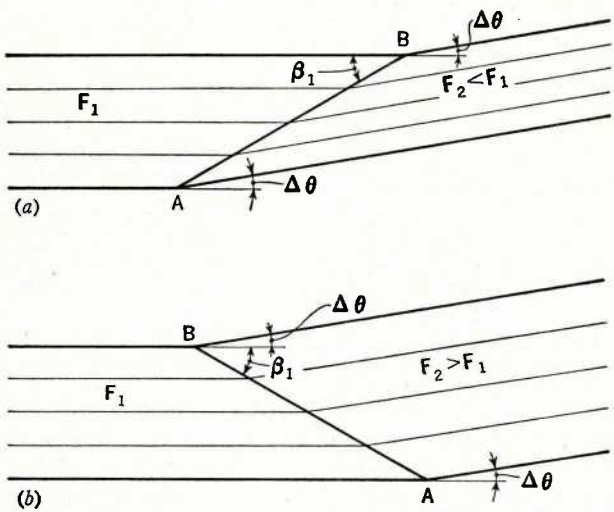

FIG. 5.—SMALL SIDE-WALL DEFLECTIONS DESIGNED TO ELIMINATE DISTURBANCES

with such problems, and with other possibilities which follow on the basis of the foregoing principles. It may also be added that a successful analysis must always very clearly be predicated on a fair prediction of the value of the initial Froude number F_1.

This outline was concerned with the principles of wave intersection, reflection, and interference employing an elementary case for illustration. More complicated systems of curved walls may be replaced by a series of short chords or tangents, each one of the latter a source of a surge or a depression front. Combinations of wave systems are limited only by the mounting difficulties of keeping account of the wave characteristics through numerous intersections and reflections. Except for this fact a useful guide to the design of hydraulic structures is thus available, provided a clear bookkeeping and numbering system can be established and followed.

Successive Waves of Equal Sign.—Before discussion of such a system, a few furthur properties of these wave fronts may be detailed by use of Fig. 6.[10] If a number of wall sections are arranged so that successive sections as shown send out positive fronts only, it is clear that the wave angles β_1 with respect to the flow between sections must increase more and more in the downstream direction. Ultimately, therefore, these fronts carrying small disturbances only must merge into larger ones imposing such height and angle changes that the angle β_1 can no longer be approximated by Eq. 5 but must be computed from Eq. 4, which shows clearly that the wave velocity of a large wave is not only larger than $\sqrt{g\,h_1}$ but even larger than $\sqrt{g\,h_2}$. Such so-called shock waves

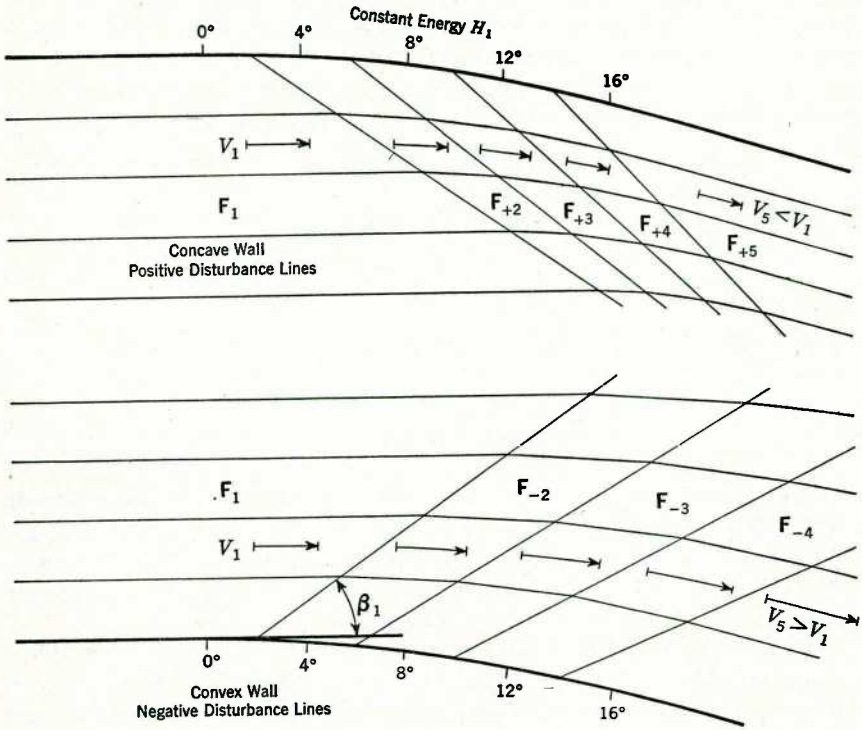

FIG. 6.—FLOW ALONG CURVED WALLS

are discussed in detail subsequently. These difficulties are not present with negative or depression fronts. With decreasing depth and increasing velocity the wave angles β_1 become smaller in the downstream direction, and angular deflections of the stream are away from the disturbance lines. Therefore, negative fronts will generally diverge, and it can easily be concluded that, within the framework of the basic assumptions made initially, so-called shock waves or disturbances with steeper and steeper fronts cannot be built up from successive negative disturbances of small magnitude.

[10] "Gas-Wave Analogies in Open-Channel Flow," by A. T. Ippen, *Proceedings*, 2d Hydraulics Conference, *Bulletin No. 27*, Univ. of Iowa Studies in Eng., Iowa City, Iowa, 1942, p. 257, Fig. 3.

Method of Characteristics

To facilitate the analysis of wave systems due to continuous disturbances, such as those in curved channels or in channel contractions or expansions, a graphical method has been devised on the basis of the preceding theory with certain ingenious changes. This development was entirely the outcome of an early analysis of supersonic flow of gases by A. Busemann[11] and is known as the "method of characteristics." At the suggestion of Mr. von Kármán this method was adopted in 1935 for use in the supercritical flow of water and was applied to the problem of flow in the curved sections of open channels during the analysis of the test data. Independently, Mr. Preiswerk[9] studied water flow through channel expansions and other problems related by analogy to the high-velocity flow of gases. The basic equation for the graphical method of solving problems of supercritical flow of water is given by Eq. 9. For the purpose of obtaining the deflections of the streamlines as a function of the characteristics of the wave fronts, the ratio (h/H) appearing in that equation will be replaced by its equivalent from the Bernoulli theorem: $1 = \frac{h}{H} + \frac{V^2}{2gH}$; or with $\bar{V} = \frac{V}{\sqrt{2gH}}$—

$$\frac{h}{H} = 1 - \bar{V}^2 \qquad (13)$$

—and $\frac{d(h/H)}{d\bar{V}} = -2\bar{V}$. Eq. 9 is thus transposed into the form:

$$\frac{1}{\bar{V}}\frac{d\bar{V}}{d\theta} = \frac{\sqrt{1-\bar{V}^2}}{\sqrt{3\bar{V}^2-1}} \qquad (14)$$

Eq. 14 represents the expression for an epicycloid between the circles of radii $1/\sqrt{3}$ and 1 as the limiting values of $\bar{V}$. Only for supercritical flow has Eq. 14 any physical meaning, since the denominator is zero for $\bar{V}^2 = V^2/(2gH) = 1/3$ which corresponds to critical flow, whereas the numerator obviously can be zero only for zero depth or $V^2/(2g) = H$.

The curve representing Eq. 14 may now be plotted between these limits noting that $d\bar{V}/d\theta = \infty$ for $\bar{V} = 1/\sqrt{3} = 0.577$ and that $d\bar{V}/d\theta = 0$ for $\bar{V} = 1$. The corresponding values (h/H) are two thirds and zero. Values between $\theta = 0°$ and $\theta = 65°\ 53'$ corresponding to $\bar{V} = 0.577$ and $\bar{V} = 1.00$ are given in Table 1. For the drawing of the so-called "characteristics diagram" the curve is best transferred to a sheet of celluloid, which is then cut to serve as a templet between the two limiting circular arcs. The diagram may be started and applied as follows: In a rectangular coordinate system the space within a sector of, say, 46° on either side of the $\bar{V}_x$-axis is subdivided into sectors 2° or 4° in central angle, and the intervals are marked by radial lines between the inner and outer limiting circular arcs starting with 0° on the $\bar{V}_x$-axis. From each point on the inner circle the epicycloid may be drawn by the templet in both directions to the outer circle. In this fashion a dense network of inter-

[11] "Gasdynamik," by A. Busemann, *Handbuch der Experimentalphysik*, Vol. IV, 1931.

secting epicycloids is obtained. Since the radial distance between the limit circles comprises all possible values of $\bar{V}$ between 0.577 and 1.00, a corresponding scale of conversion to h/H may be added as shown in Fig. 7. The physical meaning of the diagram may be demonstrated by first assuming a flow with initial values of V_1 and h_1 or $\mathbf{F}_1$ for which $\bar{V}_1$ can be computed. The diagram is next alined with its $\bar{V}_x$-axis parallel to V_1 in the plan of flow, in which the design of the boundaries is laid out. If one of the boundaries is deflected through an angle $\Delta\theta$, the streamlines adjacent to the wall will turn through the same angle and a disturbance line will originate at this point in the flow plan, beyond which the flow will be in a new direction and at a new value of $(h/H)_2$ or $\bar{V}_2$. To find the latter, one must revert to the characteristics diagram (Fig. 7). The initial value of $\bar{V}_1$ laid out along the $\bar{V}_x$-axis will be near an intersection of this axis with the two epicycloids. If the plan of flow indicates a positive disturbance, one of the branches leading inward is followed;

TABLE 1.—VALUES OF $\bar{V}$ FOR PLOT OF EPICYCLOID BETWEEN CIRCLES OF RADIUS $1/\sqrt{3}$ AND 1.0

0° TO 6°		7° TO 13°		14° TO 20°		21° TO 27°		28° TO 34°		35° TO 40°		41° TO 46°		47° TO 65° 53′	
θ	$\bar{V}$	θ	$\bar{V}$	θ	$\bar{V}$	θ	$\bar{V}$	θ	$\bar{V}$	θ	$\bar{V}$	θ	$\bar{V}$	θ	$\bar{V}$
0	0.577	7	0.709	14	0.782	21	0.840	28	0.886	35	0.925	41	0.952	47	0.972
1	0.613	8	0.720	15	0.791	22	0.848	29	0.893	36	0.930	42	0.956	48	0.975
2	0.635	9	0.731	16	0.799	23	0.855	30	0.900	37	0.935	43	0.960	49	0.978
3	0.651	10	0.742	17	0.808	24	0.861	31	0.905	38	0.939	44	0.963	50	0.980
4	0.666	11	0.753	18	0.817	25	0.868	32	0.910	39	0.943	45	0.966	65°	1.000
5	0.683	12	0.763	19	0.825	26	0.874	33	0.915	40	0.948	46	0.969	−53′	
6	0.695	13	0.773	20	0.833	27	0.880	34	0.920	..	....	..	....	....	....

in the opposite case one of the branches going outward is followed from the origin until it intersects the radial line belonging to the angle of turn $\Delta\theta$. The radius vector to this point of intersection represents the new value of $\bar{V}$. Its direction is also the direction of the streamlines beyond the disturbance line in the flow plan and its magnitude at once gives the hydraulic conditions of depth and velocity or $\mathbf{F}_2$. One may thus conclude that every point in the characteristics diagram or in the velocity plane determines the hydraulic conditions in a section of the flow plane bounded by walls or disturbance lines. Before proceeding to extend the construction of streamline patterns in the flow plane, a method must be found of constructing the disturbance lines at the same time. For this purpose another drafting device is utilized, which is based on the following theoretical considerations:

The component of the velocity normal to the wave fronts V_n was assumed to be given by $\sqrt{g\,h}$; therefore $(V_n)^2 = g\,h = g\,H - V^2/2$ and

$$V^2 = 2\,g\,H - 2\,(V_n)^2 \ldots\ldots\ldots\ldots\ldots\ldots (15a)$$

In accordance with Fig. 2 the velocity V can be related to V_t and V_n by

$$V^2 = (V_t)^2 + (V_n)^2 \ldots\ldots\ldots\ldots\ldots\ldots (15b)$$

Introducing V^2 from Eq. 15*a* into Eq. 15*b*,

$$2\,g\,H = 3\,(V_n)^2 + (V_t)^2 \ldots\ldots\ldots\ldots\ldots\ldots\ldots\ldots (16)$$

Dividing Eq. 16 by $2\,g\,H$ gives the dimensionless components $\bar{V}_n$ and $\bar{V}_t$ in

$$\frac{(V_n)^2}{1/3} + \frac{(\bar{V}_t)^2}{1} = 1 \ldots\ldots\ldots\ldots\ldots\ldots\ldots\ldots (17)$$

Eq. 17 represents an ellipse with major and minor axes of 1 and $1/\sqrt{3}$, respectively, and any radius vector from the center of the ellipse is equal to $\bar{V}$ since it is given by $\sqrt{(V_n)^2 + (V_t)^2}$. This fact is utilized as follows in connection with the characteristics diagram: An ellipse is inscribed on a transparent sheet of plastic to such a scale that the units are identical in both figures.

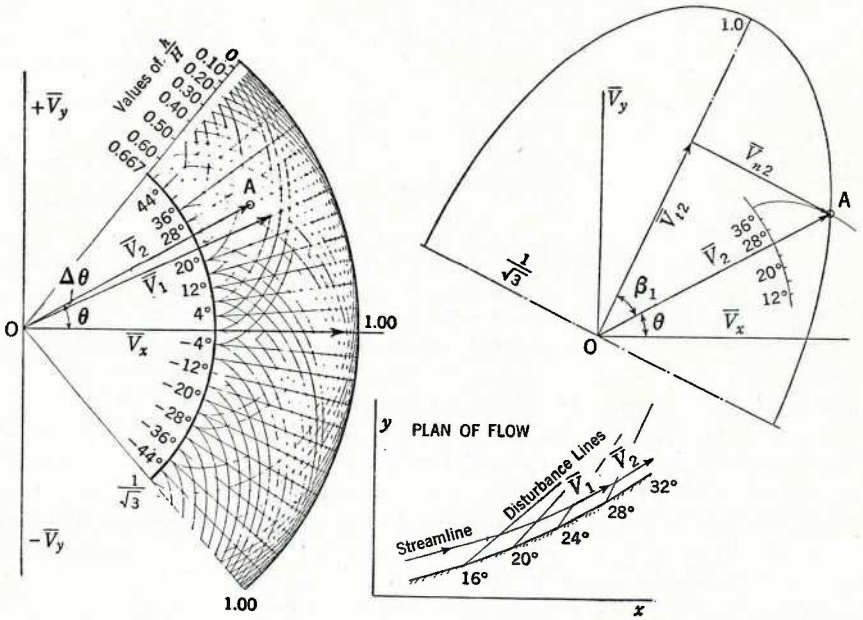

FIG. 7.—CHARACTERISTICS DIAGRAM; SUPERCRITICAL FLOW WITHOUT ENERGY DISSIPATION

If the ellipse is rotated about the center, O, so that finally the ellipse passes through the point $\mathbf{F}_1$, which defines $\bar{V}_1$ in the velocity plane, a line drawn parallel to the major axis gives the direction of $\bar{V}_{t1}$, which is identical with the direction of the disturbance line or wave front in the flow plane. Therefore, it may be drawn through the point in Fig. 7 at which the disturbance is said to originate.

An illustrative example is shown in Fig. 7 in the manner just outlined,[12] except that the point chosen for illustration is not the initial point for $\theta = 0$,

[12] "Gas-Wave Analogies in Open-Channel Flow," by A. T. Ippen, *Proceedings*, 2d Hydraulics Conference, *Bulletin No. 27*, Univ. of Iowa Studies in Eng., Iowa City, Iowa, 1942, p. 259, Fig. 4.

but one along the wall for $\theta = 24°$ with the change indicated to $\theta = 28°$ and with A marking the position on the epicycloid corresponding to $\mathbf{F}_2$ in the preceding discussion.

A detailed example solved by this method for supercritical flow through a channel contraction is given in Symposium paper No. 3. Although the ultimate application of this method permits the rapid and the almost automatic solution of fairly complex problems, anyone applying it must familiarize himself thoroughly with all its aspects and must understand the physical significance of the individual steps at the beginning. Almost any numbering system, methodically applied as the analysis proceeds, will serve satisfactorily, and for this reason no recommendations are made.

High Wave Fronts with Dissipation of Energy

Attention has already been called to the fact that a number of successive positive disturbance lines of small intensity must eventually merge, as distance from the origin increases, into a line representing a surge front of material height. The exact equation for the velocity of such a wave of finite height has been given as Eq. 3 which shows that the wave velocity or celerity is even larger than that for a small disturbance traveling at the larger depth. Consequently the wave angle is larger too in accordance with Eq. 4.

Under the heading, "Method of Characteristics," the wave angle β was approximated by the value of $\sin^{-1} 1/\mathbf{F}$ neglecting the wave height. This section will deal with the modification of the theory due to finite and considerable wave heights, especially with respect to the angle β_1 at which such a large front will assume a steady or "standing" position. Also, the previous assumption of constant energy has to be modified, since energy dissipation is associated with wave fronts of considerable height. However, for many practical cases this modification is still of minor consequence. Basic material for this section was developed by Mr. Rouse and M. P. White,[13] M. ASCE, early in 1937. Mr. Preiswerk[9] adopted Mr. Busemann's shock-polar diagram for use in the hydraulic analogy of supersonic flow in 1938. As before, the problem is the correlation of the wave angle β_1 as defined by Eq. 4 and of the angular change θ accomplished under every standing wave. Fig. 2 may again be referred to except that in keeping with the purpose of this section the angle change $\Delta\theta$ is replaced by θ, thus acknowledging that large deflections are accomplished by large changes in depth under the wave front.

From the geometry of the vectors the angle θ may be related to β_1 by: $V_{t1} = \dfrac{V_{n1}}{\tan \beta_1} = \dfrac{V_{n2}}{\tan (\beta_1 - \theta)}$, in which V_{n2} can be replaced by $V_{n2} = \dfrac{h_1}{h_2} V_{n1}$ from the continuity equation. Therefore,

$$\frac{\tan (\beta_1 - \theta)}{\tan \beta_1} = \frac{h_1}{h_2} \quad \ldots\ldots\ldots\ldots\ldots\ldots\ldots\ldots (18)$$

and, solving Eq. 18 for θ,

$$\tan \theta = \frac{\tan \beta_1 \, (1 - h_1/h_2)}{1 + h_1/h_2 \tan^2 \beta_1} \quad \ldots\ldots\ldots\ldots\ldots\ldots\ldots\ldots (19a)$$

[13] "Fluid Mechanics for Hydraulic Engineers," by Hunter Rouse, McGraw-Hill Book Co., Inc., New York, N. Y., 1st Ed., 1938.

Eq. 19*a* can be reduced to a simpler expression if the variations of h_1/h_2 and β_1 occurring in practice are introduced. Thus, for values $h_1/h_2 = 2/3$ to $1/3$ and $\beta_1 = 10°$ to $35°$, only a small error results if Eq. 19*a* is reduced to

$$\tan\theta = \left(1 - \frac{h_1}{h_2}\right)\sin\beta_1 \qquad (19b)$$

In agreement with Eqs. 4 and 19*a* the wave angle β_1 and the wave height are fixed for a given Froude number $\mathbf{F}_1$ and a given deflection angle θ. Eqs. 4 and 19*a* can be combined into one by solving for h_1/h_2 as follows:

$$\frac{h_1}{h_2} = \frac{2}{\sqrt{1 + 8\,(\mathbf{F}_1)^2\sin^2\beta_1} - 1} \qquad (20a)$$

and

$$\frac{h_1}{h_2} = \frac{\tan\beta_1 - \tan\theta}{\tan\beta_1 + \tan\theta\tan^2\beta_1} \qquad (20b)$$

Equating Eqs. 20 and solving for $\tan\theta$ gives a very useful expression without h_1/h_2 but containing the initial Froude number $\mathbf{F}_1$:

$$\tan\theta = \frac{\tan\beta_1\,(\sqrt{1 + 8\,(\mathbf{F}_1)^2\sin^2\beta_1} - 3)}{2\tan^2\beta_1 - 1 + \sqrt{1 + 8\,(\mathbf{F}_1)^2\sin^2\beta_1}} \qquad (21)$$

Normally the deflection angle θ as well as the initial value of the Froude number $\mathbf{F}_1$ would be given by design. For this case it is practical to plot Eq. 21 and to solve graphically for the angle β_1, since the solution of the equation for β_1 in terms of $\mathbf{F}_1$ and θ becomes rather involved. With β_1 known it is an easy matter to determine h_1/h_2 from Eq. 20*a* or from its graphical form. If the latter values are too large for the design in question, the wall or deflection angle θ must be reduced and the process of computation is speedily repeated with graphs such as Fig. 8.

The limiting values of θ for which the flow passes into the subcritical state below the wave front are of considerable interest. For their determination an expression would be needed involving the Froude number $\mathbf{F}_2$ below the wave front. The latter can then be given the value of unity for critical flow and the corresponding quantities for the other variables may be computed. Since a direct relationship between θ and $\mathbf{F}_2$ becomes rather involved algebraically, it is preferable to correlate h_2/h_1, $\mathbf{F}_2$, and $\mathbf{F}_1$ whereupon, by use of Fig. 8, the pertinent values of θ and β_1 are easily read from the curves.

Making use of a geometric condition evident from Fig. 2, since $(V_{t1})^2 = (V_{t2})^2$, one obtains

$$(V_{n1})^2 - (V_{n2})^2 = (V_1)^2 - (V_2)^2 \qquad (22a)$$

The continuity equation yields $V_{n2} = \frac{h_1}{h_2}V_{n1}$, whereas Eq. 2, based on the momentum relation, results in $V_{n1} = \sqrt{g\,h_1}\sqrt{\frac{1}{2}\frac{h_2}{h_1}\left(1 + \frac{h_2}{h_1}\right)}$. By definition

$\mathbf{F}_1 = V_1/\sqrt{g\,h_1}$ and $\mathbf{F}_2 = V_2/\sqrt{g\,h_2}$, so that, after various substitutions, Eq. 22*a* assumes the following form:

$$(\mathbf{F}_2)^2 = \frac{h_1}{h_2}\left[(\mathbf{F}_1)^2 - \frac{1}{2}\frac{h_1}{h_2}\left(\frac{h_2}{h_1} - 1\right)\left(\frac{h_2}{h_1} + 1\right)^2\right] \quad \ldots\ldots\ldots (22b)$$

Eq. 22*b* establishes the relationship between $\mathbf{F}_1$, $\mathbf{F}_2$, and h_2/h_1 for stationary wave fronts, its graphical solution having been added in the fourth quadrant in

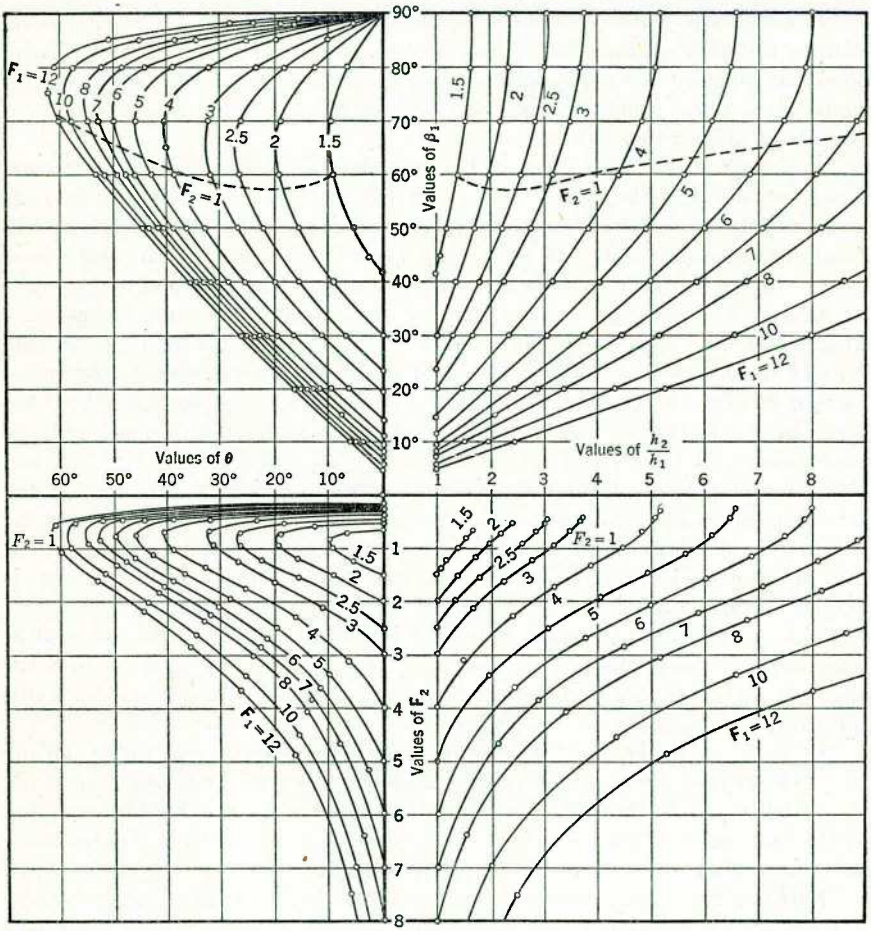

FIG. 8.—GENERAL RELATIONS FOR $\mathbf{F}_1$ VERSUS θ, β, $\frac{h_2}{h_1}$ AND $\mathbf{F}_2$

Fig. 8, in which the critical values for $\mathbf{F}_2 = 1$ are easily located as the intersections of the line for $\mathbf{F}_2 = 1$ with the lines $\mathbf{F}_1$ = constant.

A second critical condition exists for a wave angle β_1 of 90°, which reduces Eq. 4 to the relation between $\mathbf{F}_1$ and h_2/h_1 familiar from the right hydraulic

jump:

$$(\mathbf{F}_1)^2 = \frac{1}{2}\frac{h_2}{h_1}\left(1 + \frac{h_2}{h_1}\right) \quad \ldots\ldots\ldots\ldots\ldots\ldots (23a)$$

or

$$\frac{h_2}{h_1} = -\tfrac{1}{2} \pm \sqrt{2\,(\mathbf{F}_1)^2 + \tfrac{1}{4}} = \tfrac{1}{2}\,(\sqrt{1 + 8\,(\mathbf{F}_1)^2} - 1) \quad \ldots\ldots\ldots (23b)$$

Mr. Rouse has presented[13] a further version of Eqs. 19*a*, 21, and 22*b* giving the deflection angle θ in terms of h_2/h_1 and β_1.

Physical Significance.—For the purpose of this discussion a few points concerning the physical meaning of Eqs. 20 to 23, and of Fig. 8, may be stressed, to clarify some of the results of the analysis that cannot easily be established mathematically. Subsequently, they will be demonstrated graphically by a somewhat different analytical attack.

The angle θ is related to β_1 in Eq. 21, which is represented in the second quadrant of Fig. 8, in such a manner that θ varies from zero to a maximum and again to zero as β_1 increases for any given value of the Froude number $\mathbf{F}_1$ from its minimum value of $\sin^{-1} 1/\mathbf{F}_1$ to 90°. When $\beta_1 = 90°$ and simultaneously $\theta = 0$, the wall deflection cannot be the cause of the standing wave or jump. The standing wave, therefore, is dependent on some downstream disturbances, as soon as the flow below the wave front passes into the subcritical state, which is true for the right hydraulic jump, formed only under certain conditions downstream from the jump. It would seem further that flow parallel to the wall at an angle θ for subcritical conditions will only be accomplished if the downstream disturbance, combined with the wall deflection, produces a wave height of the correct magnitude, which can be computed from Eqs. 20 to 23. In other words, the equations as given no longer determine the wave angle β_1 uniquely for a given wall angle and Froude number $\mathbf{F}_1$ if the flow is subcritical below the wave front with $\mathbf{F}_2 < 1$, since the wave height is subject to downstream disturbances.

The exception to the latter statement is the case in which the value of $\mathbf{F}_1$ approaches a value of unity as the value of θ increases to ± 0, so that the slightest disturbance would cause a wave front at 90° to the oncoming flow; however, this point is purely a philosophical one.

In most practical cases the hydraulic designer will avoid wall angles causing the flow to pass through the critical state or even to approach that state, since little dependence can be placed on the theory when the slightest violation of the basic premises of the theory or inaccurate knowledge of $\mathbf{F}_1$, for instance, may cause a hydraulic jump that travels upstream.

Furthermore, a single wave front is seldom met in practice, and the flow pattern will be determined by intersecting waves and reflections of the waves from opposite walls. These phenomena place severe limitations on practical wall angles, if supercritical flow is to be maintained throughout a structure.

Returning to Fig. 8 it is seen that, for any given hydraulic conditions and geometry of channel walls, the unknown quantities are quickly obtained. For instance, if $\mathbf{F}_1$ and θ are known, β_1 can be read off immediately as can h_2/h_1 and $\mathbf{F}_2$. If the wave front seems too large, then for any desirable value of h_2/h_1 and the given value of $\mathbf{F}_1$, the corresponding values of β_1 and θ are

found. If the wave is reflected, the value of $\mathbf{F}_2$ must be known in order that the process may be repeated.

Magnitude of Energy Dissipation.—In contrast to the small changes in depth due to gradual lateral deflections of the stream along walls of small curvature, sudden changes in depth, characterized by the appearance of steep standing wave fronts, are subject to energy losses, which may be computed next. The head loss for the flow through a standing wave or jump is easily expressed by the difference in the specific heads: $H_1 - H_2 = \Delta H$; or $(h_1 - h_2) + \frac{(V_1)^2 - (V_2)^2}{2g} = \Delta H$. Making use of Eq. 22*a* and of the momentum and continuity equations, the velocity-head terms may be eliminated and the head loss may ultimately be expressed as

$$\frac{\Delta H}{h_1} = \frac{1}{4} \frac{\left(\frac{h_2}{h_1} - 1\right)^3}{\frac{h_2}{h_1}} \qquad (24)$$

The head loss remains surprisingly small even for large values of h_2/h_1. Although the head loss is expressed in terms of h_1 (which, for supercritical flow, forms a small part of the specific head), the loss remains a small quantity up to values of $h_2/h_1 = 2$ and for this value it is only one eighth of the initial depth h_1. The ratio of $\Delta H/h_1$ reaches unity for values of $h_2/h_1 = 3$. However, as the possibilities of higher values h_2/h_1 presume higher Froude numbers $\mathbf{F}_1$, the depth h_1 forms a smaller percentage of the total head H_1. Therefore, head losses do not increase as rapidly for larger values of h_2/h_1 as the ratios $\Delta H/h_1$ indicate.

The important fact for practical design is that, in general, head losses up to the ratios $h_2/h_1 = 3$ remain rather small and often may be neglected, since their influence on downstream wave angles remains within the limits of accuracy set by other approximations made in the theory. It seems that in practical design this limit of $h_2/h_1 = 3$ will seldom be exceeded.

Shock-Wave Intersection and Reflections

Limiting wall angles, as given in Fig. 8, should never be approached, since the flow in a structure will seldom be determined by the first wave front alone. Reflections on opposite walls and intersections with other wave fronts will have an important role in regard to the character of flow downstream from a disturbance. Various possibilities of basic character will therefore merit discussion. At the outset it may be stated, however, that the following discussion is limited to the range of wave heights mentioned in the preceding paragraph as being little affected by energy losses. Figs. 9 and 10 illustrate, in plan, the following cases to be discussed in order:

1. Reflection of shock wave at opposite wall;
2. Intersection of shock waves:
   a. Of different intensity;
   b. Of equal intensity;
3. Convergence of two shock fronts; and
4. Shock front and negative deflection waves.

1. *Reflection of Shock Wave at Opposite Wall.*—The first case given by Fig. 9(*a*) is the easiest of the four. The flow below the first front AB can be determined from Fig. 8 since the angle of deflection θ is given. As the wave arrives at the opposite wall at point B, the new angle of deflection is the angle of this wall relative to the flow downstream of AB. If this angle happens to be zero, the disturbance is almost wiped out; if the angle is positive, point B will be the source of a wave front determined again from Fig. 8 on the basis of flow parallel to the wall below point B crossing the flow to point C, where the process is then repeated. In the example in Fig. 9(*a*) the opposite wall remains parallel to the original direction of flow. Therefore the flow below front AB is again deflected through the same angle θ and the change from $\mathbf{F}_2$ to $\mathbf{F}_3$ is determined for this angle from Fig. 8. Each reflection brings the flow closer to subcritical conditions and eventually the wave angle will be 90° unless new energy is supplied.

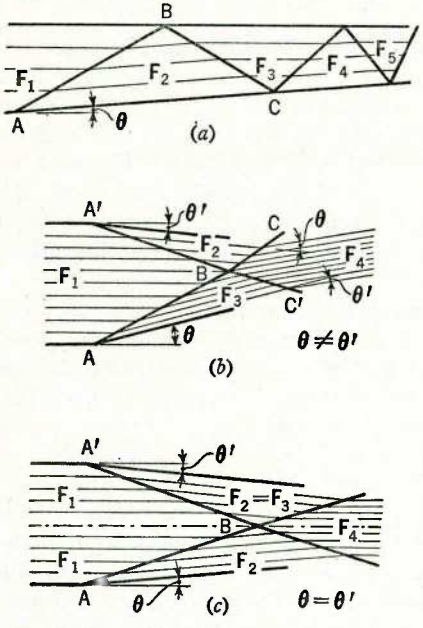

FIG. 9.—SHOCK-WAVE ANALYSIS; CONVERGING WALLS

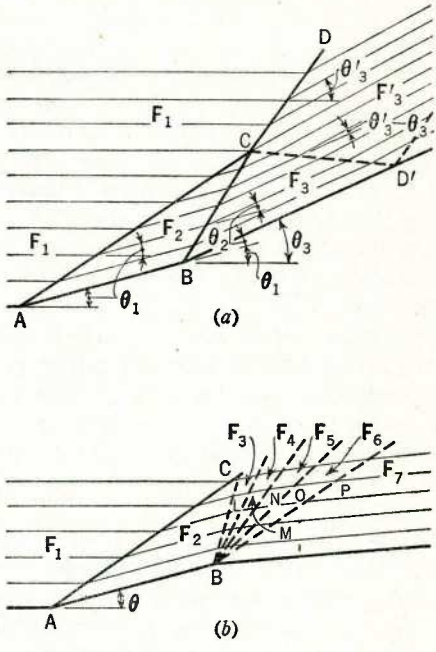

FIG. 10.—SHOCK-WAVE INTERSECTIONS FOR SUCCESSIVE WALL DEFLECTIONS

2a. Intersection of Shock Waves of Different Intensity.—The second case illustrated in Fig. 9(*b*) is somewhat more difficult. When two shock waves meet, each one thereafter will proceed with respect to altered flow conditions. Section AB must be adjusted from $\mathbf{F}_1$ to $\mathbf{F}_2$ and section A'B from $\mathbf{F}_1$ to $\mathbf{F}_3$. The intensities of the two waves in the following sections BC and BC' are not known and must be determined from the fact that the flow conditions below either one are identical. The flow below BC must have the same depth, velocity, and direction as the flow below BC'. Remembering that for most

cases the energy dissipation may be neglected in the first approximation, the new direction of flow in the field $\mathbf{F}_4$ may be determined simply as the difference of the angles θ in fields $\mathbf{F}_2$ and $\mathbf{F}_3$. In most cases the waves BC and BC′ determined on the basis of this first assumption will result in values of $\mathbf{F}_4$ from Fig. 8 which require little adjustment. The approximation becomes better as the two waves differ less in intensity and deflection angle.

2b. Intersection of Waves of Equal Intensity.—In the case of two waves of the same intensity and deflection angle the solution is obvious. The conditions are the same as if a wall were placed along the center line, and the solution is immediate. The shock-wave system on either side of the center line is identical with that illustrated in Fig. 9(*a*).

3. *Convergence of Two Shock Fronts.*—Fig. 10(*a*) presents the case of two converging shock waves, starting on the same side of the wall at points A and B and meeting in point C. The two jumps combine into a single jump CD which produces a head loss higher than the sum of the head losses by wave fronts AC and BC. If no difference in head loss existed, the solution would be simple; the direction of flow would be the same downstream from BC as it is downstream from CD, and the same Froude number $\mathbf{F}_3$ and total deflection angles would exist in this field of flow. This approximation will always be a good one. If more accuracy is warranted, it must be considered that the head below CD must be lower than that below BC and that therefore the intersection point C must be the origin of a depression wave CD′ which forms the boundary between two fields of flow characterized by $\mathbf{F}_3$ and $(\mathbf{F}_3)'$ with $(\mathbf{F}_3)' > \mathbf{F}_3$. The intensity of the depression wave must be such that by trial and error the combined effect of fronts AC and BC and of the depression wave CD′ is identical with the effect of the combined front CD; that is, to either side of a streamline drawn through C the Froude number is $(\mathbf{F}_3)'$ and the deflection angle is $(\theta_3)'$ instead of θ_3 with $(\theta_3)' > \theta_3$. In other words, the effect of the convergence of the jump is a slight additional deflection $((\theta_3)' - \theta_3)$ of the flow away from the wall below the intersection of the depression wave CD′ with the wall.

The depression wave could be treated further according to the methods previously introduced under the heading, "General Physical Background," on the basis of zero energy loss. The effect of CD′ cannot be large since, in agreement with the properties of depression waves discussed previously, negative shock waves are not possible.

4. *Shock Front and Negative Deflection Waves.*—This case involves Fig. 10(*b*) where a positive wall deflection is followed by a negative deflection of finite magnitude. The finite negative deflection of the wall is the origin of a number of depression waves BL, BM, BN, BO, etc., of small intensity as shown in Fig. 10(*b*), some of which will be able to intersect the positive front AC. The faculty of deflecting the flow through a certain small angle $\Delta\theta$, which each depression wave is assumed to have, is not impaired by its intersection with a positive front, since no energy change is involved. In most cases, however, only a few of the negative waves will reach the jump within a finite distance, and usually reflections from opposite walls take place beforehand. Thus, a combination of positive and negative wall deflections will always cause large total disturbances of the water surface, with the exception of the case in which

a positive wave from the opposite wall and of comparable deflection intensity arrives at the point of origin B of the negative disturbances.

In concluding the discussion of problems concerning intersections and reflections, combinations of steep wave fronts and of small positive or negative disturbances may be mentioned very generally. Since small disturbances can be treated without energy dissipation, their influences may be superposed directly on the field of flow subject to the action of steep wave fronts.

Polar Diagram of Shock-Wave Characteristics

Although Fig. 8 contains, in a convenient form, all possible values of the variables involved in the treatment of steep wave fronts or shock waves, it can be used only indirectly for plotting streamline patterns for flow fields with a shock-wave system. The analysis of shock waves in supersonic gas dynamics has been based, therefore, on the so-called shock-polar diagram as developed first by Mr. Busemann.[11] As its name implies, the shock-polar diagram represents a polar plot of all possible values of the dimensionless velocities upstream and downstream from a shock front similar to the plot of the same velocities on the basis of constant energy. However, since the energy does not remain constant through the finite jumps, the jump-polar diagram cannot be made of such universal character. The basic difference lies in the fact that the dimensionless velocity $\bar{V}_1 = V_1/\sqrt{2\,g\,H_1}$ will change below a jump of deflection intensity θ to the value $\bar{V}_2 = V_2/\sqrt{2\,g\,H_1}$, which is no longer identical with $V_2/\sqrt{2\,g\,H_2}$ since $H_1 > H_2$. Since curves may be plotted only for $\bar{V}_2$ (that is, for dimensionless velocities $\bar{V}_2$ in terms of H_1), the values of $\bar{V}_2$ cannot be used to find $\bar{V}_3$ below a subsequent jump 2–3. The velocity $\bar{V}_2$ must be adjusted below the jump, before the diagram can be used again, by multiplying the value $\bar{V}_2$ obtained from $\sqrt{H_1/H_2}$ which is always larger than unity. A new initial value of $\bar{V}_2\sqrt{H_1/H_2} = (V_2)'$ is found, which may then be used to determine $\bar{V}_3$ in terms of H_2. Thus, adjustments must be made continuously in accordance with changing values of H. The second difference appears in the fact that the wave celerity for finite jumps must be considered on the basis of Eq. 3, modifying the wave angles β_1 in conformance with Eq. 4.

The construction of the shock-polar curves requires the transformation of the foregoing basic equations by introducing the x-component and the y-component of the dimensionless velocities $\bar{V}_1$ and $\bar{V}_2$. Following the geometry of the vector diagram of Fig. 11,

$$\bar{V}_{n1}\,(\bar{V}_{n1} - \bar{V}_{n2}) = \bar{V}_{x1}\,(\bar{V}_{x1} - \bar{V}_{x2}) \qquad (25a)$$

and

$$(\bar{V}_{n1} - \bar{V}_{n2})^2 = (\bar{V}_y)^2 + (\bar{V}_{x1} - \bar{V}_{x2})^2 \qquad (25b)$$

All the velocities have been divided by $\sqrt{2\,g\,H_1}$, as indicated by the bar over the velocity components. In addition to Eqs. 25, the momentum relation as stated in Eq. 2 and the continuity equation as given in Eq. 1 are available while, as a fifth equation, the energy equation is used for the definition of the initial energy as $H_1 = h_1 + \dfrac{(V_{x1})^2}{2\,g}$; or

$$1 = \frac{h_1}{H_1} + (\bar{V}_{x1})^2 \quad \ldots\ldots\ldots\ldots\ldots\ldots\ldots\ldots\ldots\ldots (26)$$

Thus, all terms containing h_1 and h_2 as well as V_{n1} and V_{n2} can be replaced in terms of V_y and V_x, resulting ultimately in an equation for $\bar{V}_{y2}$ as follows:[14]

$$(\bar{V}_{y2})^2 = (\bar{V}_{x1})^2 \left(1 - \frac{\bar{V}_{x2}}{\bar{V}_{x1}}\right) \times \left[\frac{\bar{V}_{x2}}{\bar{V}_{x1}} - \frac{\sqrt{1 - (\bar{V}_{x1})^2}}{\sqrt{1 - (\bar{V}_{x1})^2 + 4\,(\bar{V}_{x1})^2 \left(1 - \frac{\bar{V}_{x2}}{\bar{V}_{x1}}\right)}}\right] \quad \ldots\ldots\ldots (27)$$

The curves of possible values of $\bar{V}_{y2}$ and $\bar{V}_{x2}$ are shown in Fig. 11 for a systematic set of values of $\bar{V}_{x1}$ varying from a maximum of $V_1/\sqrt{2\,g\,H_1} = 1$ to $V_1/\sqrt{2\,g\,H_1} = 1/\sqrt{3}$ as a minimum for critical flow.[15] A radius vector to

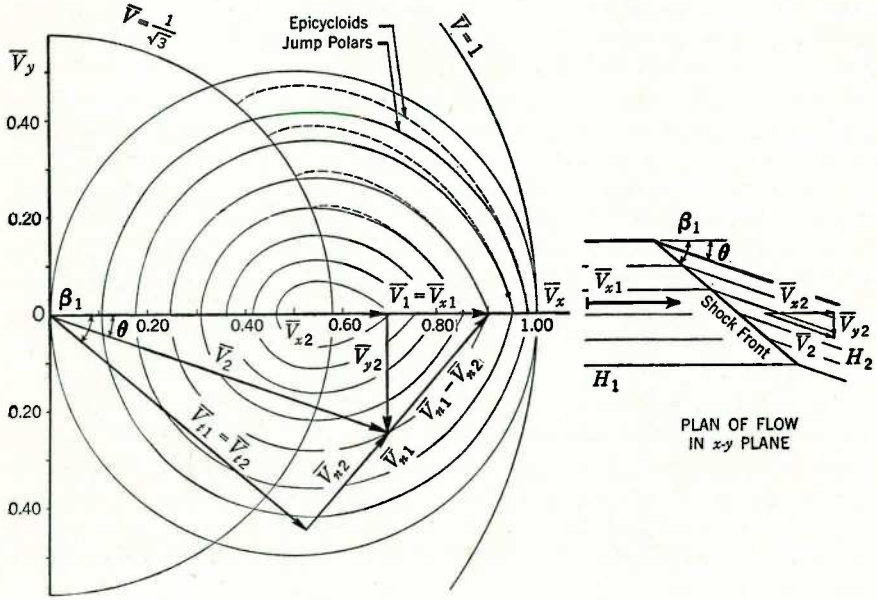

FIG. 11.—EXAMPLE SHOWING THE USE OF THE POLAR DIAGRAM, WITH $V_{x1} = 0.9$ AND $\theta = 20°$

any intersection with a curve beginning at a certain value of $\bar{V}_1 = \bar{V}_{x1}$ will give, immediately, the only value of $\bar{V}_2$ possible for the assumed direction, whereupon V_2 will be known since H_1 is given initially. Remembering also that $V_{t1} = V_{t2}$ and that the direction of these components represents the direction of the wave front, the latter may be transferred to the plan of flow as was done for the characteristics diagram in the example given. The same ellipse may be used if a graphical method is desired.

[14] "Gas-Wave Analogies in Open-Channel Flow," by A. T. Ippen, *Proceedings*, 2d Hydraulics Conference, *Bulletin No. 27*, Univ. of Iowa Studies in Eng., Iowa City, Iowa, 1942, p. 262, Eq. 20.

[15] *Ibid.*, p. 261, Fig. 6.

Only one wave front may be found at one time. With every value of $\bar{V}_2$, of course, belongs a new value of specific head, since $H_2 < H_1$, which has to be computed next as does the corresponding depth h_2. It may be sufficient to remind the reader of Fig. 8 (which relates, in a comprehensive manner, all pertinent variables) to indicate that curves of H_2/H_1 and h_2/h_1 could be plotted also as polar curves similar to the $\bar{V}_2$-curves in Fig. 11. Since shock fronts are usually not very numerous in a plan of flow, it is felt that a completely graphical solution does not offer advantages as great as does the method of characteristics, where the solution requires the drawing of a multitude of disturbance lines.

It may be noted that the polar curves for a wide range of $\bar{V}_1$-values agree quite closely with the epicycloids of the characteristics diagram as indicated in Fig. 11. One outstanding difference is the fact that the polar curves extend into the subcritical range and therefore within the circle of critical velocity with radius $\bar{V} = 1/\sqrt{3}$. As is also evident from Fig. 8, there is a maximum deflection angle θ for every curve (that is, for every initial value $\bar{V}_{x1} = \bar{V}_1$), which falls within the subcritical range of flow below the wave front and is subject to the restrictions discussed earlier in this treatment. The points $\bar{V}_2$ for $\theta = 0$ lying on the $\bar{V}_x$-axis, within the range of subcritical flow, represent the $\bar{V}_2$-values for the right hydraulic jumps.

It is desired to obtain the value of $\bar{V}_2$ in magnitude only, since its direction must be parallel to the deflected wall. In addition, the location of the shock-wave front (below which all flow is deflected through the angle θ) is to be determined. For this purpose, the $\bar{V}_x$-axis of the polar diagram is alined with the direction of flow $\bar{V}_{x1}$ in the plan of flow. A line parallel to the deflected wall is drawn in the polar diagram from the origin to its intersection with the polar curve starting from the given $\bar{V}_{x1} = 0.90$. The length of the line represents $\bar{V}_2$, which is $0.72 = V_2/\sqrt{2\,g\,H_1}$ so that V_2 is known. Through the ends of $\bar{V}_{x1} = 0.90$ and $\bar{V}_2$, the direction normal to the wave front is found; and the line normal from point O to this direction represents the wave front. The latter may then be transferred to the plan of flow, starting from the break on the wall. If another deflection is to be investigated below the first one, H_2 must be found and an adjusted value of $(\bar{V}_{x2})' = V_2/\sqrt{2\,g\,H_2}$ determined. The $\bar{V}_x$-axis is to be alined again with V_2, and the former steps are then repeated. The treatment of wave front intersections and reflections can be easily adapted to the shock-polar method on the basis of the preceding discussion.

Summary

The fact that boundary-layer influences and nonuniformities of the velocity and pressure distributions are disregarded in the theory imposes certain limitations which are discussed in detail in the Symposium papers dealing with specific practical applications. In general, it may be said that viscous forces do not seriously disturb the basic systems of disturbance lines and of finite wave fronts. Vertical accelerations are usually also of secondary order of magnitude in structures to which the elementary theory applies, since changes in the flow patterns discussed are the result of changes of the lateral boundaries only. The extension of the theory to cases of accelerated motion due to changes of specific head must be reserved for future discussion.

The assumption of a sudden change of flow conditions under a wave front was made for the convenience of analyzing wave systems and does not correspond to physical reality. Shock-wave fronts, especially, represent a finite change in velocity and depth and therefore extend in nature over a considerable distance in terms of depth. The hydraulic jump may be cited to illustrate this point. Nevertheless, the ultimate change accomplished by these standing waves is still as computed by the basic theory. The local phenomena become important only where the dimensions of the hydraulic structure concerned are small compared to the length of the transition zone. As a practical example a bridge pier may be cited, which causes standing waves comparable in height and length of transition to its own dimensions. Information on the transverse extent of hydraulic wave fronts is yet to be obtained experimentally and is tied in with the problems of boundary-layer growth and of vertical accelerations. Another more serious effect of viscous forces may be mentioned: As changes in velocity and depth occur, the balance between gravity and viscous forces existing for uniform flow is disturbed. Minor changes in specific head will result, which are not considered in the elementary theory. The effect of such changes is negligible only for local phenomena, but it is cumulative over a long distance. A small change in wave angle, for instance, will cause only a slight shift of the point of the first reflection of a wave, but the nth reflection point is displaced n times more than the theoretical one. Thus, longitudinally extended systems of waves may become subject to considerable differences by interference downstream from the original disturbance.

Except for these secondary physical phenomena which the basic analysis neglects, the elementary theory has contributed the following:

1. The primary features of supercritical flow have been rationalized on the basis of accepted principles of mechanics.
2. The general characteristics of the standing wave patterns have been developed systematically.
3. The basic requirements for sound high-velocity structures can be formulated qualitatively for the different types, and the effects of various designs can be visualized. In general, the aim of design will be toward elimination of large surface disturbances.
4. Surface disturbances can be subjected to a detailed quantitative analysis for given designs with respect to local phenomena, and basic formulas have been derived for this purpose.
5. The findings of the theory have been used to develop systematic graphical procedures for the solution of complex problems.

Acknowledgment

Considerable assistance in the preparation of the material of this paper for publication was given by Donald R. F. Harleman, Jun. ASCE, research associate in hydraulics, in the Department of Civil and Sanitary Engineering of the Massachusetts Institute of Technology. His aid is hereby gratefully acknowledged.

DESIGN OF CHANNEL CURVES FOR SUPERCRITICAL FLOW

BY ROBERT T. KNAPP,[16] M. ASCE

SYNOPSIS

Characteristics of flows around curved sections of open channels at velocities greater than the wave velocity (that is, $\mathbf{F} > 1$) are discussed in this paper. In simple curves such flows produce cross-wave disturbance patterns which also persist for long distances in the downstream tangent. These disturbance patterns indicate nonequilibrium conditions whose basic cause (when $\mathbf{F} > 1$) is that disturbances cannot be propagated upstream or even directly across the channel. Thus, the turning effect of the curved walls does not act equally on all filaments in a given cross section and equilibrium is destroyed. The paper outlines two basic methods of eliminating these disturbance patterns. Analytical design criteria are developed, and experimental verifications of the analyses are presented. The first method consists of applying a lateral force in such a way that it acts simultaneously on all filaments, causing the flow to turn without disturbing the equilibrium. Bottom banking supplies such a lateral force, and a series of vertical curved vanes across the channel has roughly the same effect. The second method employs interference patterns introduced deliberately at the beginning and at the end of the curve. Compound curves, spiral transitions, and sills all operate on this principle. Rectangular channels are uniquely suited to the interference method of treatment, since for a given channel the wave patterns are substantially independent of the flow. Trapezoidal and other nonrectangular channels should be avoided if possible, unless the flow is invariant. The fields of application of the different treatments are discussed briefly.

DESCRIPTION OF FLOW AROUND SIMPLE CURVES IN RECTANGULAR CHANNELS

One of the common types of curves in normal use for subcritical and supercritical velocities is the simple curve of constant radius in a channel of rectangular cross section. For all subcritical velocities this design is quite satisfactory. For supercritical flows, it is not satisfactory. Fig. 12 shows the surface appearance of such a curve. Very strong cross waves occur within the curve and persist for a considerable distance downstream. This type of behavior could have been predicted from the principles presented in the first Symposium paper. Thus, an examination of the mechanics of the flow shows that the only forces acting on the fluid to cause it to change its direction originate, and are applied, at the walls. At the beginning of the curve the elements next to the outer wall are forced to turn because the wall curves toward them.

[16] Director, Hydrodynamics Laboratory, California Inst. of Technology, Pasadena, Calif.

The elements next to the inner wall are induced to turn since this wall curves away from them and leaves them without support. However, the elements in the interior of the flow are unaffected at first. They continue to move in the original direction until the wall forces have had time to propagate across the channel far enough to act upon them. These wall forces appear as pressure differences and as such are propagated at the velocity of a surface wave in the channel. Fig. 13 is a diagram of such a curve having a mean radius, r. The point A is the beginning of curvature of the outer wall.[17] The first small disturbance caused by this curvature will be propagated along the line AB. Similarly, the initial disturbance produced by the inner wall is propagated along the line A_1B. All the flow upstream from the boundary ABA_1 is unaffected by the curve and thus continues to move in a direction parallel to the upstream tangent. Beyond point B the disturbance originating at A on the outer wall is no longer propagated in a straight line since the flow in this region is moving in a curved path under the influence of the inner wall. The dotted line, BM_1 indicates the path of propagation. Similarly, the disturbance originating at A_1 is propagated on the path BM. Thus, four regions of flow can be delineated as follows:

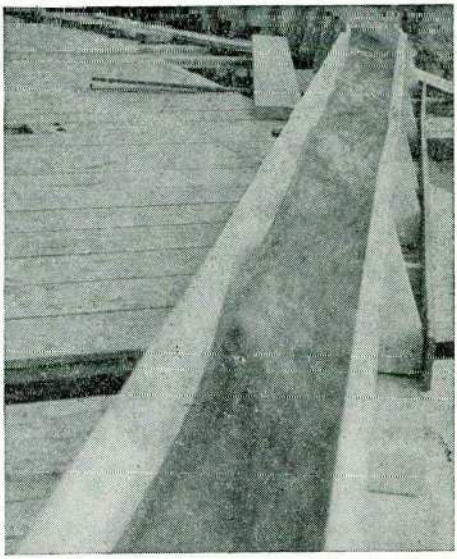

FIG. 12.—CROSS-WAVE DISTURBANCE PATTERN BELOW A SIMPLE CURVE

1. The region unaffected by either wall, lying upstream from ABA_1;
2. The region affected by the outer wall only, within ABM;
3. The region affected by the inner wall only, within A_1BM_1; and
4. The region affected by both walls, downstream from MBM_1

Along the outer wall the fluid surface rises continuously from A to M since an increasing force from the wall has been required to turn the increasing amount of flow acted upon by this wall. At point M, however, the force from the inner wall begins to act. The combined force from the two walls is more than that required to keep the flow turning with the same curvature as that of the channel. Hence, the pressure, and consequently the liquid surface along the outer wall, begin to drop. The reverse condition holds on the inner wall. The liquid surface drops continuously from A_1 to M_1. At the latter point the effect

[17] "Curvilinear Flow of Liquids with Free Surfaces at Velocities Above That of Wave Propagation," by R. T. Knapp and A. T. Ippen, *Proceedings*, 5th International Cong. for Applied Mechanics, Cambridge, Mass., 1938, p. 533, Fig. 1.

of the outer wall comes into play and therefore the surface begins to rise again. It is evident from Fig. 12 that conditions do not become stabilized when the difference in elevation between the outer and inner walls is again just sufficient to cause the flow to turn with the channel curvature. This equilibrium also is passed through rapidly. The surface continues to drop along the outer wall and to rise along the inner wall to new maxima and minima located at each reflection point of the continuing disturbance paths ABM_1— and A_1BM (Fig. 13). These reflections will conform to the normal laws of wave mechanics. Maxima will occur at all reflection points of the continuation of the path A_1BM and corresponding minima will occur along the continuation of ABM_1.

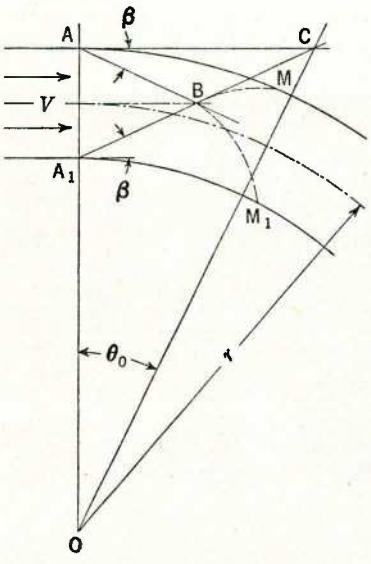

FIG. 13.—DIAGRAM OF FLOW ENTERING A CURVE

CALCULATION OF LIQUID SURFACE PROFILES ALONG THE WALLS

In order to calculate the liquid surface it is necessary to define the assumptions to be used. In the general case, these include: (*a*) Two-dimensional flow, (*b*) constant velocity across the cross section, (*c*) horizontal channel, and (*d*) frictionless flow. Assumptions (*c*) and (*d*) do not exclude the application of the results to inclined channels since, if the flow is in equilibrium, the slope compensates for the friction.

With these assumptions, and the principle of the conservation of energy, Mr. von Kármán[6] derives

$$\theta = \sqrt{3}\sin^{-1}\sqrt{\frac{h}{2H/3}} - \sin^{-1}\sqrt{\frac{h}{2(H-h)}} + (\text{a constant}) \quad \ldots\ldots (28)$$

from which the change of depth along the walls at the beginning of the curve can be calculated.[18] Angle θ is the angle of turn of the channel wall. Positive values of θ signify a turn toward the channel axis. Eq. 28 is not very convenient to use analytically, although this difficulty may be overcome by using it in a graphical form. A study of the experimental data for a series of flows of this type suggests a simplifying assumption. On the basis of the dual conditions, just specified, of frictionless flow and conservation of energy, the velocity in any filament must change as the depth changes, since the sum of the depth and the square of the velocity must remain constant. The flow around the outer wall, being the deepest, should be the slowest. Measurements indicate, however, that the velocity around the outer wall remains constant, or even in-

[18] "Curvilinear Flow of Liquids with Free Surface at Velocities Above That of Wave Propagation," by R. T. Knapp and A. T. Ippen, *Proceedings*, 5th International Cong. for Applied Mechanics, Cambridge, Mass., 1938, p. 532, Eq. 3.

creases slightly, whereas along the inner wall it decreases. The deviations are caused by the varying effects of friction on the different elements of the channel. These measurements justify the replacement of the condition of conservation of energy with the approximation that the magnitude of the velocity remains constant. For high-velocity flow the depth represents a comparatively small fraction of the specific head; therefore any possible change in depth can produce only a relatively small change in velocity. On the basis of this assumption the expression for the depth, h, can be derived in the following manner: Consider an open channel with liquid flowing in it at a velocity, V, and a depth, h. If the velocity, V, is supercritical—that is, if V is greater than $\sqrt{g\,h}$—a pressure disturbance can be propagated only at an angle $\beta = \sin^{-1}\frac{\sqrt{g\,h}}{V}$ to the direction of V. If such a pressure wave is propagated across the channel (say, as the result of the liquid encountering a slight bend in the channel), the pressure difference will act normal to the wave front—that is, normal to the angle β. The effect of the pressure difference at the wave front on the velocity, V, will be equal to the change in momentum of the flow normal to the wave front. Thus, if the angle of turn is $d\theta$, the change in depth produced by this change in angle can be expressed as follows:

$$\frac{dh}{d\theta} = \left|\frac{-V_n}{g}\right|\frac{dV_n}{d\theta} \qquad (29)$$

By Fig. 13 $V_n = V \sin\beta$; and, assuming V constant,

$$dV_n = V\cos\beta\,d\theta \qquad (30)$$

Eq. 30 assumes that $d\theta/2$ is small compared to β. Eq. 29 now becomes

$$\frac{dh}{d\theta} = \frac{V^2}{g}\sin\beta\cos\beta \qquad (31)$$

Introducing in Eq. 31 the relationship previously defined that $\sin\beta = V/\sqrt{g\,h}$, and the expression that follows directly from it, that $\tan\beta = \sqrt{g\,h}/\sqrt{V^2 - g\,h}$, Eq. 31 may be transformed to

$$d\theta = \frac{dh}{\sqrt{h\left(\frac{V^2}{g} - h\right)}} \qquad (32a)$$

If Eq. 32*a* is integrated from 0 to θ,

$$h = \frac{V^2}{g}\sin^2\left(\beta_1 + \frac{\theta}{2}\right) \qquad (32b)$$

in which β_1 is the original wave angle corresponding to the depth, h_1, upstream from the disturbance.

Eq. 32*b* is much simpler than Eq. 28 and gives results agreeing equally well with experimental measurements for high velocities. It must be re-

membered that Eq. 31 is an approximation. However, Eq. 28 is also an approximation, because, among other things, it assumes a constant velocity across the cross section at the entrance to the curve. In the actual case this velocity is not constant. It should be possible to calculate the water-surface profile on the basis of actual velocity distribution instead of utilizing this assumption of constant velocity. However, in most cases the requirements are not rigorous enough to demand this refinement.

There is a close relationship between the wave angle, β, and the Froude number, **F**; and sin β is simply the reciprocal of **F**. Thus either can be used to characterize the state of the flow if the velocity is greater than the critical velocity. The Froude number is more generally used because it retains its significance for subcritical velocities as well as for supercritical ones since physically it is simply the ratio of the flow velocity to the velocity of propagation of a wave with respect to the fluid. On the other hand, the wave angle, β, has no significance for subcritical flow since under these conditions it does not exist.

Neither Eq. 28 nor Eq. 32*b* gives the law locating the maxima and minima along the walls, because they do not contain the factors that determine these locations. Fig. 13 furnishes a basis for estimating their location. As previously stated, the first maximum on the outer wall occurs at point M, which is the reflection point of the disturbance which originates at A_1. The path is straight from point A_1 to point B since the water depth, and hence the wave velocity, is constant. From point B to point M the path is curved, because the water depth (and therefore the wave velocity) is increasing, and also because the direction of flow has been changed by the effect of the outer wall. The path BM may be computed by the methods outlined in the first Symposium paper. Usually it is sufficient to estimate the location of the first maximum and minimum by assuming that they occur at intersections of the line OC with the outer and inner walls. Fig. 13 shows that θ_o represents a half wave length of the disturbance pattern. Its value is given by the expression:

$$\theta_o = \tan^{-1} \frac{b}{\left(r + \frac{b}{2}\right) \tan \beta_o} \qquad (33)$$

Therefore, subsequent maxima should occur at $3\,\theta_o$, $5\,\theta_o$, etc., along the outer wall. If by some method the wave pattern could be eliminated and the flow brought to equilibrium within the curve so that the difference in depth between the inner and outer walls would just produce the pressure required to balance the centrifugal force, the difference in depth across the channel would be

$$h_2 - h_1 = \frac{V^2 b}{r g} \qquad (34)$$

The depth along the outer wall should be $h_o + \frac{V^2 b}{2 r g}$. For $\theta = \theta_o$ (first maximum on the outer wall) Eq. 32*b* gives nearly twice this depth. The disturbance

pattern that oscillates about the equilibrium depth, therefore, has a wave length of $2\,\theta_o$ and an amplitude of $\frac{V^2\,b}{2\,r\,g}$.

Disturbance in Downstream Tangent

The disturbance pattern (that is, the pattern of cross waves superimposed on the equilibrium superelevation) continues into the downstream tangent. The wave length now becomes $\frac{2\,b}{\tan\beta_o}$. Furthermore, because of the sudden change of curvature, a new disturbance of amplitude $\frac{V^2\,b}{2\,r\,g}$ originates at the end of the curve. This new cross-wave pattern has a maximum on the outer wall (at the point of tangency). The wave length is the same as that of the original disturbance, since it is determined by the same factors. The resulting disturbance pattern in the downstream tangent is the sum of these two patterns. In general, they are out of phase and the resultant pattern is dependent on the phase angle. Thus, if a simple curve at equilibrium discharges into the downstream tangent, the resulting disturbance pattern will have an amplitude of $\frac{V^2\,b}{2\,r\,g}$ with a maximum occurring on the outer wall at the end of curvature. A similar curve having a disturbance pattern of $\frac{V^2\,b}{2\,r\,g}$ superimposed upon equilibrium conditions will produce no disturbance pattern in the downstream channel if the disturbance within the curve has a minimum on the outer wall at the end of curvature. Curves of lengths θ, $3\,\theta$, $5\,\theta$, etc., will have a maximum on the outer wall at the end of curvature and will produce a disturbance pattern in the downstream channel having maxima of $\frac{V^2\,b,}{r\,g}$ which is double that of the pattern below a curve operating at equilibrium. It will be noted that the disturbance in the downstream tangent may have a greater amplitude than the corresponding one within the curve but that the actual depth of flow along the wall is never greater than it is on the outer wall within the curve, nor less than it is along the inner wall. The explanation of this anomalous result is that in the tangent the equilibrium condition about which the disturbance oscillates is the constant-depth flow, whereas in the curve the corresponding equilibrium condition is variable flow depth in the cross section, with superelevation on the outer wall, and depression on the inner wall.

Channel with Multiple Curves

In the field most channels are made up of a series of curves separated by tangents of varying lengths. The disturbance pattern in the lower curves and tangents can become very complicated since each curve affects the disturbance in its downstream tangent and the disturbance in each tangent affects the performance of the following curve. It was just shown that the disturbance in the downstream tangent is a maximum when a maximum exists at the end of the outer wall of the preceding curve. The same reasoning will

show that the disturbance in a curve will be a maximum whenever a minimum point exists on the outer wall at the beginning of curvature. Thus it is possible by a particularly unfortunate combination of length of curve and of intermediate tangent, to build up an extremely high disturbance pattern.

Calculation of the Water-Surface Contours

In general it is sufficient for design purposes to calculate the water-surface profile along the two walls of the channel. However, it is possible to calculate the entire water surface by the method of characteristics described in the first Symposium paper. The method of characteristics is not applicable when the wave fronts become steep or break. If the vertical accelerations are high some disagreement may be found, but in general this will be confined to a limited zone and thus will not affect the validity of the calculations as a whole.

There are two sources for additional energy losses in curves over those existing in straight channels. Even if equilibrium conditions are established by proper methods of treatment, the cross section of the flow is distorted by the superelevation in such a way as to decrease the effective hydraulic radius and thus increase the frictional losses. Losses are most apparent in the zone of decreased depth. The second major source of loss occurs only if the disturbance pattern is strong enough to produce breaking waves, which correspond to shock waves in supersonic flow of gases. If the wave breaks, an appreciable amount of energy is lost. However, if the surface wave does not break, it represents a very small amount of energy loss. A qualitative proof of this statement is the number of oscillations required for the damping in the downstream channel of a disturbance pattern produced in a curve. Field conditions usually permit the use of radii large enough to avoid breaking waves. Thus, in general, it can be stated that, for supercritical flow, the additional energy losses in curves are of little significance either in the calculation of the disturbance pattern or in the determination of the hydraulic gradient of the channel as a whole.

Available Methods for the Reduction of Superelevation in Curves and in the Downstream Tangents

Summary of Flow Characteristics Which Affect Method of Treatment.—Before discussing the possible ways of reducing the superelevation in curved channels, it will be well to review briefly the salient physical characteristics of high-velocity flow around curves, as follows:

1. The flow velocity is greater than the velocity of the surface wave (that is, $F > 1$). Therefore, disturbances cannot travel directly across the channel, but only at the oblique angle determined by the ratio of the wave velocity to the flow velocity.

2. In channels, as normally designed, the side walls are expected to do the turning. This is basically a nonequilibrium process because the effect of a change in wall alinement is not propagated directly across the channel, and therefore cannot immediately affect the entire flow.

3. The form of the disturbance produced when water flows from a straight to a curved channel or vice versa is oscillating and has the properties of a wave train.

Banking.—The most logical method of eliminating the disturbance pattern is to remove its cause. Since it is impossible to act on all the elements of flow at once by a change in direction of the side walls, it would be desirable to employ some better method of applying the lateral force to change the flow direction. The obvious way of applying a lateral force simultaneously to all the fluid elements is by the use of a bottom cross slope—that is, by banking. This cross slope, S_c, can easily be calculated by equating the gravity component along the cross slope to the centrifugal force determined by the radius and velocity. The result is

$$\tan \phi = S_c = \frac{V^2}{r g} \ldots\ldots\ldots\ldots\ldots\ldots\ldots\ldots (35)$$

It should be emphasized that, with the proper use of banking, all the force necessary to change the direction of the flow is supplied by the cross slope. The walls do nothing except conform to this change of direction. In banking it is not feasible to change the cross slope of the channel instantaneously from a level bottom to the value indicated by Eq. 35. The banking requires an appreciable change in elevation, which can be obtained either by raising the bottom on the outside of the curve, or by lowering it on the inside—or by a combination of the two. To avoid shock, the banking must be introduced gradually and, to follow the path of the stream, the walls must have a decreasing radius of curvature that just matches the increase of cross slope. The most elegant design of a banked bottom would be one in which the center of gravity of the flow followed the mean slope of the channel.

One characteristic of a banked curve is that equilibrium conditions are obtained for only one velocity of flow, and hence for only one depth and one rate of flow. All other flows will show disturbance patterns similar to those in untreated curves. The magnitude of the disturbances will be determined by the degree of departure from equilibrium velocity.

Multiple Curved Vanes.—Eqs. 32*b* and 34 show that for a given depth, velocity, and radius of curvature, the maximum superelevation varies directly with the width of the channel. Therefore, if a given curve is divided into a series of narrower curves by concentric vertical vanes, the superelevation in the subchannels will be correspondingly reduced. Furthermore, the disturbance in the channel below the vanes will dissipate rapidly because of the absence of the vanes that supported the differences in elevation.

Interference Treatments.—The fact that the disturbances produced at the beginning and at the end of a simple curve are wave trains suggests that they might be eliminated by proper interference patterns—that is, by the deliberate introduction of similar disturbances of equal magnitude but of opposite phase. In the flow around a curve of constant radius, the equilibrium condition requires a superelevation of $\frac{V^2 b}{2 r g}$ on the outside wall and a corresponding drop along the

inner wall. The disturbance wave pattern oscillates about this equilibrium condition with a wave height practically equal to the equilibrium change in elevation. For complete "interference" the counterdisturbance should have this same wave height. The original disturbance has a minimum point on the outer wall and a maximum point on the inner wall at the beginning of curvature. Therefore, the counterdisturbance should be introduced with a maximum on the outer wall and a minimum on the inner wall at the same point. The opposite conditions exist at the end of curvature. There are several ways of producing the required counterdisturbances, three of which will be discussed briefly—compound curves, spiral transitions, and diagonal sills. All three of these treatments are complete in themselves and do not require auxiliary measures, such as banking of the bottom, to accomplish the desired result. It is possible to combine methods, but such combinations will not be discussed in this paper. It may have been noted that in this discussion of interference treatments, no attention has been paid to the production of a disturbance pattern having the correct wave length. The reason is that the wave length is a function of the velocity and the channel width; hence, the counterdisturbance will automatically have the correct wave length to match the original disturbance. Therefore, care must be taken to obtain a conterdisturbance of the right amplitude and phase. No attention needs to be paid to the wave length except as it is used in establishing the correct phase.

Compound Curves.—A simple curve produces a disturbance pattern having an amplitude and a wave length that can be determined quite accurately. Therefore, it is logical to employ a section of a simple curve to produce the counterdisturbance pattern required to interfere with the one formed by the main curve.

The length of curve most effective in producing a disturbance pattern is a half wave length since this length produces the maximum disturbance for a given radius of curvature. It is also the minimum length in which the disturbance from both inner and outer walls has had time to affect the entire flow. This maximum is on the outer wall, which is where it should be to interfere with the disturbance produced by the main curve. This curve length as measured on the outer wall is $\frac{B}{\tan \beta_o}$. The equivalent central angle is

$$\theta' = \tan^{-1} \frac{b}{\left(r_i + \frac{b}{2}\right) \tan \beta_o} \quad \ldots\ldots\ldots\ldots\ldots\ldots (36)$$

In Eq. 36, r_i is the radius of the counterdisturbance section, not that of the main curve. The required radius for this section is just twice that of the main curve as it is desired to produce a disturbance of one half that caused by the main curve. Thus, the interference pattern must have a wave height equal to $\Delta h/2$, or

$$\Delta h_i = \frac{V^2 b}{2 r g} = \frac{V^2 b}{r_i g} \quad \ldots\ldots\ldots\ldots\ldots\ldots (37a)$$

From Eq. 37*a* it follows directly that

$$r_i = 2\,r \ldots\ldots\ldots\ldots\ldots\ldots\ldots\ldots\ldots\ldots (37b)$$

in which Δh_i is the height of the interference pattern. Therefore, if a simple curve of radius r is preceded by a section of another simple curve, whose length is $\frac{b}{\tan \beta_o}$ and whose radius is $2\,r$, the flow will rise gradually to the equilibrium value and remain in this condition throughout the entire length of the main curve. However, if the main curve terminates abruptly in a downstream tangent, a disturbance pattern will be formed therein having a wave height of $\frac{V^2 b}{2 r g}$. Similar reasoning to that used in developing the design for the upstream counterdisturbance section will show that an identical section applied at the downstream end of the curve will produce the interference pattern required to eliminate the disturbance in the downstream tangent. Fig. 14 shows the

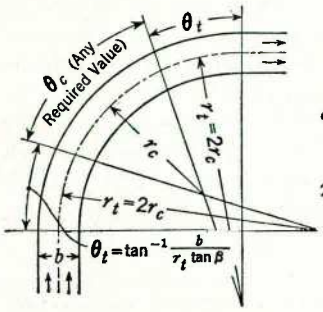

FIG. 14.—DESIGN CRITERIA FOR A COMPOUND CURVE

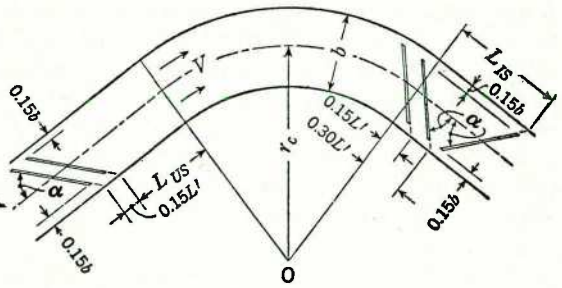

FIG. 15.—PLAN OF SILL INSTALLATION

construction of such a compound curve which will operate with no disturbance pattern either in the curve itself or in the downstream channel.

Spiral Transitions.—Spiral transition curves have been suggested to replace constant-radius transitions. The suggestion is probably traceable to the use of spiral transitions in railroad and highway construction. The spiral can be made to produce satisfactory conditions at the beginning and at the end of the main curve. For that matter, many other designs of transition curves can be found which will be equally satisfactory, provided that the transition curve, whatever its design, must produce a simple disturbance pattern which has a maximum on the outer wall at the beginning of curvature of the main curve and a wave height as given in Eq. 34. One fundamental fact must always be borne in mind: As previously shown, no configuration of curved walls used with a flat bottom channel can produce a change in direction of a high-velocity flow under conditions that maintain equilibrium in all points of the flow. Thus, the primary purpose of the transition curve, whatever its shape, is only the production of the interference wave pattern necessary to cancel out the one produced by the main curve. The fact that the external appearance of the

flow shows no evidence of a disturbance pattern is no indication of the absence of the interference phenomenon.

Diagonal Sills.—Diagonal sills on the channel bottom can be used to produce the necessary interference pattern. The effect of a diagonal sill is to produce a change in direction in the lower layer of the flow, which is quite rapidly averaged throughout the entire cross section by the mechanism of momentum exchange. The over-all result can be approximated by calculating the lateral force exerted on the sill by the flow. This force must produce a corresponding lateral change in momentum in the flow. If the force is equated to the product of the mass rate of flow and the change in lateral velocity, the latter can be calculated readily. The vector sum of the lateral and longitudinal velocities gives the resulting direction of the flow below the sill. Since the mass rate of the total flow is used, the direction will be the average for the entire flow.

If skin friction is neglected, the only force that the fluid can exert on a sill will be normal to the face. This force is equal and opposite to the rate of change of momentum of the flow. Its magnitude is obtained by computing the rate of change of momentum of the water that hits the sill. This layer of water has the width of the channel and the height of the sill. It can be assumed to travel with the average flow velocity and to turn through the angle that the sill makes with the channel axis. This layer of water will mix rapidly with the remainder of the flow above it. Therefore, the average angle through which the entire flow is turned can be computed by applying the principle of conservation of momentum to obtain the resulting lateral component of velocity. Thus, if the sill height is d, the angle of sill inclined to the channel is α, and the angle of curve of the entire flow is θ'_s,

$$\theta'_s = \tan^{-1} \frac{d}{h} \frac{\sin 2\alpha}{2} \quad \ldots\ldots\ldots\ldots\ldots\ldots\ldots\ldots (38)$$

Eq. 38 shows that the sill has maximum effectiveness when $\alpha = 45°$, and this is confirmed by laboratory tests. Experiments indicate, however, that a smoother disturbance is obtained with a sill angle of 30° with very little loss in effectiveness. The required magnitude of the counterdisturbance produced by the sill is governed by the same consideration as that which governs the magnitude of the counterdisturbance produced by the upstream and downstream sections of the compound curve. The same reasoning, therefore, indicates that θ'_s should be $\theta_o/2$ in which θ_o is the central angle of the half wave length in the main curve, given by Eq. 33. It is not practical to attempt installations for values of θ'_s greater than 10°, as too great a sill height would be required.

On first consideration, the desirable location for the diagonal sills would appear to be with their downstream end at the beginning of curvature on the outer wall. The corresponding position at the end of the curve would be to have the downstream end of the sill at the end of curvature on the inner wall. However, the disturbance produced by a diagonal sill is not as smooth as that resulting from a simple curve. This is particularly true of the first maximum produced. Subsequent maxima become smoother and more similar to those caused by a simple curve. Experiments have shown that the best location for

the diagonal sills is as indicated in Fig. 15. The distance L_{US} is given by the expression:

$$L_{US} = \frac{b}{\tan \beta_o}\left[\frac{1.12}{\left(1 + \frac{3\,\Delta h_i}{2\,h_o}\right)^{\frac{1}{2}}} + \frac{0.0313}{\left(\frac{h_i}{h_o}\sin \beta_o\right)^2}\right] \quad \ldots\ldots\ldots (39)$$

The first term in the brackets is a correction for the increase in velocity of the finite disturbance over that of an infinitesimal wave; the second term is an addition for the distance downstream from the toe of the sill at which the maximum disturbance occurs. The symbol h_i denotes the depth of the disturbance produced by the sills and Δh_i is $h_i - h_o$. For normal cases the value of the bracket term will lie between 0.9 and 1.15. Eq. 39 should be used with caution if the correction factor falls outside this range since the experimental verification of the empirical coefficients is rather meager.

Another laboratory finding is also incorporated in Fig. 15. Two sills are shown instead of one at each location. Also the sills end a short distance from the walls. Both modifications are for the purpose of eliminating undesirable local disturbances and of broadening the main disturbance to make it approach the wave form produced by the curved transition section that the sills are replacing. The group of three sills at the end of the curve replace the downstream transition section of the compound curve method of treatment and perform the same necessary function—that is, the elimination of the disturbance in the downstream tangent. All the sills shown in Fig. 15 should have heights one half of that indicated by Eq. 38 since they act in pairs.

Fields of Application of Different Treatments for Rectangular Channels

The treatments described have different fields of use. Banking is most adaptable to major channels that ordinarily operate at or near the design flow. It offers the only method for preventing, completely, the rise in elevation of the water surface in the curve. This requires that the banking be obtained entirely by depressing the inner wall, which usually involves costly excavation. The effect of banking can be decreased or completely nullified by improper wall design. Banking does not produce equilibrium conditions for flows above or below the design capacity. However, for the lower flows, the disturbances produced stay below the design flow line.

The use of multiple curved vanes is rather restricted. They are not desirable for channels carrying debris unless the vane spacing can be made considerably larger than the maximum size of debris to be expected. In case it is necessary to bridge such a channel at the curve, an economical design may be made by using the vanes as bridge piers.

Compound curves offer the most desirable solution for most high-velocity channels. If properly designed, they appear to offer a completely satisfactory solution, not only for the design discharge, but also for all lower discharges.

Spiral or other complicated transition curves are not recommended for any normal application. They simply add to the cost of both the design and the

construction with no commensurate improvement in the flow characteristics over that secured by the use of compound curves.

Diagonal sills should be used primarily as a remedial measure in existing channels which have been designed with simple circular curves or other unsatisfactory forms. For such applications, they offer the possibility of changing quickly and economically a completely unsatisfactory condition of flow into one that is at least acceptable. However, diagonal sills operate best at the design rate of flow. For lower flows, the disturbance produced is too large and thus there is some residual pattern both in the curve and in the downstream channel. This is usually not serious for, as in the case of the banked bottom, the superelevations produced by the disturbance pattern fall below the flow line for the design discharge. This disturbance pattern at low flows may have one somewhat intangible by-product. If the channel in question happens to be used for flood-control purposes or for similar uses in which maximum flows are rather unusual, the sight of the disturbance pattern at low flows may cause uneasiness and distrust among the adjacent residents. This is particularly true if overtopping of the channel would be serious. The inexperienced observer is likely to reason that, if a low flow shows such a pronounced disturbance pattern, higher rates are certain to cause increasing superelevations and major flows are sure to cause failure. The engineer may encounter considerable difficulty in explaining that the reverse is true—that the channel performance improves as the flow rate increases.

It must be expected that the maintenance costs for curves with diagonal sills will be higher than those for either banked or compound curves, especially if the flow is debris laden. However, experience has shown that wood timbers bolted to the bottom of concrete channels form quite satisfactory sills even for relatively large channels carrying heavy debris loads. If sills are used with extremely high-velocity flows, cavitation will occur (see subsequently in Fig. 31). Cavitation itself will tend to increase rather than decrease the effectiveness of the sills but the resulting damage may destroy them.

Nonrectangular Channels

A good indication of the problems involved in high-velocity flow in nonrectangular curved channels is obtained by examining two unique advantages of the rectangular cross section which hold for all interference type curve treatments:

1. For a given channel with a given slope, the wave angle remains nearly constant over a wide range of flows; and
2. The channel width is constant.

From these two characteristics it follows that the disturbance pattern in and below a given curve is constant in configuration and location irrespective of the rate of flow. The significance of this statement has already been stressed—that is, designs using interference pattern methods of treatment are satisfactory for all flows within the design maximum.

In a nonrectangular channel the wave angle changes with depth since the wave and flow velocities no longer vary at the same rate. The surface width

likewise varies with depth. This means that the wave pattern varies with the flow.

Therefore it must be concluded that curve treatments using the interference method will be much less satisfactory for nonrectangular cross sections than for rectangular cross sections. For example, in nonrectangular channels both compound curves and sills produce interference patterns of the right phase for only one rate of flow. If the channel width varies rapidly with the discharge, this phase shift may even change the interference into a reinforcement and thus increase materially the superelevation in and below the curves. Fig. 34, subsequently, shows such a shift produced by a change in the discharge in a trapezoidal channel. It is suggested, therefore, that the use of nonrectangular cross sections for high-velocity curved channels be avoided wherever possible, especially for applications involving wide ranges of discharge.

Experimental Confirmation

The experimental confirmation of these methods of controlling high-velocity flows in and below curves was obtained during a study conducted in the Hydraulic Structures Section of the Hydrodynamic Laboratories of the California Institute of Technology under the direction of the writer. Much of the experimental work and analysis was done by the author of the first Symposium paper. The study was sponsored by the Los Angeles County Flood Control District, which needed design information for its network of flood-control channels, many of which had steep gradients and high velocities. The first objective was the determination of the physical phenomena involved, and the second objective, the development of methods of treatment for the curved sections of high-velocity channels. Although the Los Angeles County Flood Control District was deeply concerned with the design of a specific group of channels, it was felt that it would be more profitable to conduct the study from this fundamental basis with a view to developing analytical methods of design, rather than to adopt a model study technique and be satisfied with specific solutions for only this particular group of channels.

The equipment consisted primarily of two brass channels, one having a rectangular cross section and one a trapezoidal cross section. They were designed so that under normal flow conditions the sectional areas would be the same. They were both provided with abnormally high walls to permit the investigation of high superelevations. The rectangular channel was 18 in. wide and 14 in. deep; and the trapezoidal channel was 12 in. wide at the bottom, 12 in. deep, and had side slopes of 1 on $1\frac{1}{2}$. The channels were mounted on a platform 100 ft long, which was adjustable to any desired slope up to 1 in 10. A water-circulating system was provided with a maximum rate of flow of 6 cu ft per sec. The flow was measured by a set of three venturi meters having slightly overlapping ranges. Fig. 16 shows the plan and elevation of this equipment,[19] and Figs. 17 and 18 illustrate some of the details of construction. Water depth and surface contours were measured by point gages mounted on rails accurately adjusted to be parallel to the bottom of the

[19] "Experimental Investigations of Flow in Curved Channels," by A. T. Ippen and R. T. Knapp (abstract of results and recommendations, U. S. Engr. Office), Los Angeles, Calif., 1938, p. 2.

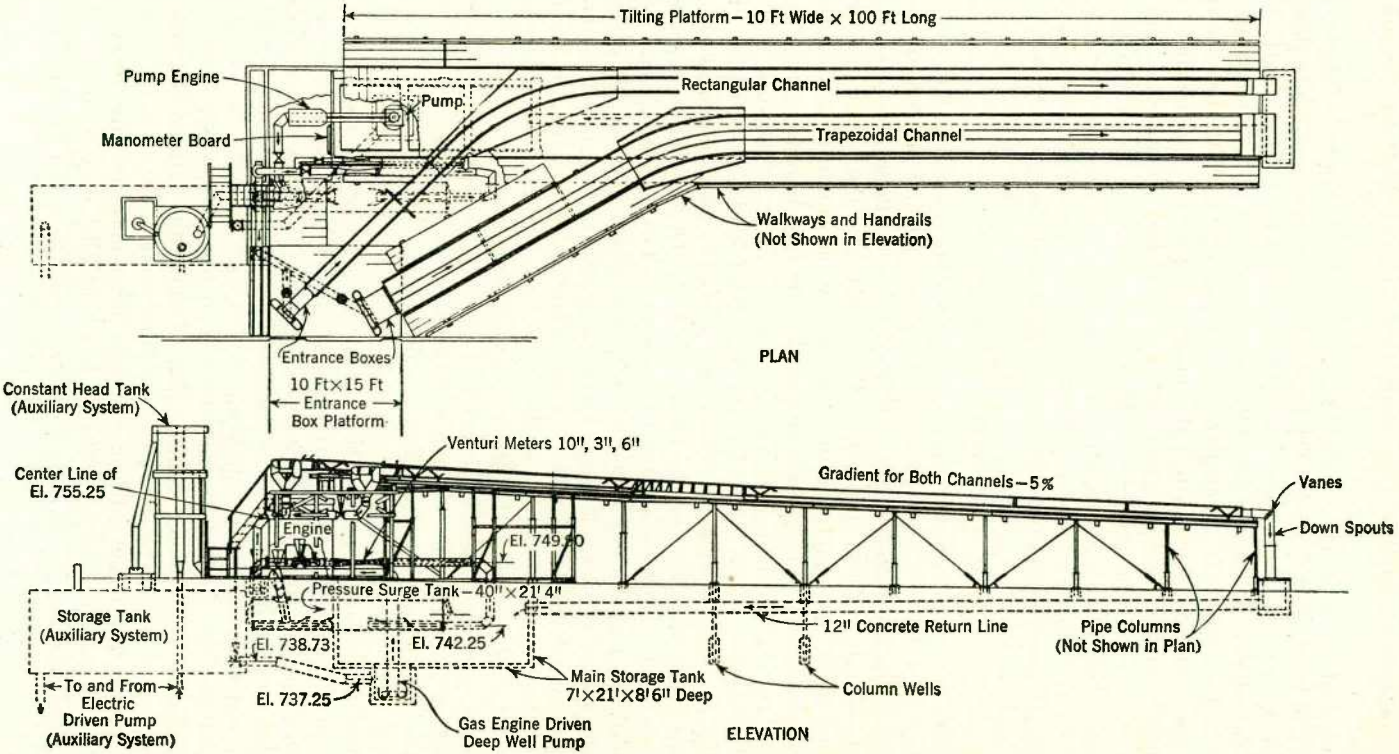

FIG. 16.—PLAN AND ELEVATION OF EXPERIMENTAL CHANNELS

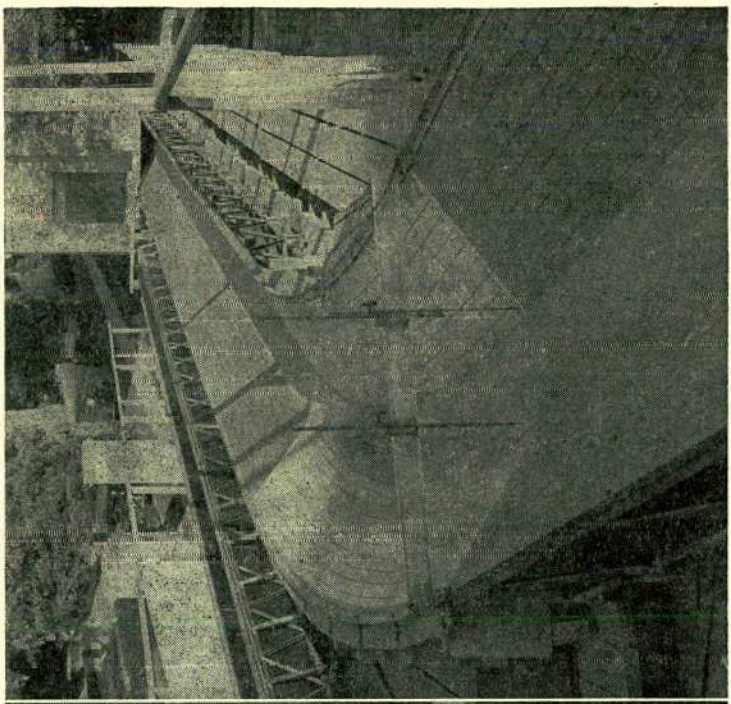

FIG. 18.—CURVE IN TRAPEZOIDAL CHANNEL

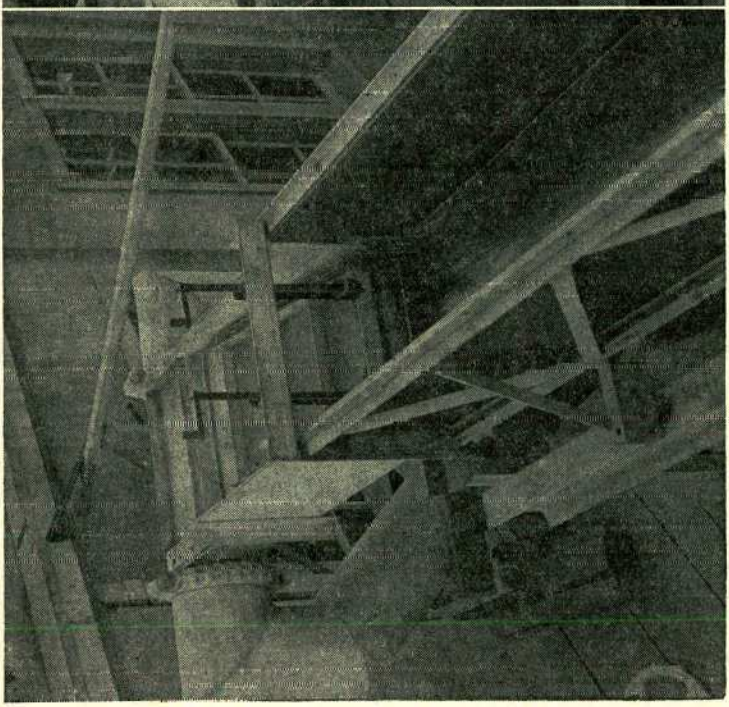

FIG. 17.—ADJUSTABLE ENTRANCE NOZZLE

channel. Velocity profiles were obtained by pitot tubes mounted on the same carriage. Considerable care was taken in each run to secure equilibrium conditions between the slope and the velocity of flow. In addition, check runs were made with velocities both above and below the equilibrium value to determine the effect of departures from equilibrium. It was found that the equilibrium requirements were not critical; conditions always remained practically constant through the experimental stretch, because, at the slopes used, a long length of channel is necessary to produce appreciable changes in velocity

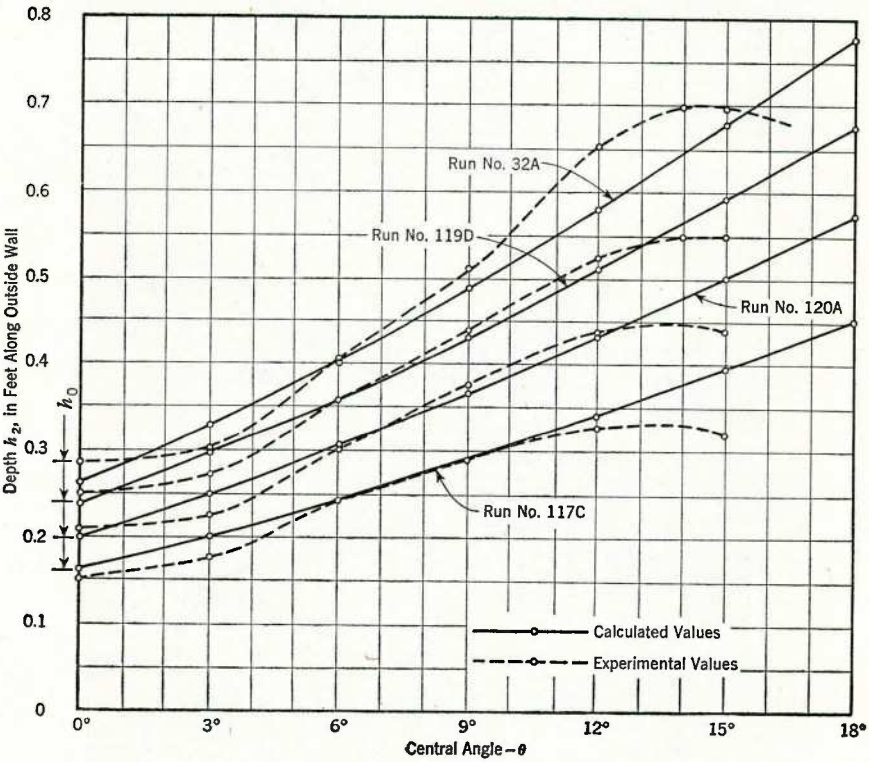

FIG. 19.—COMPARISON OF EXPERIMENTAL AND CALCULATED VALUES OF OUTER WALL SURFACE PROFILES IN A CURVE OF 25-FT RADIUS

or depth. A total of 156 experimental runs was made in the two channels and in the auxiliary adjustable slope section. Each run had from one to seven divisions. A wide range of slopes and Froude numbers were covered. The data presented in this paper are only representative samples.

Nearly all the experiments were performed in the rectangular channel. This was partly due to the limited time available. An additional restriction to the work on the trapezoidal channel resulted from the growing realization of the inherent characteristics of high-velocity flow in curves and the resulting basic limitations imposed upon the use of all cross sections in which the width

varied with the depth of flow. A sufficient number of experiments was run in the trapezoidal channel to demonstrate clearly the reality of these limitations.

Constant Radius Curves; Rectangular Channel.—Fig. 19 shows a comparison, for four different rates of flow, of the observed values versus the calculated values for the water-surface profile along the outer wall from the beginning of curvature to the first maximum. These measurements were made in a curve having a mean radius of 25 ft. Fig. 20 shows a parallel set of runs for a 50-ft curve. Table 2 shows a similar comparison for the height and location of all

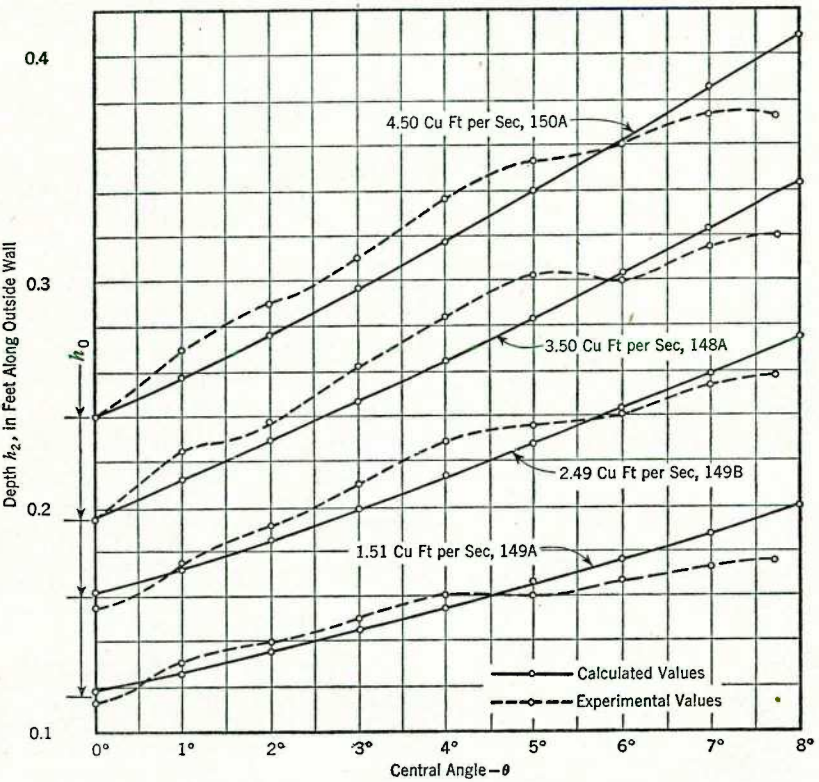

FIG. 20.—COMPARISON OF EXPERIMENTAL AND CALCULATED VALUES OF OUTER WALL SURFACE PROFILES IN A CURVE OF 50-FT RADIUS

the maxima in the curve and for two sets of maxima in the downstream tangent. These are the same runs shown in Fig. 19. Within the curve the distance between maxima varies from 0.914 to 1.066 of the calculated value, whereas in the downstream tangent, the corresponding ranges are 0.868 to 1.262. Variations of approximately the same magnitude are to be found in the depths. These variations are probably the result of: (*a*) Frictional damping of the disturbance pattern; (*b*) deviation from uniform velocity in the flow; and (*c*) variations in wave velocities caused by variations in the wave heights. Occa-

sionally it may be desirable to introduce these secondary effects into the analytical treatment. However, in most designs there are other elements of uncertainty, of equal or greater magnitude, which make increased accuracy unnecessary. For example, the slope of steep channels on natural terrain

TABLE 2.—MAXIMUM SUPERELEVATION IN AND BELOW

Run No.	Flow, Q, in cubic feet per second	Depth, h_o, in feet	Froude number, F	Computed h', in feet	Computed θ_o, by Eq. 37	Computed $L' = \frac{b}{\tan\beta}$	In the Curve, at the Outside Wall[a]: First Maximum $\frac{h}{h'}$	First Maximum $\frac{\theta}{\theta_o}$	Second Maximum $\frac{h}{h'}$	Second Maximum $\frac{\theta}{2\theta_o}$	Distance to end of curve (EC) θ/θ_o
(1)	(2)	(3)	(4)	(5)	(6)	(7)	(8)	(9)	(10)	(11)	(12)
117C	2.49	0.160	3.29	0.387	14° 33′	6.68	0.868	0.928	0.895	1.014	0.137
120A	3.51	0.199	3.28	0.496	14° 47′	6.79	0.905	0.914	0.935	1.066	0
119D	4.52	0.236	3.25	0.584	14° 46′	6.78	0.942	1.015	0.951	1.016	0
32A	5.51	0.260	3.45	0.693	15° 30′	7.13	1.010	0.967	1.002[c]	1.000	−0.06[c]

[a] Ratios of measured values to computed values. [b] In Cols. 14, 16, 18, and 20, L is the measured

usually varies quite rapidly. Thus the velocity at any given cross section is seldom in equilibrium with the slope, which increases the difficulty in estimating the velocity. Furthermore, the effective roughness usually involves as much uncertainty as that just shown in the location of the maxima.

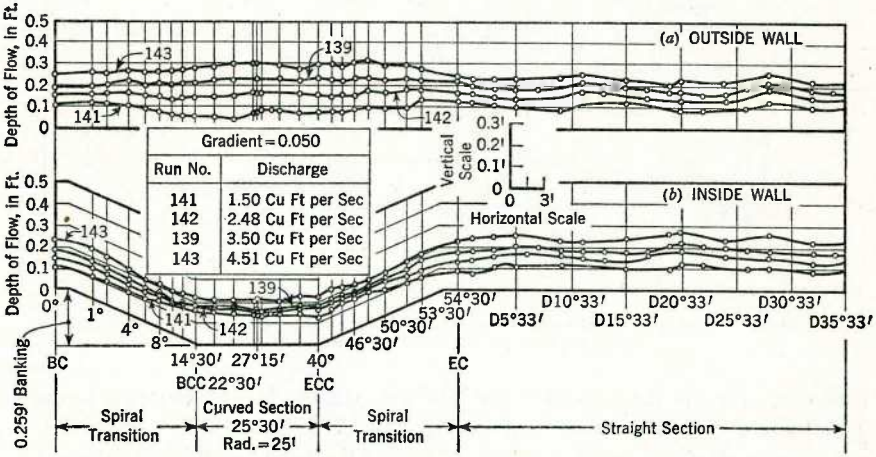

FIG. 21.—SURFACE PROFILES FOR CURVE WITH BANKED BOTTOM TREATMENT

Banked Curves; Rectangular Channel.—Fig. 21 shows a run made with a banked channel having spiral transitions calculated to match the bottom transition. The banking was accomplished entirely by depressing the inner wall, keeping the outer wall at a constant slope throughout the curve. In accordance

with the analysis, there is practically no change in the depth on the outer wall in and below the curve. (In the several illustrations, the points of curvature and compound curvature, beginning and end, are designated BC, EC, BCC, and ECC, respectively.) Figs. 22 and 23 show the surface contours and the velocity

THE CURVE; TESTS WITHOUT SILLS; RECTANGULAR CHANNEL

Below the Curve[a,b]								Distance, in Feet, Between Successive Maxima on the Same Side			Run No.
First Maximum				Second Maximum							
Inside Wall		Outside Wall		Inside Wall		Outside Wall					
$\frac{h}{h'}$	$\frac{L}{L'}$	$\frac{h}{h'}$	$\frac{L}{L'}$	$\frac{h}{h'}$	$\frac{L}{L'}$	$\frac{h}{h'}$	$\frac{L}{L'}$	L_{do-1}	L_{di-1}	L_{do-2}	
(13)	(14)	(15)	(16)	(17)	(18)	(19)	(20)	(21)	(22)	(23)	(1)
0.631	0.868	0.762	0.973	0.628	1.197	....	....	1.841	2.170	....	117C
0.688	0.884	0.867	0.884	0.700	1.178	0.617	1.178	1.768	2.062	2.356	120A
0.693	0.958	0.856	0.885	0.757	1.180	0.647	1.180	1.843	2.065	2.360	119D
0.620	0.910	0.815	0.883	0.700	1.262	0.721	1.080	1.793	2.145	2.342	32A

lengths between successive maxima on opposite sides. [c] One half foot below the end of the curve.

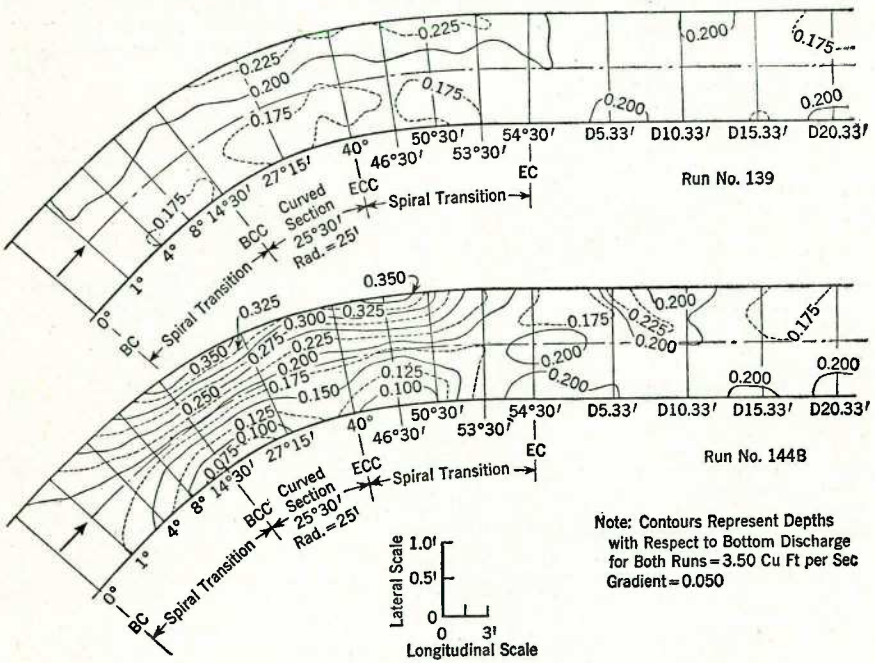

FIG. 22.—SURFACE CONTOURS FOR SPIRALED CURVE WITH BANKED BOTTOM TREATMENT

distribution observed in the curve for the same conditions. Fig. 24 shows two additional water-surface profiles for the same curve. These are for the same dis-

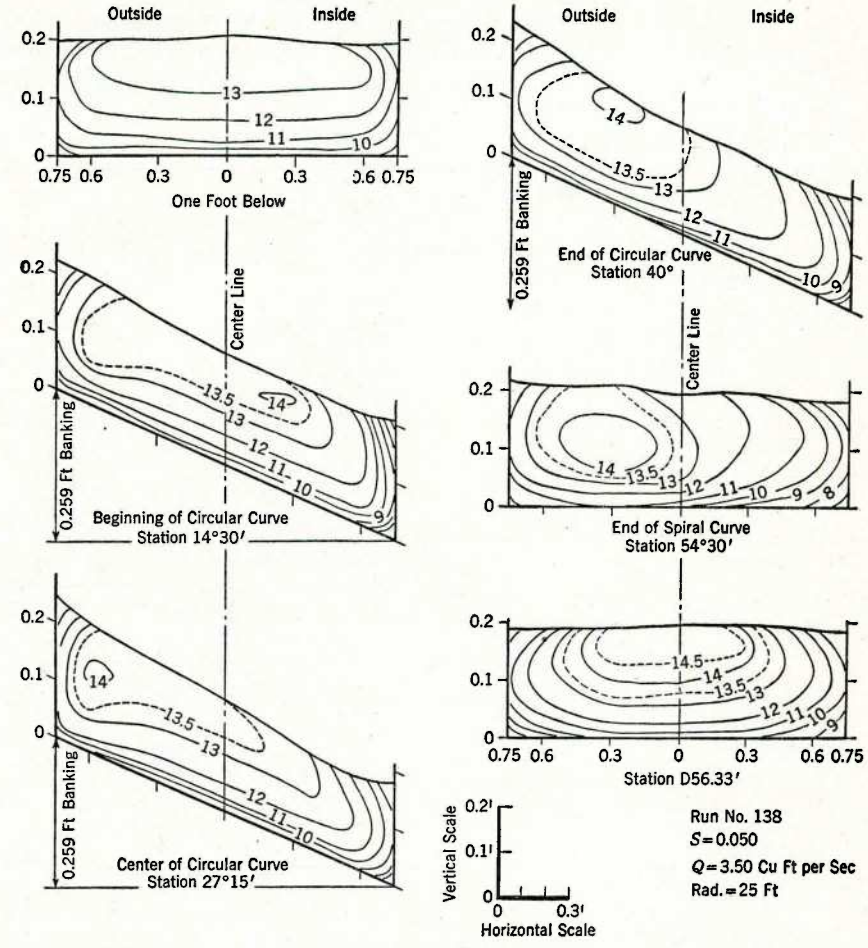

FIG. 23.—TYPICAL SECTIONS SHOWING VELOCITY DISTRIBUTION FOR A CURVE WITH BANKED BOTTOM TREATMENT

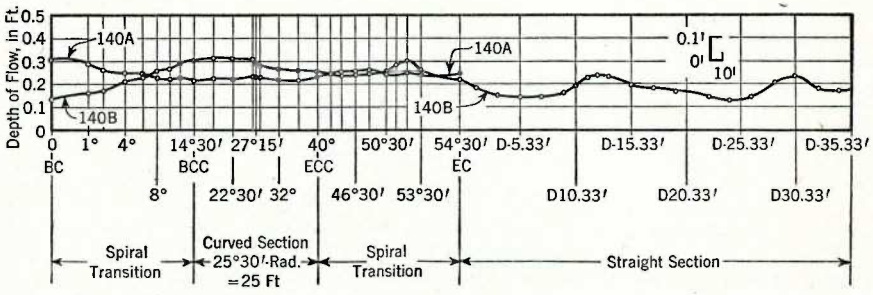

FIG. 24.—OUTER WALL PROFILES FOR BANKED CURVE; HIGH AND LOW APPROACH VELOCITIES

charge as that represented in Fig. 21. However, the velocity of approach for run 140A is lower than the equilibrium value for which the angle of banking was computed. The velocity of approach for run 140B was higher than the equilibrium value. The behavior is exactly as would be expected. In the curve the

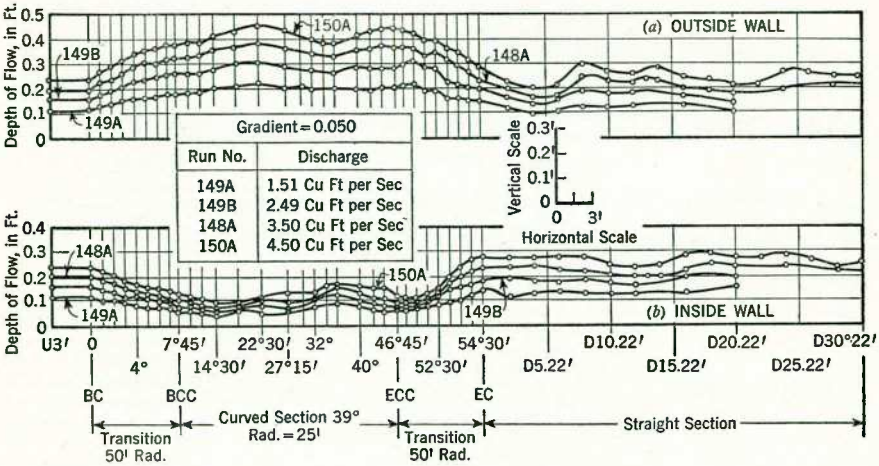

FIG. 25.—SURFACE PROFILES FOR COMPOUND CURVE TREATMENT

superelevation along the outer wall drops for the low approach velocity because the centrifugal force is not sufficient to overcome the cross slope. Therefore there is a flow toward the inside wall of the channel. The opposite condition

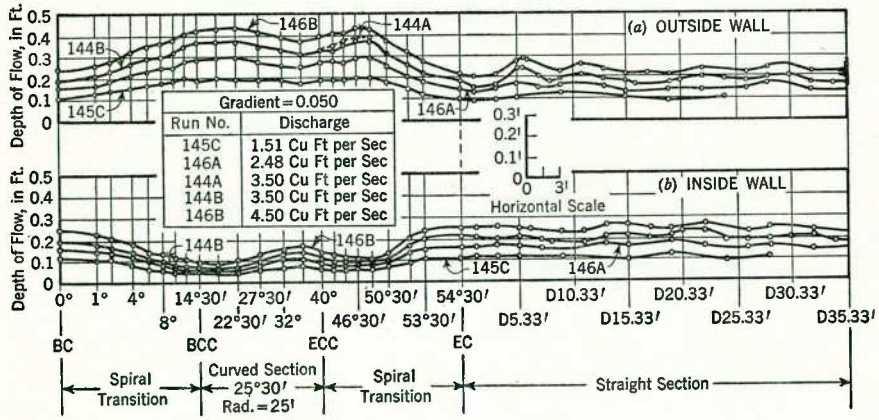

FIG. 26.—SURFACE PROFILES FOR SPIRAL TRANSITION TREATMENT

is true for the high velocity of approach. Both these runs show small but appreciable disturbance patterns in the downstream channel.

Compound Curves with Circular Transition Sections; Rectangular Channel.—Fig. 25 shows the surface profile along the outer wall for compound curves

designed to have circular transition sections of double the radius of the main curve and with lengths equal to one half of the wave length of the disturbance pattern. The superelevation increases in the transition section, remains nearly constant throughout the main curve, and falls to the initial value in the down-

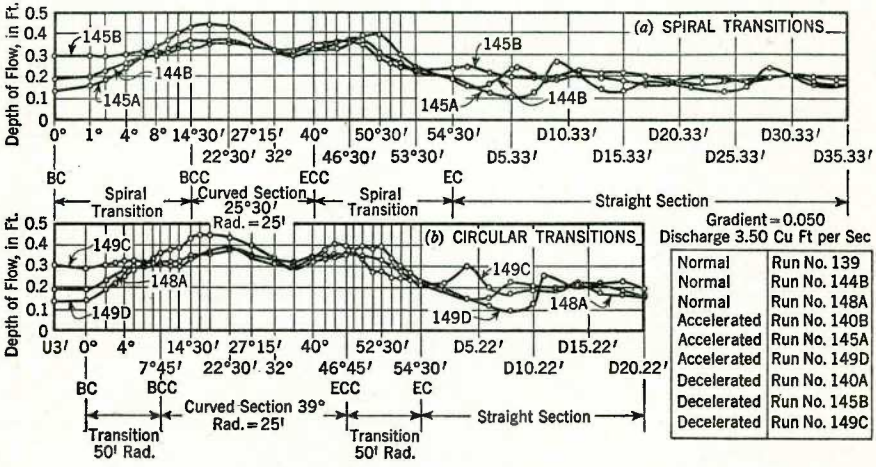

FIG. 27.—OUTER WALL PROFILES FOR SPIRAL AND CIRCULAR TRANSITIONS; HIGH, NORMAL, AND LOW APPROACH VELOCITIES

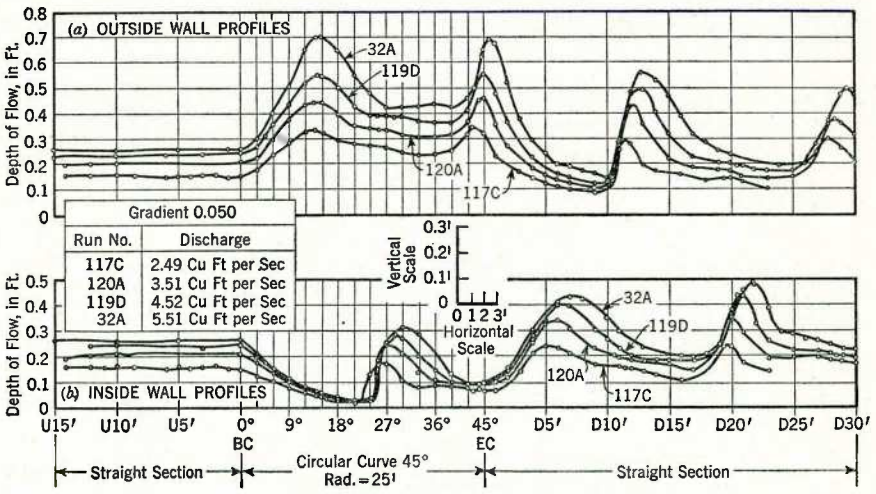

FIG. 28.—SURFACE PROFILES FOR SIMPLE CIRCULAR CURVE WITHOUT TREATMENT

stream transition section. A small disturbance pattern is visible which shows that complete interference was not obtained. The measurements indicate that, if the velocity of approach had been slightly lower, the curve would have behaved exactly in accordance with the predictions. Profiles for different flows are shown in Fig. 25. Although the curve was designed for the dis-

charge of run 148A, the performance was equally satisfactory for the other three flows.

Spiral Transitions; Rectangular Channel.—Fig. 26 shows the surface profiles for similar flows in a curve of 25-ft radius having spiral instead of circular transitions. Its behavior is nearly identical with that of the curve having circular transitions. Both curves were designed for a total turn of 54° 30″. The center-line length of the curve with circular transitions was 30.53 ft, whereas with spiral transitions it was 36.43 ft. Thus, the latter curve is approximately 16% longer, although no better. Fig. 27 shows similar profiles for both types of compound curves for velocities of approach differing from the equilibrium values. Again the performances of the two curves are similar. A comparison of these results with Fig. 24 shows that the sensitivity to deviations from the design velocity is about as low as that of the banked bottom design.

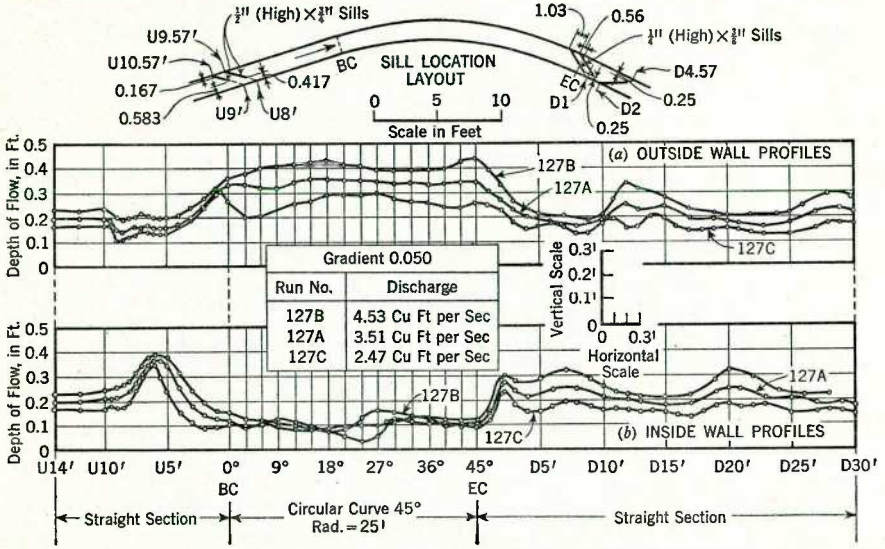

FIG. 29.—SURFACE PROFILES FOR SILL TREATMENT

Submerged Sills; Rectangular Channel.—The effect of submerged sills can be seen by a comparison of Figs. 28 and 29 which show the wall profiles for the same flow conditions in the same curve with and without sills above and below the curved section. Fig. 30 shows the surface contours for one of the three discharges shown in Fig. 29. It will be seen from Figs. 28 and 29 that the sill treatment produces very acceptable flow conditions.

Experimental Comparison of Effectiveness of Various Designs for Rectangular Channels.—Table 3 shows the comparative effectiveness of various corrective designs in similar rectangular channels having the same slope, the same main radius, and the same total angle of turn. The sets of runs are for nearly identical rates of flow. The curves with sills have slightly higher disturbances in and below the curved section than do other methods of treatment. The

TABLE 3.—Relative Effectivness of Corrective Designs for Rectangular Channels[a]

Run No.	Flow, Q, in cubic feet per second	Relative Measurements; Percentages of the Design Value of Q or of the Design Value of h_o (0.198 Ft)						Distance from End of Curve (EC) to Downstream Maximum[b]	
		Flow, Q	Depth, h_o	Maximum Disturbance					
				Curve Section		Downstream Section			
				Outer wall	Inner wall	Outer wall	Inner wall	Along outer wall	Along inner wall
(1)	(2)	(3)	(4)	(5)	(6)	(7)	(8)	(9)	(10)
				(*a*) Normal Curve					
117*B*	2.49	71.2	80.8	175.6	85.8	149.0	123.2	1.69	2.87
120A	3.51	100.3	100.5	225.0	121.7	217.0	178.7	1.77	2.94
119D	4.52	129.2	119.2	277.6	142.3	250.0	223.0	1.91	3.02
				(*b*) Single Sills Above the Curve Only[c]					
117B	2.49	71.2	80.3	165.0	68.7	166.1	124.7	1.77	2.87
119C	3.51	100.3	100.0	197.8	69.7	208.6	157.0	1.77	0.88
117A	4.52	129.2	119.6	245.9	92.9	243.0	202.6	1.77	3.02
				(*c*) Multiple Sills Above and Below the Curve					
127C	2.47	70.6	84.8	150.4	65.1	102.0	119.1	2.06	0.32
127A	3.51	100.3	100.5	180.1	66.7	125.7	138.3	1.77	0.32
127B	4.53	129.6	118.2	223.0	81.3	169.1	163.0	1.77	1.03
				(*d*) Circular Transition; r = 50 Ft					
149A	1.51	43.2	57.1	106.6	35.3	58.1	61.2	1.80	2.98
149B	2.49	71.2	80.3	149.4	52.0	87.4	79.8	1.21	2.39
148A	3.50	100.0	98.5	190.8	102.0	116.1	108.6	1.21	2.68
150A	4.50	128.7	120.2	226.6	126.7	143.3	130.8	1.21	2.68
				(*e*) Spiral Transition					
145C	1.51	43.2	60.1	103.0	54.0	60.6	61.6	1.37	2.85
146A	2.48	70.8	80.8	151.0	80.8	86.8	90.8	0.78	2.85
144B	3.50	100.0	97.5	187.2	103.5	122.7	111.6	0.79	2.26
146B	4.50	128.7	122.2	220.0	124.7	146.4	128.8	0.86	2.26
				(*f*) Spiral Transition with Banking					
141	1.50	42.8	58.1	69.2	83.3[d]	61.6	61.6	3.00	3.00
142	2.48	70.8	80.8	92.9	95.0	89.4	92.9	1.67	3.00
139	3.50	100.0	97.5	120.3	95.5	109.6	110.6	1.96	3.00
143	4.51	129.0	122.7	160.5	116.1	129.8	136.9	1.67	3.00

[a] The main radius of all curves used in this series was 25 ft. [b] Location of a point of downstream maximum expressed as half wave lengths from the end of curve for a flow of 3.5 cu ft per sec (6.794 ft). [c] The three runs in Table 3(*b*) are for qualitative comparison only, because sill conditions are not identical. [d] The reference bottom for the banked channel is depressed along the inner wall.

compound curves and the spiral transitions with and without banking all show quite comparable performance as regards disturbance in the downstream channel. Within the curve itself the least disturbance is shown by the banked curve, as would be expected

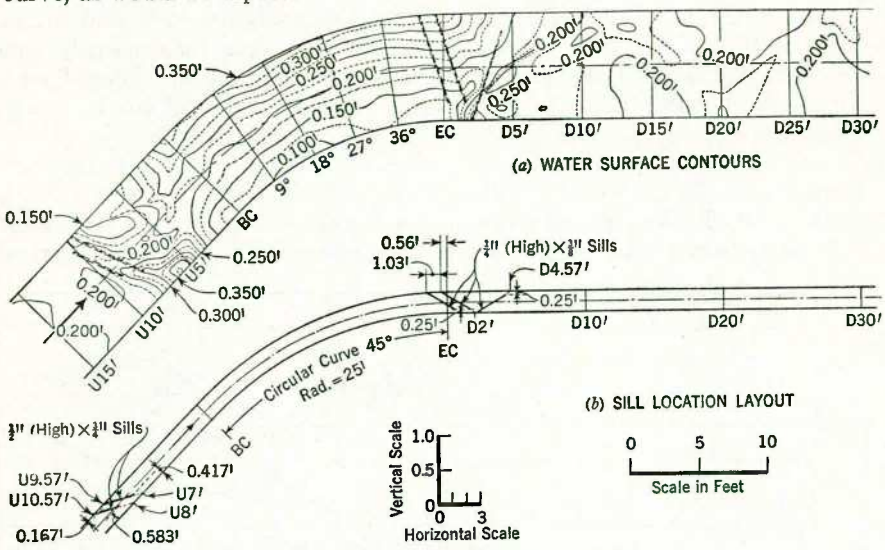

FIG. 30.—SURFACE CONTOURS FOR SILL TREATMENT

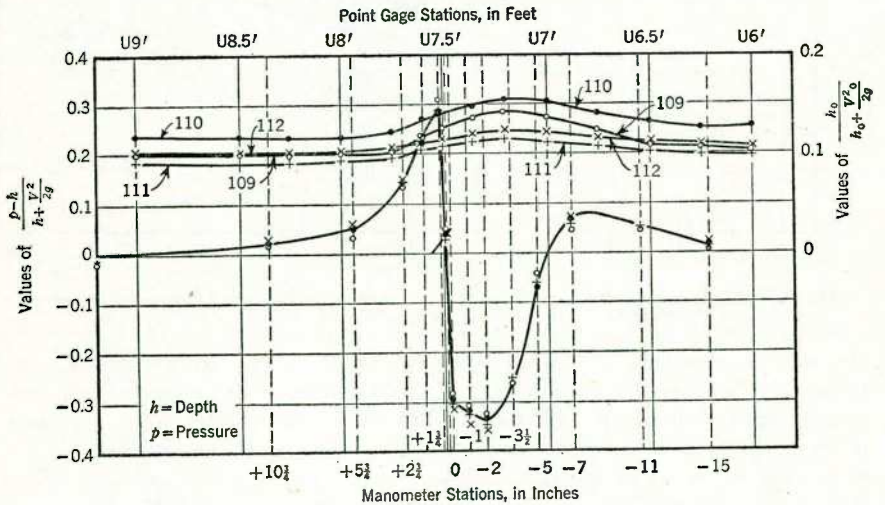

FIG. 31.—BOTTOM PRESSURE DISTRIBUTION ABOVE AND BELOW SILL

In using sills one factor must be remembered. A low pressure region forms on the downstream side of each sill which is very effective in producing the desired deflection of the flow. In channels having extremely high velocities, especially if accompanied by low depths, it is possible for the pressure in

this region to drop enough to form an air passage to the surface, with the result that the flow springs clear of the bottom. This action reduces greatly the effectiveness of the sill and causes unsatisfactory operation. Fig. 31 shows the pressure along the bottom above and below the sill installation. This sill was normal to the channel; hence, the pressure differences are somewhat higher than for the inclined sill. The measurements show that, for extremely high velocities and large depths, cavitation may occur below the sill. For all such conditions the other methods of treatment, such as compound curves, are to be recommended.

There are a few additional points to be borne in mind in making the comparison between analytical results and experimental measurements. First, uniform velocity was assumed throughout the cross section. The deviations from uniformity found in real channels will affect the surface configuration.

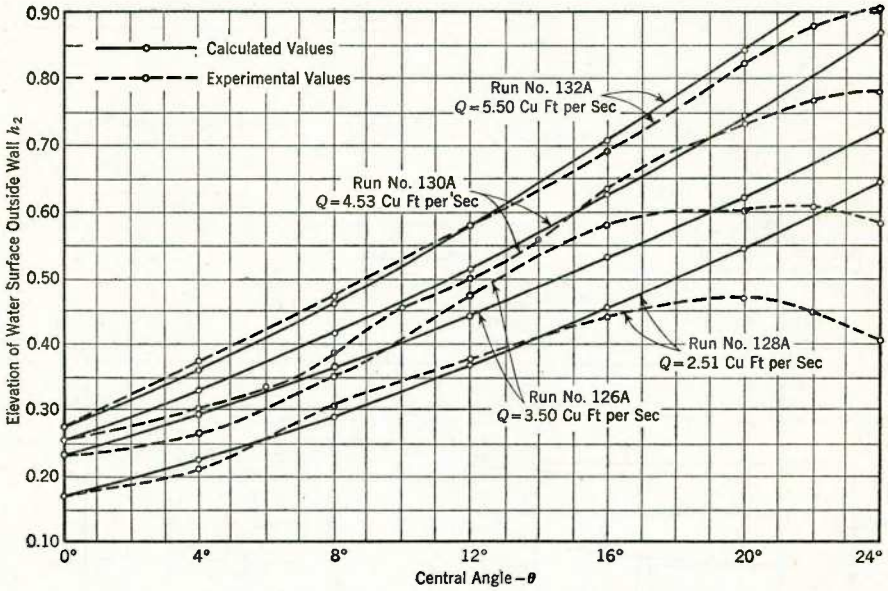

FIG. 32.—COMPARISON OF EXPERIMENTAL AND CALCULATED VALUES OF OUTER WALL SURFACE PROFILES IN A TRAPEZOIDAL CHANNEL CURVE OF 25-FT RADIUS

For normal conditions the departures from uniform velocity are not enough to cause significant discrepancies. However, serious departures from uniformity may occur below the junction of two channels or below the entrance of an auxiliary into the main channel. Another departure from the assumptions may be found in the cross section itself. The analysis assumes a true rectangular channel. In the field many rectangular channels have an appreciable invert in the bottom. The effect of this invert may be quite noticeable for low rates of flow but usually disappears for design flows.

Trapezoidal Channels.—In discussing the methods of treatment, the characteristics of nonrectangular channels were referred to briefly, but no modifica-

tions of the analysis were proposed to permit their use. The trapezoidal channel is one of the most common forms of nonrectangular cross section. The approximate method of analyzing its behavior is rather obvious and can be outlined as follows: Since the depth is not constant, the wave velocity must vary throughout the cross section. However, approximate velocities can be computed by using the average depth. The effective channel width is influenced by the amount of superelevation. Again, a fair approximation of the wave pattern can be obtained by using the width of the water surface in the upstream channel. The rise along the outer wall can likewise be computed on the basis of the average channel depth, if the datum is determined by the average depth measured down from the water surface. Fig. 32 is a comparison between the calculated and measured elevations in a trapezoidal channel which had the same hydraulic characteristics as the rectangular channels just discussed. The slope, hydraulic radius, and mean radius of curvature were all identical. The central angle of the trapezoidal curve was 30° instead of 45° because of the space limitations of the laboratory. Fig. 33 shows the cross section within the curve for a discharge of about 80% of the design. This section illustrates one of the dangers of trapezoidal channels for high-velocity flow. As a first approximation, the water surface may be considered as an inclined plane. If the slope of the outer wall had been flatter, it is apparent that the superelevation would have been much greater. Presumably, if the water surface and the outer wall had been parallel, the superelevation would have been limited by only the velocity head available in the channel, assuming sufficient curve length to develop equilibrium.

A comparison of the disturbances in rectangular and trapezoidal channels indicates that the superelevations are always greater in the trapezoidal channel.

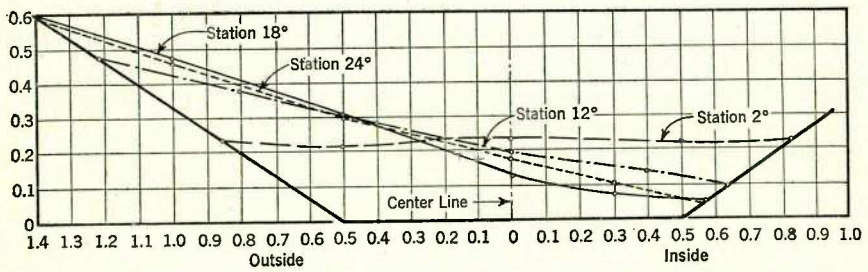

FIG. 33.—COMPOSITE CROSS SECTION SHOWING VARIATION WITH POSITION ALONG THE CURVE

This effect follows directly from the increased surface width. It was observed during the experiments that there seems to be a larger amount of energy stored in the "swing" of the trapezoidal disturbance pattern so that it appears to damp out less rapidly than in the rectangular section. Figs. 34(*a*) and 34(*b*) are views of the disturbance in and below the curve for two rates of flow. It will be noted that the maximum superelevation on the outer wall of the curve moves downstream toward the end of curvature as the rate of flow increases.

This downstream travel is accompanied by a disproportionate increase in the magnitude of the disturbance pattern in the downstream tangent. This result is to be expected from a consideration of the physical configuration involved since it was shown that the disturbance in the downstream tangent becomes greatest when the last maximum in the curve occurs on the outer wall at the

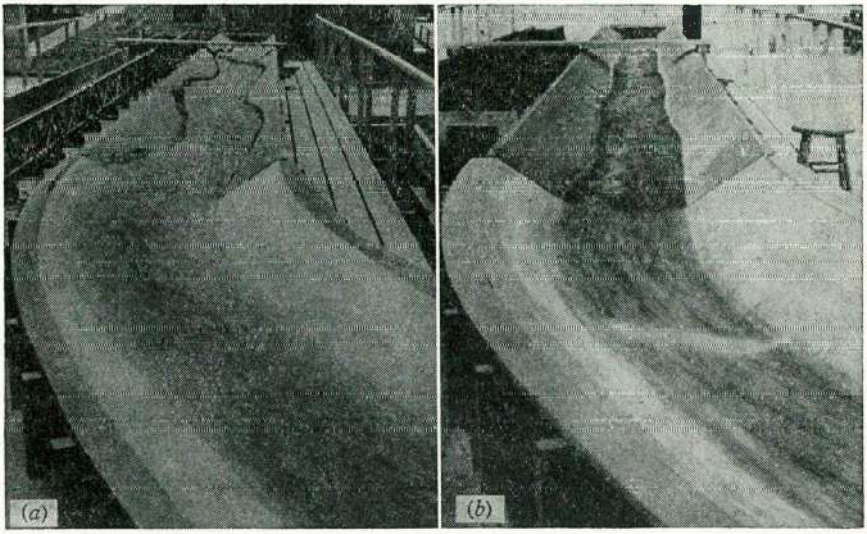

FIG. 34.—DISTURBANCE PATTERN IN AND BELOW THE CURVE IN A TRAPEZOIDAL CHANNEL: (*a*) HIGH FLOW AND (*b*) LOW FLOW

end of curvature. The violent behavior of the flow in this particular example is due to the specific length of the curve and is not typical for all trapezoidal curves. For example, if the curve had been either appreciably shorter or longer with all other factors remaining the same, the disturbance pattern in the downstream tangent would have decreased as the flow increased instead of increasing as shown in Figs. 33 and 34.

LIMITS OF APPLICATION

The analysis and treatments proposed in this paper apply only to channels with supercritical velocities. Furthermore, for channels operating with Froude numbers between 1 and 1.5, the results may be rather erratic because of the fundamental instability of the flow in this region. Minor disturbances cause disproportionate effects and may easily produce a jump which suddenly reduces the velocity to below that of the wave velocity. As the Froude number becomes greater than 1.5, the stability increases rapidly and, with it, the reliability of the calculations. One rather unexpected result of this situation is that these methods of calculation and treatment may be used with great confidence for very high velocities which would otherwise be most difficult to handle. The major limitations on the high-velocity end are air entrainment and cavita-

tion. These limitations apply much less to compound curves and curves with banked bottoms than they do to simple curves and to the use of sills.

The scope of this paper has been limited to the conditions of flow in which the average velocity is constant—that is, when the friction loss is in equilibrium with the slope. The treatments are valid for the small accelerations or decelerations due to the constantly changing slopes usually encountered in the field. However, the high accelerations in spillways and similar structures are not covered. The physical principles underlying this treatment of open-channel flow for supercritical velocities are obviously applicable to nonequilibrium conditions as well. Examples of such treatments are found in other parts of this Symposium. There are undoubtedly many other cases not yet examined which can be solved by considering the unique characteristics of supercritical flow.

DESIGN OF CHANNEL CONTRACTIONS

By Arthur T. Ippen,[1] M. ASCE, and John H. Dawson,[20] Jun. ASCE

Synopsis

Channel contractions for subcritical flow are designed for minimum energy losses by proper streamlining of the boundaries. Efficient and economic solutions are achieved with relatively little difficulty. If supercritical flow exists, the accent of design is shifted to the reduction or eventual elimination of the standing wave patterns which appear as a result of such flow, in accordance with the principles discussed in the first Symposium paper. So far these designs have envolved from experimental cut-and-try processes with models. This third Symposium paper endeavors to show, on the basis of experimental evidence, that the basic principles of supercritical flow can be applied in a satisfactory manner to the design of typical channel contractions and that solutions may be found with a minimum amount of surface disturbance patterns. Furthermore, the magnitude of the standing waves may be predicted adequately, as well as their location within the channel contraction. The method of eliminating waves in the downstream channel is discussed for a basic form of channel contraction.

General Problems of Design

The design of channel transitions has received the attention of hydraulic engineers in the past and has been formulated into a number of suggestions and procedures. The theoretical basis of these procedures is supplied by the principles of nonuniform flow applied, successively, to short channel sections. Variations of velocity and depth induced by the conveying boundaries are assumed to occur only along the channel axis. Basic surface curves identical for all longitudinal sections are derived in first approximation by assuming that the total head remains constant, and refined surface curves are obtained by considering the friction losses in the direction of flow. The velocities and depths at any station are assumed to be unaffected by curvature of the lateral boundaries and, hence, constant in transverse sections. The primary aim of economical design is a minimum of energy loss.

The design of channel transitions for supercritical velocities, on the other hand, must be attacked quite differently because of the occurrence of standing waves. The basic principles of the theory have been discussed in the first Symposium paper. The primary conclusions with respect to the problem in question are that, in economically feasible structures, standing waves cannot be avoided, and that their characteristics must therefore be explored carefully to insure successful design. Velocities in supercritical flow will vary in magnitude

[20] Associate Prof., Civ. Eng. Dept., Oklahoma Inst. of Technology, Oklahoma Agri. and Mech. College, Stillwater, Okla.

and direction in a systematic fashion in transverse sections, and surface elevations will not be constant. The effect of a transition is not confined to the immediate vicinity of the structure as in subcritical flow, but may affect the flow conditions downstream from the transition for very long distances. Design for a minimum of standing waves, therefore, is the particular goal for flow at supercritical velocities so that economical structures may result. The various phases of the flow through contractions were attacked by a number of investigators[21,22,23,24,25] at Lehigh University and at the Massachusetts Institute of Technology (M.I.T.) during the years from 1938 to 1947. Although considerable experimental work remains to be done, it is felt that a summary of the essential findings is desirable and may prove useful in similar work directly concerned with structures of this type.

Contractions Composed of Circular Arcs

The first systematic attack on the problem was made in the Hydraulic Laboratory of Lehigh University with a channel contraction composed of two equal circular arcs along each wall as shown in the diagram of Fig. 35. This

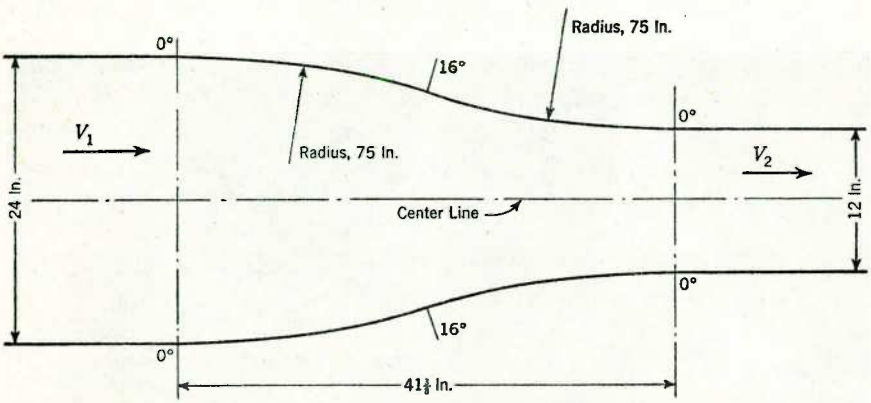

Fig. 35.—Contraction Composed of Circular Arcs

case was chosen as one that might be typical of a contraction designed from conventional knowledge of open-channel flow. The photographs of Fig. 36, taken in the downstream direction, show clearly the problem to be faced with supercritical flow in such contractions. The surface of the stream is traversed

[21] "The Effects of Lateral Contractions on Supercritical Flow in Open Channels," by J. H. Dawson, thesis presented to Lehigh Univ. at Bethlehem, Pa., in 1943, in partial fulfilment of the requirements for the degree of Master of Science.

[22] "Design of a Sharp Angle Contraction in Supercritical Flow," by D. P. Rodriguez, thesis presented to Lehigh Univ. at Bethlehem, Pa., in 1943, in partial fulfilment of the requirements for the degree of Master of Science.

[23] "Experimental Relation Between Sudden Wall Angle Changes and Standing Waves in Supercritical Flow," by D. Coles and T. Shintaku, thesis presented to Lehigh Univ. at Bethlehem, Pa., in 1943, in partial fulfilment of the requirements for the degree of Bachelor of Science.

[24] "Theoretical Investigation of Standing Waves in Hydraulic Structures," by A. A. Stone, thesis presented to the Massachusetts Inst. of Technology at Cambridge, Mass., in 1946, in partial fulfilment of the requirements for the degree of Master of Science.

[25] "Standing Waves in Supercritical Flow of Water," by M. P. Barschdorf and H. G. Woodbury, thesis presented to the Massachusetts Inst. of Technology at Cambridge, Mass., in 1947, in partial fulfilment of the requirements for the degree of Master of Science.

by large standing waves which, in height, exceed considerably the initial depth of flow. The converging arcs in the upstream part and the reversed arcs in the downstream part of the contraction were chosen to be equal and with a 16° central angle each. The contraction was from a 2-ft width to a 1-ft width for the downstream channel. These two conditions, therefore, determined the radius of curvature of 75 in. and the length of the contraction. The channel contraction was set into a steel flume, which was 2 ft wide at its upper end and 1 ft wide in the longer reach of 30 ft below the contraction. For any flow the flume was adjusted in slope to give uniform flow conditions for the initial Froude number. Proper velocities and depths could be established for any Froude number between $\mathbf{F} = 2$ and $\mathbf{F} = 12$ by discharging the water into the flume through a rectangular nozzle, whose opening could be adjusted to give a certain desired depth. All water quantities were determined by a calibrated venturi meter in the supply line from a constant-head tank. The entire surface within the contraction, and for a sufficient distance downstream from the contraction, was mapped for the runs presented in Fig. 37. Normally, however, only the side-wall elevation and the center-line elevation were determined for all stations along the contraction and downstream tangent.

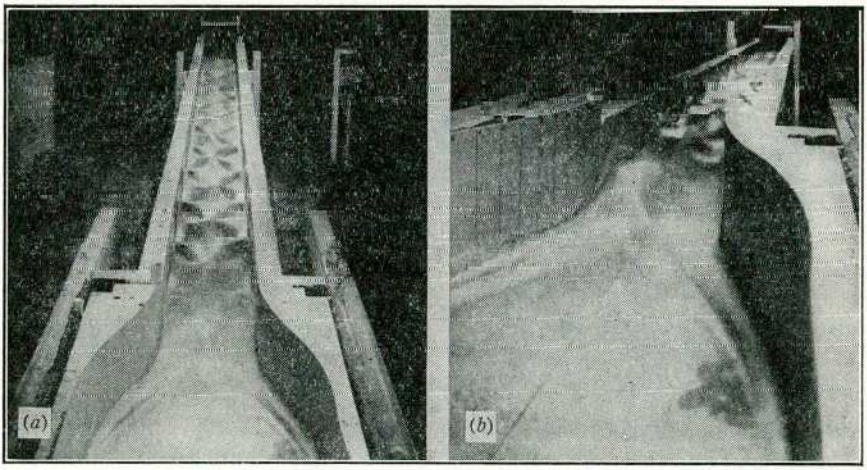

FIG. 36.—STANDING WAVE PATTERNS CAUSED BY VERTICAL-ARC CONTRACTIONS

Surface Contours in Circular-Arc Contractions.—The differences in the surface elevations between subcritical flow and supercritical flow are strikingly apparent from the configurations of the constant-depth lines in Fig. 37. Fig. 37(*a*) shows distinctly that the usual assumption of essentially constant depths in transverse flow sections is basically fulfilled for this run at a Froude number of $\mathbf{F}_1 = 0.358$. Fig. 37(*b*), for a Froude number of $\mathbf{F}_1 = 4$, shows clearly the essentially different surface contours for cases of supercritical flow. The characteristic feature of flow remaining undisturbed within the center of the contraction is especially apparent. This can easily be explained on the basis of

disturbance lines discussed in the first Symposium paper. The increases in depth caused by converging side walls can only be communicated along disturbance lines at a wave angle β_1 to the oncoming flow. Positive lines tending to converge originate along the first or concave part of the wall, and diverging or negative lines emanate from the convex part of the contraction. In Fig. 38 a theoretical solution showing the disturbance lines on the basis of the method of characteristics is given for comparison with the actually measured surface lines. The converging lines result in steep wave fronts which clearly have their counterpart in Fig. 37(*b*). The diverging or negative lines extend from Station 16° on downstream, resulting in a depth along the wall at the end of the contraction which reverts to the normal depth.

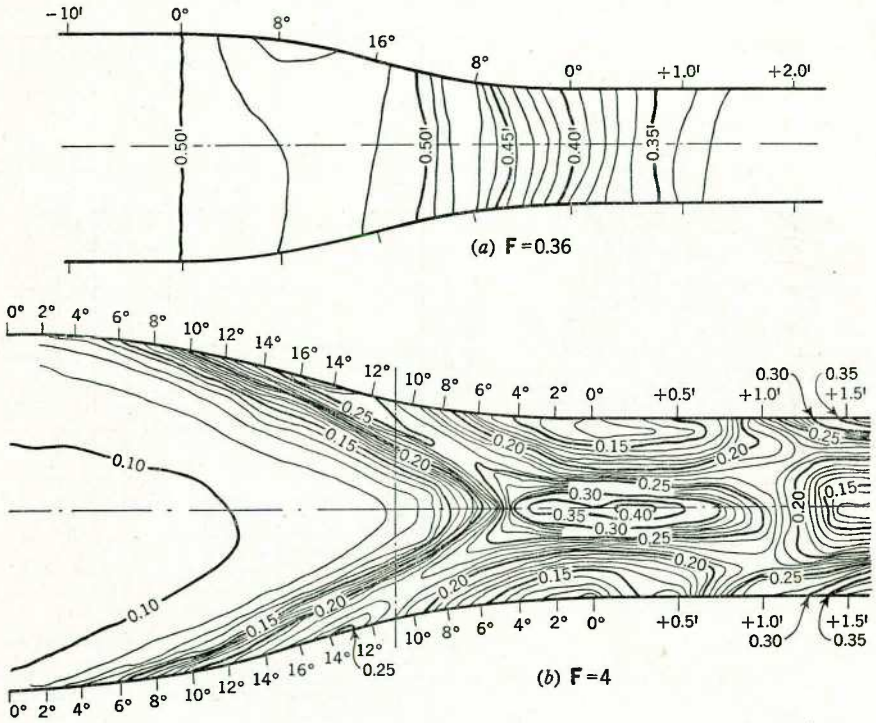

FIG. 37.—CONTOURS OF WATER SURFACE IN A CONTRACTION COMPOSED OF CIRCULAR ARCS

Wall Profiles.—The characteristic variations in depth along the side walls are revealed distinctly by the profiles in Fig. 39 for a range of Froude numbers and for the same contraction. The theoretical profiles are plotted for direct comparison with the measured surface lines. According to the principles discussed in connection with Fig. 3 in the first Symposium paper, all theoretical lines must show a sharp break at the beginning of the curved wall, since the curvature at that section increases from zero to $1/r$ and since the velocity at

the wall is assumed equal to the normal velocity V_1. At Station 16° there must be a peak, because at this point the curvature is reversed suddenly in the example investigated. This point would correspond to the peak obtained along the outside of a channel curve where the first negative disturbance is

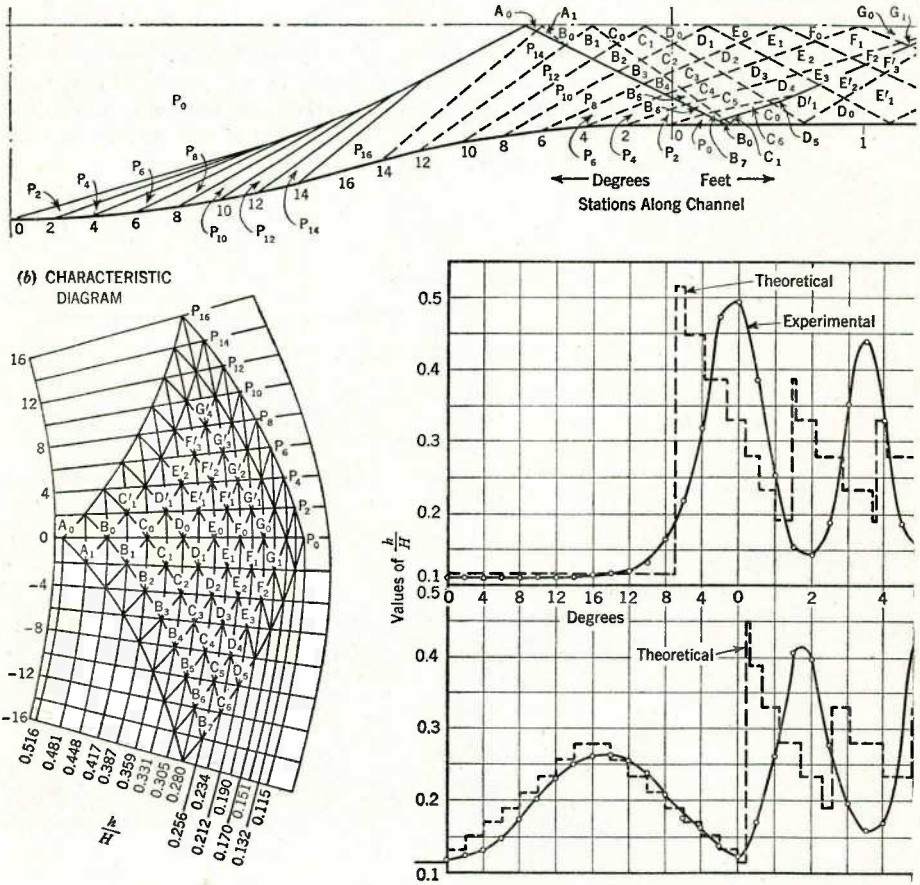

FIG. 38.—THEORETICAL ANALYSIS OF FLOW THROUGH A CONTRACTION COMPOSED OF CIRCULAR (*c*) COMPARISON OF CENTER-LINE SURFACE PROFILES;

reflected. The only difference is that, in the latter case, the negative impulse is created locally instead of being produced at the opposite wall and being transmitted along a negative disturbance line. Since the total angular turn of the reverse curve must also be 16°, the depth along the wall must revert to the initial depth h_1, and the Froude number **F** of the flow at the end of the contraction should again be the same as at the entrance, at least along the walls. The complication arising from this requirement is not difficult to see: The continuity condition obviously does not permit the same velocity and depth to exist in the narrower section as in the wider entrance. It follows that depth and velocity must vary across the end section in such a way as to satisfy the

continuity condition. A fundamental weakness of this type of contraction is thus exposed.

The lowest initial Froude number that would not result in a hydraulic jump being formed in the contraction was **F** = 3. The discrepancy between theo-

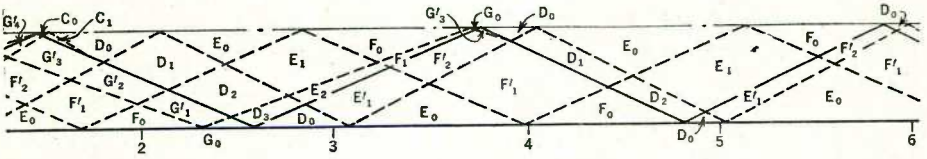

(*a*) PLAN OF CONTRACTION AND DISTURBANCE LINES

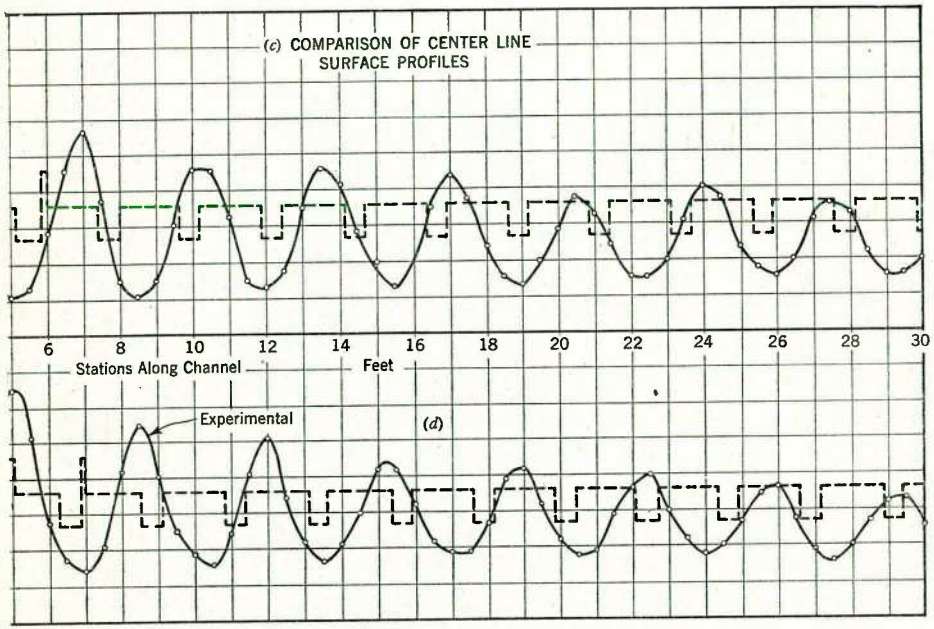

ARCS, **F** = 4: (*a*) PLAN OF CONTRACTION AND DISTURBANCE LINES; (*b*) CHARACTERISTIC DIAGRAM; AND (*d*) COMPARISON OF SIDE-WALL SURFACE PROFILES

retical and measured profiles is explained by the fact that the Froude number of the wave is too near the critical, and therefore small changes in velocity result in large changes in depth. The counterpart of this case is found for a right hydraulic jump when the undulating stage is reached and unstable conditions are approached. In actual practice such conditions are to be avoided. The theory, it is to be remembered, too, neglects vertical accelerations, which assume relative importance in the present case. The agreement between theory and measurement is very close for **F** = 4 to **F** = 8 as far as height of the total disturbance is concerned. Only when **F** = 12 is there a serious discrepancy apparent. This difference is explained by the fact that the maximum

depth along the wall is now seven times the initial depth, a case in which vertical accelerations must become excessive. Such a ratio of h/h_1 would certainly not be permissible in practice and would clearly call for a longer transition with smaller central angles for the arcs composing the side walls.

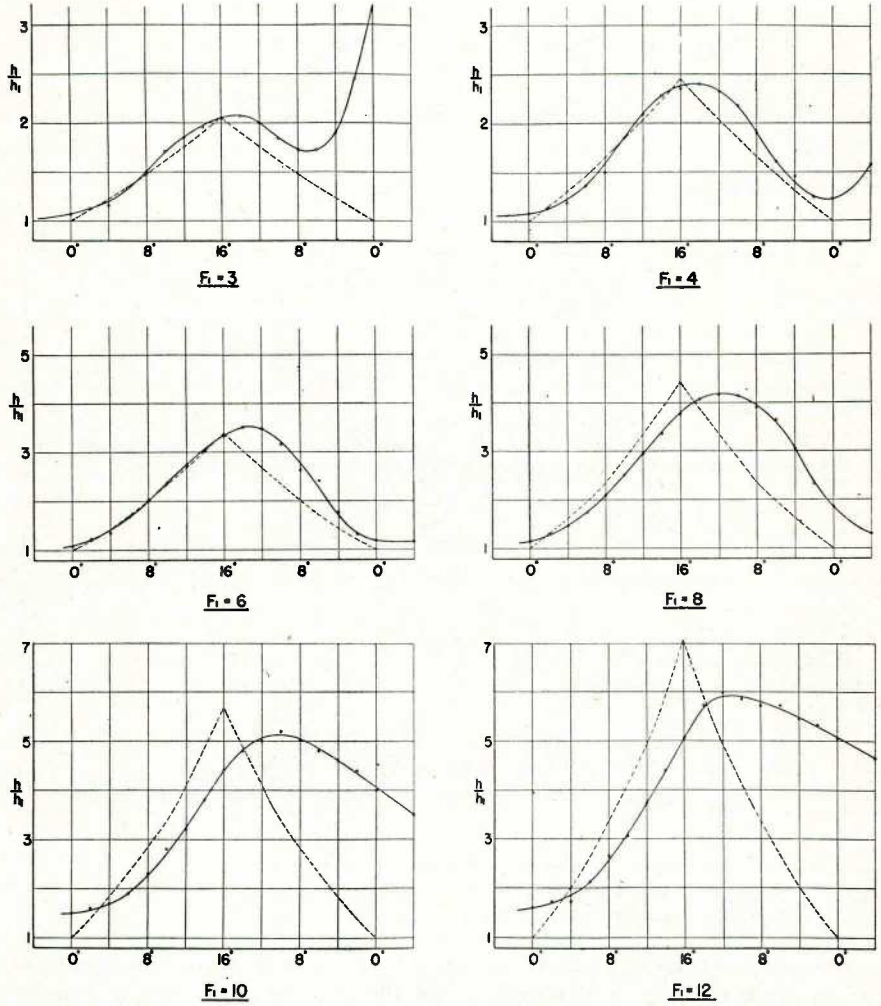

FIG. 39.—MEASURED AND THEORETICAL WALL PROFILES FOR CIRCULAR-WALL CONTRACTION

It is not the magnitude of **F** which causes the difficulty, but the fact that the central angle of the circular-wall sections is excessive for high values of **F**. A longer transition therefore is indicated, which might be designed for a curvature determined by a specified ratio of h/h_1. The permissible central angle can easily be read from the curve in Fig. 3 for such a ratio, once the starting point has been determined from the flow conditions at the entrance.

The theoretical profiles in the example chosen are symmetrical with the maximum point since the curvature of the two arcs composing the converging wall is the same. The maximum will not be changed, regardless of a change in curvature of both arcs or of one of the arcs, as long as the central angles remain the same. The wall profiles therefore may easily be made unsymmetrical if, for example, a larger radius is used for the downstream arc than for the upstream one. Nevertheless, a given depth change is always associated with a given change in direction, or in θ; and at the point of the same total angular change along the wall the same depth must occur for given initial conditions, always assuming, of course, that no disturbance line reaches the wall from the opposite side.

Boundary-Layer Effects.—In comparing the measured profiles in Fig. 39 with the theoretical profiles it is noted, first, that usually the measured profile shows a somewhat delayed and smooth rise as compared to the aforementioned sharp initial break at the entrance. Second, the peak does not consist of a cusp, as shown by the computed profile, but is broad and rounded. Both differences are explained by the effect of the velocity distribution along the wall. The velocity increases from zero to the normal velocity within a certain finite distance from the wall, which implies that the angular change is not transmitted to the main flow immediately. The initial angular change $\Delta\theta$ is accomplished within a zone of lower Froude numbers and, therefore, with smaller elevation changes. The steep rise of the profile is delayed until the zone of higher velocities is affected. This boundary-layer influence is felt also at the peak of the profile, since the negative influence of the reversed curvature is similarly delayed and takes effect only gradually through the boundary layer adjacent to the wall. Although this influence of the boundary layer is quite noticeable in the small-scale experiments, for conditions in large structures a better conformance to the theoretical profiles must be expected since the boundary-layer thickness for large structures is considerably reduced relative to the other dimensions.

Related Types of Contractions.—The question may now be asked as to whether the findings presented for this circular-arc contraction are basic and unavoidable for such channel contractions in supercritical flow. To give a general answer, a few additional forms may be discussed in principle on the basis of the theory and with the aid of Fig. 40. The Froude number $\mathbf{F}_1$ may be assumed to increase from one case to another while the wall alinement is kept the same for each type of contraction. It can be seen that a given type of contraction might, instead, have been varied in length to produce the various wave patterns discussed on the basis of the same Froude number. However, the former basis of comparison is chosen as the more convenient. It may also be stated that, in order to make the comparison systematic, cases which are obviously impractical are still included to illustrate certain points. The probable wave patterns have been sketched into three plan views (cases 1, 2, and 3 of the three types of contraction, A, B, and C). However, only the initial disturbance lines and the basic shock waves are indicated, so that the lines of reflected disturbances may not obscure the fundamental problem.

Types A, B, and C, case 1, have little practical significance. Since the wave angles are normally small, extremely long contractions would be required

for the waves to intersect as far upstream as is shown. Cases A1 and B1 are better than case C1, since the positive waves reach the opposite wall within the convex range of wall curvature, whereas case C1 has some positive waves reflected within the concave range—thus causing still higher elevations along this wall. Case B1 will have the most pronounced shock wave because the converging positive disturbance lines are so crowded together; the rise in cases A1 and C1 will not be so steep, but of the same ultimate magnitude. Case A1 and, especially, case B1 are more advantageous than case C1 in that the positive disturbances are partly canceled, and somewhat lower diamond waves result in the downstream channel. However, these conditions may exist only for very long contractions or for large wave angles near critical depth, and, therefore, are not expected to occur in practice.

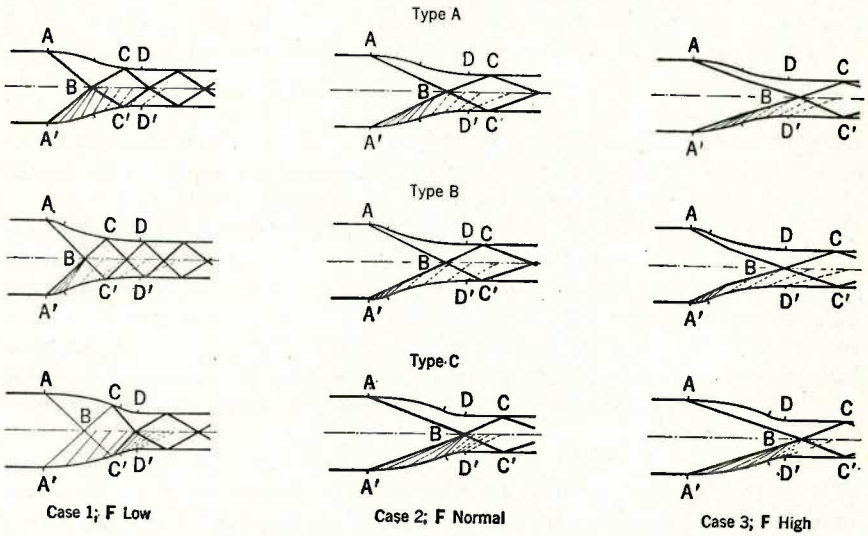

FIG. 40.—CONTRACTIONS COMPOSED OF CIRCULAR ARCS, SHOWING SCHEMATIC DISTURBANCE LINES

Types A, B, and C, case 2, are characterized by having the first wave intersection farther downstream, and they are marked "**F** normal" because the conditions of permissible wave height for given Froude numbers and desirable lengths of contractions would result in patterns of this type. Case C2 is the most undesirable since the "wave-decreasing" influence of the convex walls is shifted downstream, and a maximum depression along the walls may lie in the same cross section as the intersection of the shock waves with its resulting maximum depth. The highest differentials of depths are obtained and, therefore, the maximum disturbances in the channel downstream. In solution A2 this tendency is somewhat relieved, and in B2 the converging lines are so far upstream that some of the negative disturbances may reach the shock fronts in advance of their point of intersection—thereby reducing their heights.

For types A, B, and C, case 3, all the shock-wave intersections are moved too far downstream, which results in large disturbances, if such conditions can be maintained at all. There are indications that for cases A3 and B3 the contraction is too short because the Froude numbers appear to be too high. Although peaks may be relatively somewhat lower for cases A3 and B3 than before (due to the effect of the negative impulses from the convex wall sections), the occurrence of maxima and minima near the same cross section indicates large downstream disturbances.

Summary.—Of all the contractions, B2 will probably perform best. The maximum depth in the center, however, will differ little from solution A2, and smaller downstream disturbances may be expected due to wave interference in this case. In designing such circular contractions, therefore, the characteristics of this type may be followed. In the following section, however, a more systematic approach is indicated toward basically better designs.

Straight-Wall Contractions

General Principles of Design.—The aim of rational design for supercritical flow must be oriented, first, toward lower standing waves and, second, toward reduction or possible removal of standing wave patterns in the channel section downstream from the contraction. As stated, the total deflection angle θ determines the wave height, regardless of the degree of curvature of the side walls. It is logical, therefore, to decrease this angle θ to a minimum. For the contractions discussed in the preceding section, decreasing values of θ are obtained by inserting longer straight-wall sections between the circular sections. Thus, for contractions of the same length, increasing curvatures result for the circular parts, but the deflection angles are decreased. The minimum angle θ is had by connecting the upstream and downstream tangent points by straight lines, possibly rounding the corners slightly for the sake of appearance.

TABLE 4.—Reduction in Maximum Wave Height (See Fig. 8)

Froude No., F_1	$\theta = 8°$; Straight Contraction			Central Angle = 16°; Circular-Arc Contraction		
	h_2/h_1	h_3/h_2	h_3/h_1	h_2/h_1	h_3/h_2	h_3/h_1
2	1.35	1.35	1.82	(1.82)	....	Hydraulic jump
3	1.50	1.40	2.10	2.10	1.80	3.78
4	1.63	1.50	2.44	2.46	1.83	4.50
6	2.00	1.67	3.34	3.41	2.05	7.0
8	2.31	1.83	4.23	4.45	2.25	10.0
10	2.70	2.00	5.40	5.61	2.40	13.5

Table 4 serves to illustrate the reduction in maximum wave height for a contraction of given longitudinal extent as a function of the Froude number. The values of h_2/h_1 and h_3/h_1 are listed for a contraction composed of circular arcs of 16°, central angle, and for a straight-wall contraction of 8°, deflection angle. The ratio h_3/h_1 represents, in each case, the theoretical depth ratio for the zone immediately below the first shock-wave intersection and is assumed to be indicative of the highest possible disturbance. The ratios h_3/h_1 naturally

become excessive for the higher Froude numbers from a practical point of view, but they are considered here only for the sake of comparison.

The design procedure for a straight contraction is simple: For an initial Froude number $\mathbf{F}_1$ and for a permissible depth increase h_2/h_1 the wall angle θ and $\mathbf{F}_2$ can be found from the diagram in Fig. 8 of the first Symposium paper. The first shock wave can be regarded as reflected at the center (see Fig. 41) by its image wave from the opposite wall. Since the depth and velocity beyond this point of reflection or intersection determine the height and location of the disturbances downstream; and, since the angle θ must be the same for the initial and reflected waves, the diagram is used again to determine h_3/h_2 and $\mathbf{F}_3$ with the values of θ and $\mathbf{F}_2$ found previously. The ratio h_3/h_1 can then be

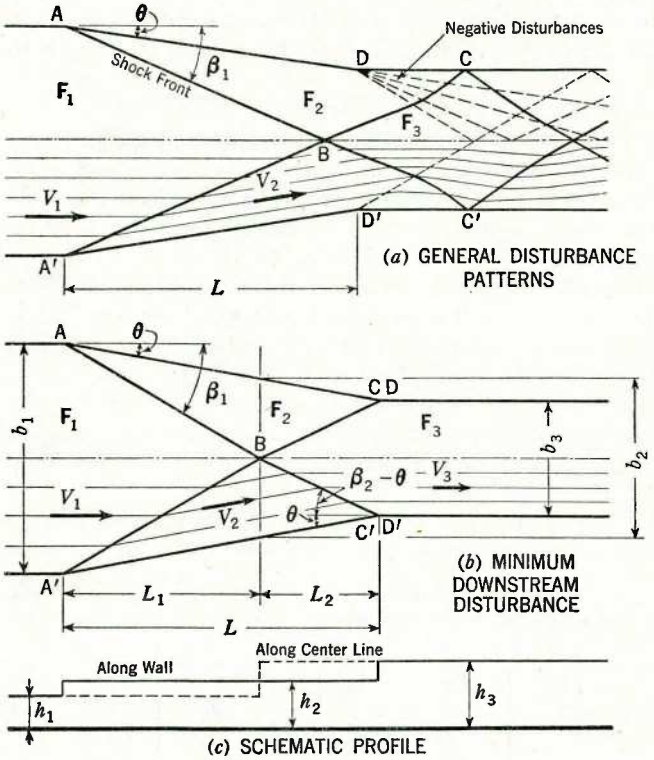

FIG. 41.—DESIGNS OF STRAIGHT-WALL CONTRACTIONS

readily computed and should normally not be higher than three. Fig. 41(*c*) will show immediately whether the hydraulic quantities are safe in so far as they remain sufficiently supercritical. In practice, wall angles so small (and, therefore, contractions so long) that a second reflection along the wall takes place within the contraction are improbable. Theoretically, however, the story is not changed in this case; another set of values of h_4/h_3 and $\mathbf{F}_4$ are to be added to the computation with the same angle θ.

Wave Patterns in Channel Below Contraction.—In the preceding section it was shown that, on the basis of the theory, better hydraulic performance is always obtained for contractions with straight walls rather than with circular-wall alinements due to the smaller total angle of deflection. The additional aim of design is to reduce the standing waves in the channel downstream from the contraction. If the length of channel contraction in relation to initial flow conditions is ignored, the shock waves set up by the converging walls are subject to the negative disturbances originating at points D and D′ (see Fig. 41(*a*)) in a rather haphazard fashion. In the discussion of the various possible wave patterns sketched in Fig. 40, the location of the shock-wave intersection B with respect to points D and D′ is shown to have a definite influence on the wave height in the downstream channel. Maximum disturbances result with points B, D, and D′, lying in the same cross section. Minimum disturbances are to be expected if the reflected shock waves are made to meet the walls at points D and D′, since then the deflecting effects of shock waves and walls tend to cancel each other. This cannot easily be accomplished with **S**-shaped wall contractions unless straight sections are introduced between the concave and convex wall sections. However, it is possible to design straight-wall contractions as indicated in Fig. 41(*b*) to meet this requirement for low disturbances. The disturbance might even be reduced to zero in such a case, provided the basic assumptions of the theory could be satisfied.

To what extent these assumptions are violated remains for further discussion. At this point the geometric conditions in relation to hydraulic flow conditions may be established for such designs in accordance with the notations in Fig. 41(*b*). The deflection of the flow at points A and A′ at the channel entrance causes symmetrical shock waves which cross the channel at an angle β_1 and meet at point B at the center. They are reflected to the walls and on their way proceed through a new flow field characterized by the parameter $\mathbf{F}_2$. If they meet the wall (as assumed) at CD and C′D′, theoretically, there remain no disturbances because the flow has been directed parallel to the walls in the downstream channel by synchronizing the deflection effect of the waves BC and B′C′ with the deflection effect of the wall. Since the deflection angle θ is the same for both, no disturbance is obtained. It is difficult to correlate, mathematically, the geometric and hydraulic conditions for this special case although the setup appears simple enough. The following relations hold:

$$L = L_1 + L_2 = \frac{b_1}{2 \tan \beta_1} + \frac{b_3}{2 \tan (\beta_2 - \theta)} \quad \ldots\ldots\ldots\ldots (40)$$

also,

$$L = \frac{b_1 - b_3}{2 \tan \theta} \quad \ldots\ldots\ldots\ldots\ldots\ldots\ldots\ldots (41)$$

Continuity conditions yield $b_1 h_1 V_1 = b_3 h_3 V_3 = Q$; or

$$\frac{b_1}{b_3} = \frac{h_3 V_3}{h_1 V_1} = \left(\frac{h_3}{h_1}\right)^{3/2} \left(\frac{\mathbf{F}_3}{\mathbf{F}_1}\right) \quad \ldots\ldots\ldots\ldots\ldots\ldots (42)$$

In agreement with Eqs. 19 to 22 of the first Symposium paper and Eqs. 40 to 42, all conditions are available to determine the shape of a contraction. It probably is impossible to eliminate from Eq. 40 the variables β_1 and β_2 and to replace them in terms of h_1/h_3, θ, and $\mathbf{F}_3/\mathbf{F}_1$. Therefore, the procedure must be one of trial and error as follows: For a given value of $\mathbf{F}_1$ a certain reduction in width is required from b_1 to b_3. The assumption of a desirable depth change h_3/h_1 is made, and $\mathbf{F}_3/\mathbf{F}_1$ is thus given by Eq. 42. Provided $\mathbf{F}_3$ is not too close to the critical value, Fig. 8 may be employed to determine the deflection angle θ by trial and error. Assuming a value of θ, the corresponding values of h_2/h_1 and $\mathbf{F}_2$ are read from that graph. A second determination using the same θ and replacing $\mathbf{F}_1$ by the $\mathbf{F}_2$ just obtained will yield a value of h_3/h_2. Multiplying h_2/h_1 by h_3/h_2, the trial value of h_3/h_1 is obtained. If this is not the desired value, the process has to be repeated with an adjusted value of θ until agreement is reached between the assumed h_3/h_1 and the one obtained by trial. The procedure using this diagram is extremely fast. The length L follows from Eqs. 40 and 41.

In general, long contractions will result for low values of h_3/h_1 and high values of $\mathbf{F}_1$. Ratios of $h_3/h_1 = 2$ and $h_3/h_1 = 3$ seem advisable in order to reduce the length of contractions, provided $\mathbf{F}_3$ stays well above the critical value.

If the contraction cannot be designed to the correct angle θ, disturbances must be expected to continue into the downstream channel, as indicated in Fig. 41(*a*). The maximum height of these disturbances may then be determined as in the foregoing procedure. The process is repeated twice with a given angle θ, since the maximum depth h_3/h_1 will occur at least within a narrow zone below the wave intersection B. It will then recur intermittently along side walls and center line, provided points C and C′ lie below points D and D′. The respective positions of points D and C tend to modify the height of the downstream waves, since points D and D′ are the origins of negative disturbance lines. It is felt, however, that the limitations imposed on the theory by the basic assumptions would render a possible theoretical analysis of surfaces downstream from the contraction of little practical significance.

The following summary may express the results of this theoretical investigation briefly:

1. Straight-wall contractions are always better than curved-wall contractions from the standpoint of maximum wave height and compared on the basis of equal length.

2. For given reductions in channel width, correct deflection angles θ may be found, which result in minimum disturbances in the downstream channel.

Vertical Accelerations and Boundary-Layer Influence.—The actual physical features of shock-wave fronts differ from the ones assumed in the basic theory to a considerable extent, as is indicated schematically in Fig. 42. First, vertical fronts, represented by single lines in plan and having negligible longitudinal dimensions, are arrived at in the elementary theory; and, second, the velocity is assumed constant over the depth.

The flow is assumed to expand under the front instantaneously, in accordance with the deflection imposed on the stream by the side wall. It has

already been shown that the existence of a boundary layer along the channel sides will modify the rate of rise or depression of the water surface there. In the theory this assumption is one of convenience, and the actual appearance of the shock wave is considerably modified under the influence of the neglected

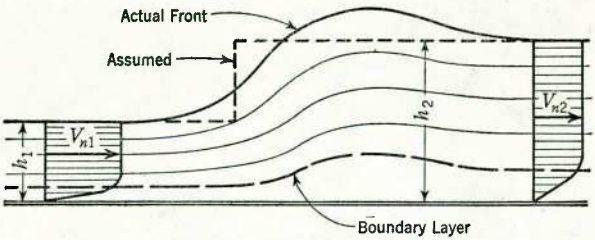

FIG. 42.—SCHEMATIC COMPARISON OF ACTUAL AND ASSUMED WAVE FRONT

factors. The flow will expand rather gradually in the case of low waves, whereas, for higher fronts, the surface slope approaches the vertical with eventual overturning or breaking of the wave. Surface rollers, familiar from the hydraulic jump, are formed. Steep fronts naturally cause high vertical accelerations and, therefore, considerable deviations from the assumed hydrostatic pressure distribution under the front. Thus, the wave fronts are characterized locally by depths which are higher than those calculated. However, within a short distance the depths revert closely to the theoretical depths as soon as the streamlines again are parallel to the bottom. The fact that wave fronts extend longitudinally and are distorted vertically in the case of high vertical accelerations must be considered in analyzing experimental results. The longtitudinal dimensions of the front should be small as compared to the dimensions of the structure to be tested. The phenomena of wave reflection and intersection are equally influenced and modified by the physical discrepancy between theoretical assumption and actuality. However, basic wave patterns must remain valid regardless of these local effects.

In Fig. 42 the boundary layer along the bottom is indicated to an exaggerated extent by a dashed line. This boundary layer will increase disproportionately in thickness under the wave front since the low momentum of the fluid within this layer is not sufficient to overcome the adverse pressure gradient under the front. This fact will change the so-called displacement thickness of this layer and will be equivalent to a rise in elevation of the bottom, thus decreasing the specific head of the flow. A slight change in the height of the front and in its location may result. Although this discussion is helpful in the analysis of experimental trends, refinements of the theory do not seem warranted for the purpose of this paper.

EXPERIMENTAL RESULTS WITH STRAIGHT-WALL CONTRACTIONS

The two phases of the problem with straight contractions were the subject of several experimental studies at Lehigh University and at M. I. T. As shown previously the basic theory and the experimental results obtained for curved side walls agree satisfactorily (see Fig. 39), giving disturbances corresponding

to the maximum deflection angles. The statement made previously that straight-wall contractions are more satisfactory due to smaller deflection angles has already been supported by theoretical evidence in Table 4; it remains, there-

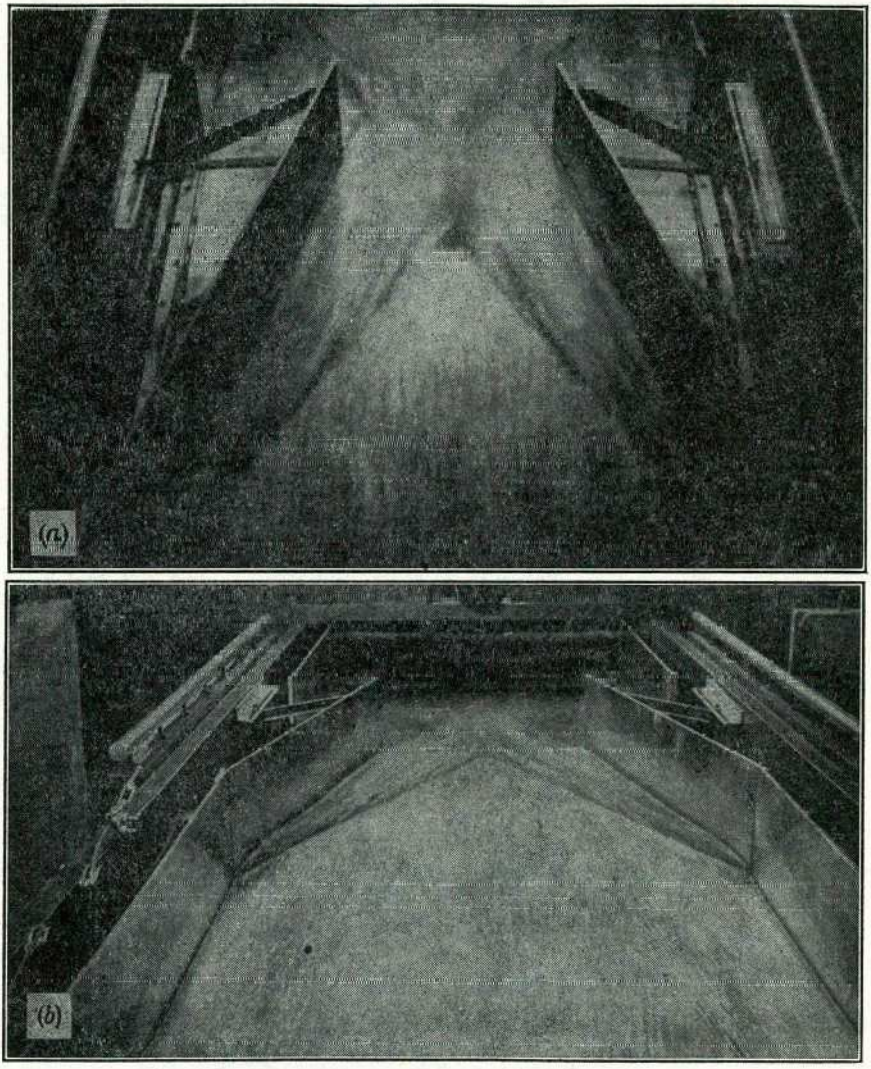

FIG. 43.—VIEWS, FACING DOWNSTREAM, OF CONTRACTION COMPOSED OF STRAIGHT WALLS; $F = 3.86$ AND $\theta = 15°$

fore, to present experimental confirmation of the basic equations. Two sets of results are available for this purpose.

M. P. Barschdorf and H. G. Woodbury,[25] in a flume constructed of aluminum plates for accurate work at the Hydraulic Laboratory at M. I. T.,

arranged for movable side walls, so that wall angles of θ from 3° to 30° could be established. For Froude numbers between 3 and 4 they conducted a series of experiments measuring the pertinent features of the standing waves produced for wall deflection angles from 3° to 30°. A sufficient number of transverse profiles were determined by point gage to obtain the wave heights and wave angles independently of the local effects discussed in the preceding section. The photographs of Fig. 43 are two views facing downstream into the contraction with a wall angle of $\theta = 15°$ and for a Froude number of $\mathbf{F} = 3.86$. The

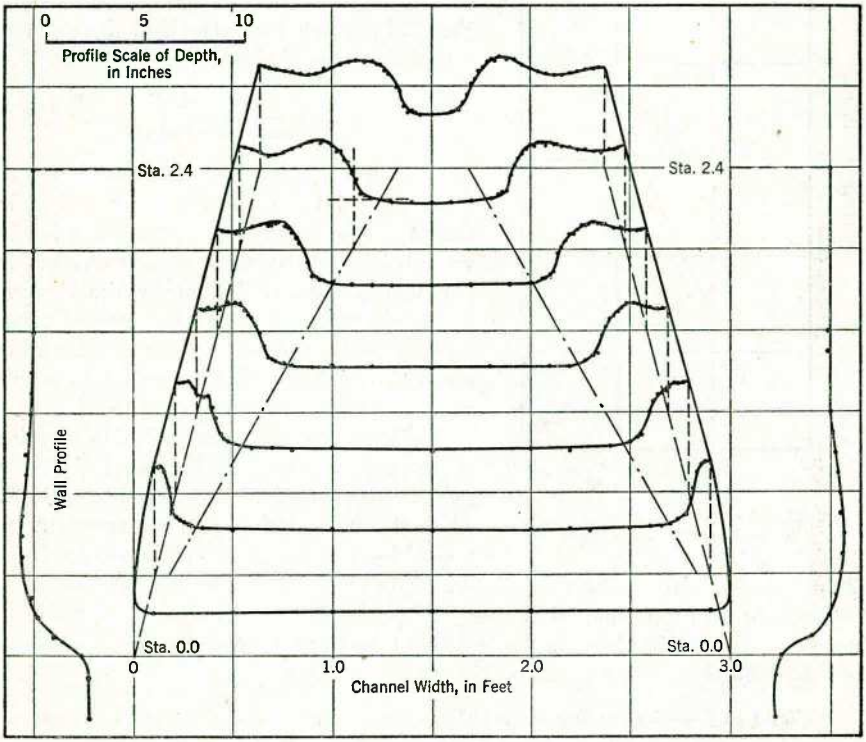

FIG. 44.—SURFACE PROFILES OF STANDING WAVES IN STRAIGHT-WALL CONTRACTION; $\mathbf{F} = 3.86$ AND $\theta = 15°$

surface profiles for all runs were plotted in distorted scale in isometric form as shown for the preceding example in Fig. 44. The initial rise of the surface near the front above the equilibrium depth is apparent, whereas beyond this local disturbance the depth along the wall returns to a more or less constant value. Side-wall profiles are also plotted and show clearly the constancy of depth h_2 along the wall.

In Table 5 a comparison is presented of measured and theoretical values of wave angle β_1 and of the depth ratio h_2/h_1. All theoretical values of β_1 and h_2/h_1 were determined from the known quantities of θ and $\mathbf{F}_1$ by graphs equiva-

lent to Fig. 8. Wave angles β_1 were determined by averaging the wave fronts vertically at each station and by drawing straight lines through the wave front locations thus obtained. From Table 5 it is seen that excellent agreement was obtained for this Froude number $\mathbf{F}_1$ as far as ultimate values of h_2/h_1 are concerned. The values of β_1 varied from -12% to $+5\%$ about the theoretical value of β_1 for the different deflection angles from 3° to 24°. The general trend obtained consistently for only slightly different Froude numbers is best illustrated in Fig. 45 in which the ratio K of sines of the actual β_1 to the theoretical β_1—

$$K = \frac{\text{actual sin } \beta_1}{\text{theoretical sin } \beta_1} \quad \ldots\ldots (43)$$

—is plotted against the deflection angle θ. Since the minimum possible value of β_1 is $\sin^{-1} 1/\mathbf{F}_1 = 15°0'$, the influence of the wave height on the value of β_1 is smaller for low values than indicated by the theory, and larger than the theoretical values when h_2/h_1 greatly exceeds values of 2. This result shows that vertical accelerations will affect the location of the wave front.

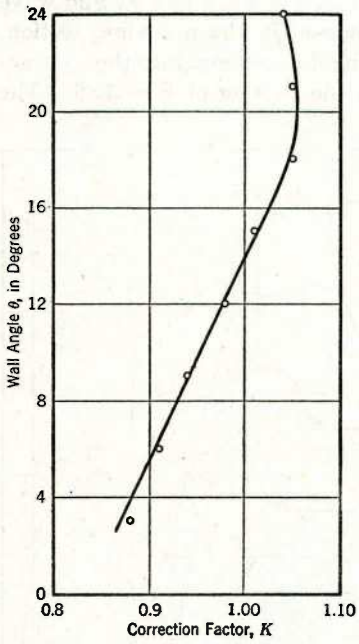

FIG. 45.—PLOT OF CORRECTION FACTOR K AGAINST WALL ANGLE θ

This tendency appeared also in a series of tests conducted at Lehigh University by D. Coles and T. Shintaku,[23] Jun. ASCE, when the wall angle was kept constant at $\theta = 6°$ for a range of Froude numbers from $\mathbf{F}_1 = 3$ to $\mathbf{F}_1 = 10$. Their results are summarized in Table 6. Although the ratios h_2/h_1 are obtained fairly easily from the measurements, the angle β_1 is not so readily available from the data and depends somewhat on the method of interpretation.

TABLE 5.—COMPARISON OF MEASURED AND THEORETICAL VALUES OF β_1 AND h_2/h_1 FOR A FROUDE NUMBER OF $\mathbf{F}_1 = 3.86$

Wall angle	Theoretical[a] β_1	Measured β_1	Theoretical h_2/h_1	Measured h_2/h_1	Percentage Variation from Theory	
					β_1	h_2/h_1
3°	17° 35′	15° 30′	1.21	1.24	−11.8	2.3
6°	20° 15′	18° 15′	1.47	1.47	− 9.9	0
9°	23° 10′	22° 45′	1.70	1.73	− 1.2	1.7
12°	26° 30′	26° 7′	2.00	2.00	− 1.5	0
15°	29° 30′	29° 55′	2.22	2.22	+ 1.4	0
18°	32° 25′	34° 15′	2.49	2.47	+ 5.6	−0.70
21°	35° 45′	38° 00′	2.72	2.71	+ 6.3	−0.3
24°	39° 18′	41° 20′	2.99	3.01	+ 5.2	+0.6

[a] Minimum value is 15° 00′.

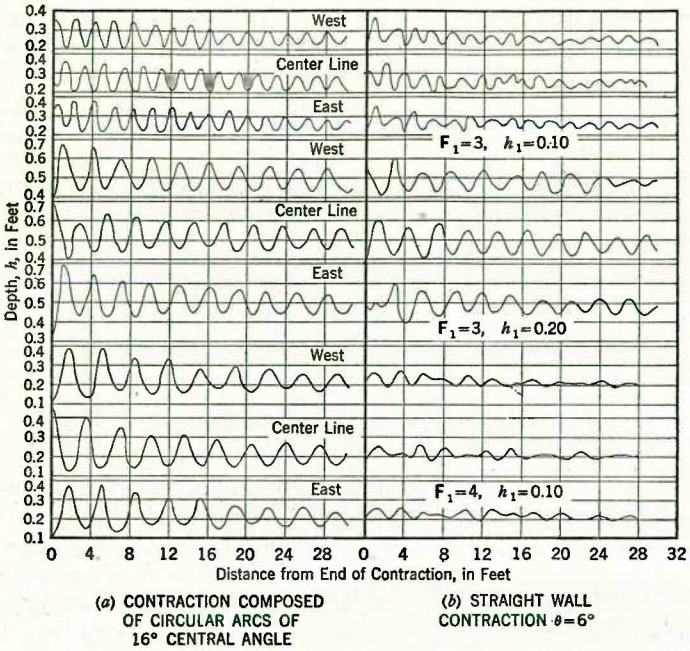

FIG. 46.—WALL AND CENTER-LINE PROFILES; $F = 4$ AND $h_1 = 0.10$

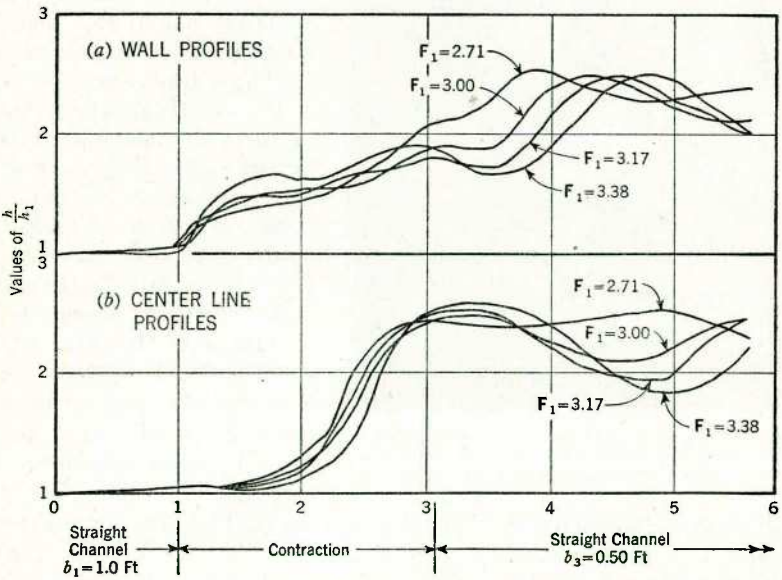

FIG. 47.—WALL AND CENTER-LINE PROFILES FOR STRAIGHT-WALL CONTRACTION; $\theta = 6.9°$

Essentially the basic theory stands confirmed by the experimental findings in laboratory flumes for a practical range of F_1 from 3 to 8 and of h_2/h_1 from 1 to 3. Its usefulness for design is readily apparent within the limitations discussed.

Disturbance Pattern in Channel Below Contraction.—Several studies were finally made to compare disturbances from contractions in the channel down-

TABLE 6.—COMPARISON OF MEASURED AND THEORETICAL VALUES OF β_1 AND h_2/h_1 FOR VARYING FROUDE NUMBERS AND CONSTANT WALL ANGLE $\theta = 6°$

Froude No.	Theoretical β_1	Measured β_1	Theoretical h_2/h_1	Measured h_2/h_1
3.00	25° 10′	22° 00′	1.38	1.31
4.00	19° 30′	18° 40′	1.47	1.52
6.00	15° 00′	15° 10′	1.75	1.73
8.00	12° 20′	12° 45′	2.00	2.17
10.00	11° 10′	10° 30′	2.30	2.88

stream. Fig. 46(*a*) shows the dimensionless depth profiles along the walls of the channel and its center line, starting at the end of the contraction for the circular-arc contraction and with maximum deflection angles of 16°. Although the comparable straight-wall contraction should have been built with $\theta = 8°$ to obtain a contraction of the same length, a longer contraction with $\theta = 6°$ was built to extend its usefulness into the range of lower Froude numbers. These profiles are shown in Fig. 46(*b*) as before for the same hydraulic conditions. The improvements with respect to wave height are readily seen.

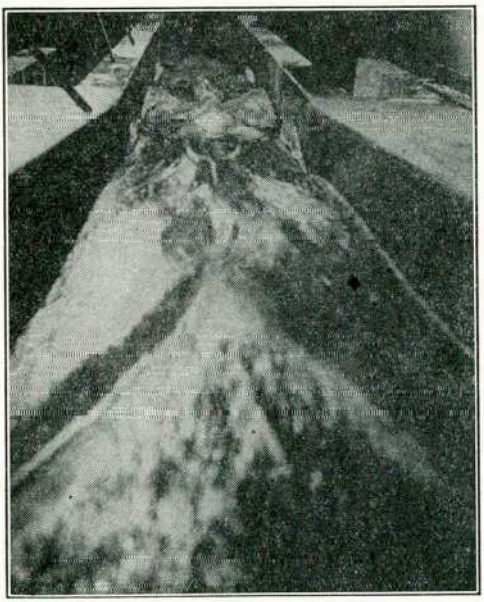

FIG. 48.—FACING DOWNSTREAM TOWARD SURFACE DISTURBANCES FOR A STRAIGHT-WALL CONTRACTION; F = 4

In addition, attention is called to the fact that the disturbances for $F = 4$ are actually less than for $F = 3$ for the same contraction. This fact indicates that the contraction at $F = 4$ more nearly satisfied the requirements of correct design as indicated in Fig. 41(*b*), whereas, for $F = 3$, the points of intersection and reflection of the wave fronts were located so as to cause maximum disturbances.

Previous to this study D. P. Rodriguez[22] designed a correct straight-wall contraction for $F = 4$ and for a reduction ratio of $b_1/b_3 = 2$. The angle θ for this case was computed to be 6.9°. Tests were then made on a one-sided contraction in the Lehigh flume. The best profiles were found not for $F = 4$

but for **F**-values of about 3, as indicated in Fig. 47 showing the various wall and center-line depth profiles. This result, although not anticipated at that time, is due to the fact (established later) that the actual wave angle β_1 for this wall angle and Froude number is smaller than the computed value (see Table 5). Therefore, a longer contraction is indicated than is obtained from the theory. It is also for this reason that the wall angle of 6° was chosen in the study reported by Messrs. Coles and Shintaku.[23] With this smaller wall angle the improved profiles for **F** = 4 in Fig. 46(*b*) were obtained. A photograph

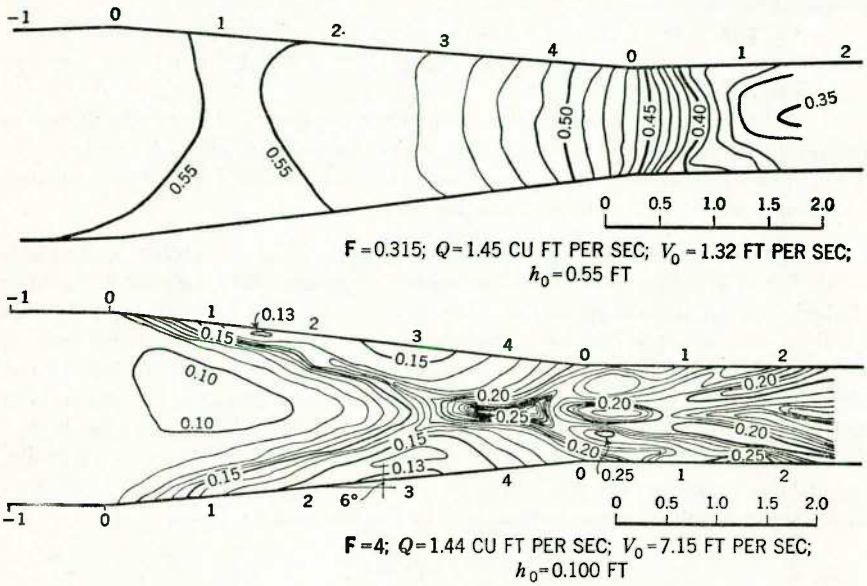

FIG. 49.—CONTOURS OF WATER SURFACE IN A STRAIGHT-WALL CONTRACTION FROM 2 FT TO 1 FT

showing this contraction with flow conditions near **F** = 4 is given in Fig. 48, which readily shows the improvement in the surface disturbances when compared to views in Fig. 36. A further graphical illustration of this case is supplied by the surface contour maps of Fig. 49. Fig. 49 gives the surface for **F** = 0.315—that is, for subcritical flow, which is equivalent to the case plotted in Fig. 37(*a*) and does not show any essential difference. For the case of supercritical flow with **F** = 4, Fig. 49 may be compared to Fig. 37(*b*), and the reduction in the depths produced along side walls and along center lines is seen to be considerable.

CONCLUSION

The experimental evidence presented in the preceding section is not sufficient to establish corrections of general validity for the application of the elementary theory. However, by and large, it is adequate to show that the basic phenomena are predictable from the theory. Only minor corrections

need be applied because of factors not included in the theory (such as the influence of gravity and friction forces) and because of the vertical accelerations under the shock-wave fronts. Further experimentation is to be directed toward a systematic coverage of these influences. The limited aims of the present paper may be summarized under the following points:

1. The behavior of a typical channel contraction composed of circular arcs was explored experimentally for a wide range of Froude numbers;
2. The flow conditions predictable from the thoery were compared to experimental measurements;
3. On the basis of these results the physical requirements of channel contractions for supercritical flow were defined as distinct from those for subcritical flow;
4. A basic design form was developed for supercritical flow conditions to reduce wave heights and disturbances in the downstream channel; and
5. Typical contractions designed with straight converging walls were tested and found to conform essentially to the requirements.

It is thus established that channel contractions for supercritical flow can be designed specifically to avoid excessive standing wave heights by proper choice of both deflection angles and length for given reductions in width. Straight-wall contractions are normally superior to curved-wall contractions, as long as the channel bottom is level crosswise and of constant slope in the direction of flow. Warping of the bottom and large changes in longitudinal slope have not been included in this paper, although improvements in the standing wave patterns can be attained experimentally by such methods. Additional experimental work and an extension of the theory are needed to cover these phases of supercritical flow in channel contractions.

Acknowledgment

Much of the experimental work reported in this paper was done by graduate students in the hydraulics laboratories of Lehigh University and of the Massachusetts Institute of Technology. Their contributions are acknowledged by extensive reference to their theses submitted to the two institutions for advanced degrees. It remains to express grateful appreciation for the extensive assistance received from the respective laboratory staffs on the construction of the equipment and during the performance of the experimental work.

DESIGN OF CHANNEL EXPANSIONS

By Hunter Rouse,[26] M. ASCE, B. V. Bhoota,[27] Assoc. M. ASCE, and En-Yun Hsu[28]

Synopsis

Following an introductory discussion of supercritical flow in divergent channels, the matter of channel design is discussed under three sequent headings: (1) Surface configuration at abrupt expansions; (2) efficient curvature of expanding boundaries; and (3) elimination of disturbances at the end of transitions. The extent of the agreement between elementary wave theory and experimental measurement is shown, and the results are presented in the form of generalized diagrams convenient for rapid exploration and preliminary design.

Introduction

In the design of hydraulic structures it is often necessary to provide for the lateral expansion of flow emerging at high velocity from a closed conduit, sluice gate, spillway, or steep chute. If such a transition section is made to diverge too rapidly, the major part of the flow will fail to follow the boundaries; if the divergence is too gradual, on the other hand, waste of structural material will result; and, finally, if local disturbances are produced by incorrect boundary form, either at these points or farther downstream the walls may fail to confine the flow. Any particular problem of this nature, to be sure, may be subjected to cut-and-try investigation through model tests, with results which are necessarily restricted to the specific model form. An exact and general analytic solution, unfortunately, is still a matter for the future, and may be approached only through application of sound physical principles as discussed in the first Symposium paper. However, a step in this direction has been made in the development of reasonably general relationships among the several major variables involved, by means of which an approximate solution may be obtained for a great range of boundary conditions.

As in other problems of steady flow in an open channel of nonuniform cross section, the variation in velocity and depth through a channel expansion will depend on the geometry of the channel boundaries, the rate of flow, and the fluid properties. Under boundary geometry must be considered the form of the channel walls, the slope and form of the floor, and the surface roughness of floor and walls. In a strict sense, under fluid properties one should consider the density, specific weight, viscosity, and surface tension; except in small models, however, or under conditions in which boundary shear is of particular

[26] Director, Iowa Inst. of Hydr. Research, State Univ. of Iowa, Iowa City, Iowa.
[27] Engr., Foreign Div., The Dorr Co., Bombay, India.
[28] Research Associate, Iowa Inst. of Hydr. Research, State Univ. of Iowa, Iowa City, Iowa.

moment, both surface tension and viscosity are of very minor importance, and the two remaining properties then reduce to their ratio $\gamma/\rho = g$, the gravitational acceleration.

If these different independent variables are combined by the Π-theorem [29] of dimensional analysis into a series of dimensionless ratios, as many length ratios will be obtained as are necessary to describe the relative geometrical proportions of the boundary, together with a flow parameter of the Froude type. The latter is generally written in the form:

$$\mathbf{F} = \frac{V}{\sqrt{g\,h}} \qquad (44)$$

in which V is the mean velocity and h is the mean depth of the approaching flow.

For given boundary conditions, the relative form of the free surface and the relative velocity distribution will depend solely upon the magnitude of the Froude number. As in all cases of open-channel flow, the critical magnitude $\mathbf{F} = 1$ marks the border between two wholly different types of surface configuration and velocity distribution. For Froude numbers less than unity, the depth then being greater than the critical, a gradual enlargement of the cross section will result in a gradual increase in mean surface elevation and a corresponding reduction in mean velocity. For Froude numbers greater than unity, the depth then being less than the critical, the same gradual enlargement of the cross section will result in a gradual reduction in mean surface elevation and a corresponding increase in mean velocity. However, only if the divergent boundaries are continuous planes (which is physically impossible if the transition is to begin and end with other than zero and infinite cross-sectional areas) will the depth of flow and the magnitude of the velocity be constant over any normal section. In other words, at the beginning and at the end of the transition the local curvature or angularity of the walls and floor will produce disturbances which make it impossible to handle such a problem satisfactorily on the elementary basis of mean velocity and mean depth. For Froude numbers less than unity (which are not the concern of the present paper), the boundary may be designed and the flow pattern may be evaluated in much the same manner as for the corresponding transition in a closed conduit. On the other hand, for Froude numbers greater than unity, the problem of design and evaluation becomes one of gravity-wave analysis, since each increment of the boundary deflection may be considered to generate an incremental surface wave which crosses the flow at an angle depending upon the Froude number and the boundary form; only through determination of the cumulative effect of all such waves may the depth and velocity at each and every point be predicted.

As has been described in the first Symposium paper, there is at hand a graphical method which permits the direct construction of streamlines, "isovels," and water-surface contours for any boundary form, provided that: (1) The channel walls are vertical and the floor is horizontal, (2) the energy

[29] "Fluid Mechanics for Hydraulic Engineers," by Hunter Rouse, McGraw-Hill Book Co., Inc., New York, N. Y., 1938, pp. 13–18.

loss due to boundary resistance is negligible, and (3) the pressure is hydrostatically distributed. These provisions may at first glance appear decidedly restrictive, but they become less so as they are considered individually. Vertical channel walls are common; indeed, sloping walls are generally to be avoided in nouniform high-velocity flow because of their tendency to exaggerate surface disturbances. Channel floors are seldom horizontal, however, and the boundary resistance is never completely negligible; on the other hand, slight to moderate slopes of either the floor or the total-head line generally have an influence which is secondary to that of the wall expansion, and such effects are in fact compensative rather than additive. Moreover, only in the case of relatively abrupt curvature at the beginning or the end of the expansion is the existence of nonhydrostatic zones to be expected, and these may be effectively eliminated by proper easing of the transition curve. Only two factors, in actuality, tend to limit the graphical method in its use for the complete design of a well-proportioned expansion. First, its application depends upon prior knowledge or assumption of the boundary geometry, so that determination of the best form of transition involves the tedious process of trial and error. Second, if (as is usually the case) a hydraulic jump is to form at the end of the expansion, the method offers no clue as to the inherent stability (or, more likely, instability) of the phenomenon. As a matter of experience, the formation of a jump or standing wave by other than the boundary curvature (for instance, by backwater from a downstream control) may lead to an asymmetric pattern of flow within the transition which is still wholly unpredictable.

Since the purpose of this paper is the provision of general rather than specifically detailed information on the behavior of high-velocity flow in any channel expansion and on the preliminary design of particular expansion structures, primary attention (once the agreement between theory and experiment has been shown to be satisfactory) is focused upon the reduction of all experimental data to a few composite diagrams from which the basic details of design may be determined. Both the experiments and the generalization of the experimental results group themselves naturally into three subdivisions of the problem—first, the characteristics of a high-velocity jet expanding upon a level floor; second, the effects of boundary curvature in the zone of divergence; and, third, phenomena accompanying the return to uniform flow at the end of the transition.

All experiments described herein were conducted at the Iowa Institute of Hydraulic Research of the State University of Iowa under a project sponsored by The Engineering Foundation and the Committee of the Hydraulics Division, ASCE, on Hydraulic Research. The first part of the project, including the construction of equipment, was undertaken as a doctoral dissertation by Mr. Bhoota,[30] and the second part as a master's thesis by Mr. Hsu,[31] who then completed the investigation as a staff member of the Iowa Institute. Messrs. C. H.

[30] "Characteristics of Supercritical Flow at an Abrupt Open-Channel Enlargement," by B. V. Bhoota, thesis presented to the State University of Iowa, at Iowa City, Iowa, in December, 1942, in partial fulfilment of the requirements for the degree of Doctor of Philosophy.

[31] "Characteristics of Supercritical Flow at a Gradual Open-Channel Enlargement," by En-Yun Hsu, thesis presented to the State University of Iowa, at Iowa City, Iowa, in February, 1946, in partial fulfilment of the requirements for the degree of Master of Science.

Hsia and M. M. Hassan, Assoc. M. ASCE, assisted in various phases of the analysis. The entire project was under the direction of Mr. Rouse.

Essentially the same equipment (see Fig. 50) was used for all experiments. Water was supplied from constant-level tanks, through 4-in. lines and 8-in. lines containing calibrated elbow meters, to a pressure tank 2.5 ft in diameter and 5 ft long. One end of the pressure tank was provided with three interchangeable nozzles yielding rectangular jets 0.4 ft by 0.4 ft, 0.3 ft by 0.6 ft, and 0.25 ft by 1.0 ft in cross section—that is, having width-depth ratios of 1, 2, and 4. Rates of discharge were such that flow at any Froude number from 1 to 8 could be established. Flush with the bottom of the nozzle outlet sections was a level table, normally horizontal but adjustable to a maximum slope of approximately 10° and provided with a suitably hooded waste trough. This

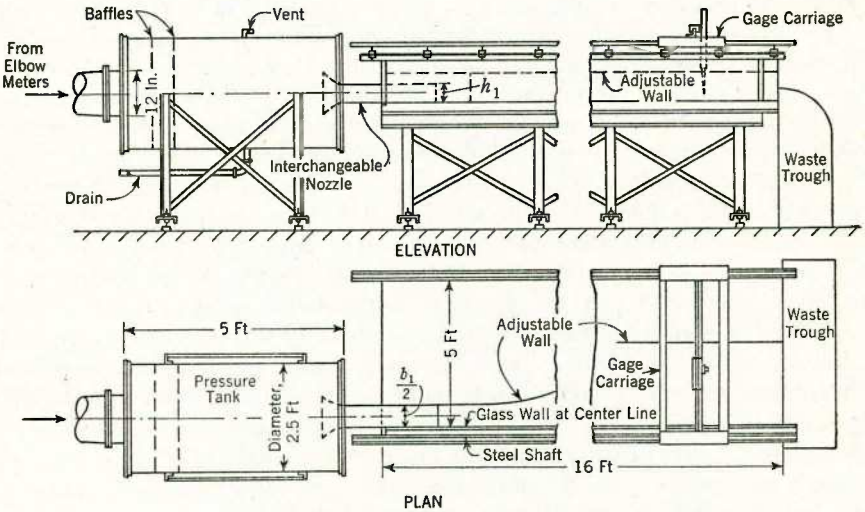

FIG. 50.—SCHEMATIC REPRESENTATION OF EXPERIMENTAL APPARATUS

table was originally 5 ft wide and 8 ft long, and was covered with oiled hardboard except for a plastic section with floor piezometers. It was later doubled in length and paved with finished concrete throughout. A gage carriage traveling on steel shafts above the table permitted three-directional movement of a point gage or pitot tube to any part of the test section. Through the earlier experiments one edge of the table was alined with the outer edge of each nozzle, a glass wall extending down the assumed line of symmetry of the transition for purposes of observation. That such elimination of one half of the flow pattern introduced negligible error was shown when the full transitions were later tested.

CHARACTERISTICS OF FLOW AT AN ABRUPT EXPANSION

The extreme case of a channel expansion is represented by the abrupt termination of the side walls, the channel floor continuing at the same slope.

If h_1 and V_1 represent the depth and mean velocity of the approaching flow, b_1 is the channel width, x and y are the longitudinal and lateral coordinates (measured from the outlet section and the center line, respectively) of a point of depth h, and if no other factors than the acceleration of gravity are assumed to influence the flow, these variables may be combined into the following dimensionless relationship:

$$\frac{h}{h_1} = f_1\left(\frac{x}{h_1}, \frac{y}{h_1}, \frac{b_1}{h_1}, \mathbf{F}_1\right) \ldots\ldots\ldots\ldots\ldots\ldots (45)$$

Evidently, the relative depth at any point of the flow should depend upon the relative coordinate location, the relative width of the channel outlet, and the Froude number of the approaching flow. The form of this functional relationship, of course, cannot be predicted through dimensional considerations, but must depend upon either physical analysis or experimental measurement.

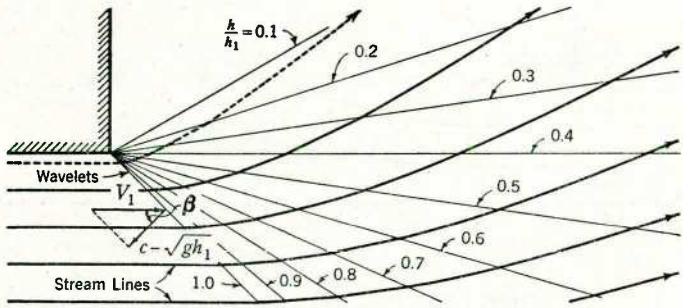

FIG. 51.—PATTERN OF FLOW NEAR THE ABRUPT END OF A CHANNEL WALL

The elementary wave theory indicates that the flow in the neighborhood of the end of either wall will begin to change in direction only as it passes the first negative wavelet (see Fig. 51), which lies at the angle $\beta = \sin^{-1}\sqrt{g\,h_1}/V_1 = \sin^{-1} 1/\mathbf{F}_1$ to the initial flow direction. From then on the streamlines may be considered to continue deviating through a series of infinitesimal steps, the angle of each succeeding wavelet depending upon the local magnitude of the continuously changing ratio of V to $\sqrt{g\,h}$—that is, the local Froude number. Each wavelet represents, in effect, a line of constant depth, so that proper selection among the infinite series of wavelets will yield the systematic series of surface contours shown in Fig. 51.

If now the zone is investigated in which the wavelets from the two opposite sides of the outlet begin to intersect, it will be seen (Fig. 52) that the resulting pattern of interference will yield a rather complex variation in depth and velocity of flow. The surface contours may again be determined by a rather laborious analysis of each element of the pattern in accordance with the elementary wave theory, but a far more rapid solution may be obtained by the graphical method of characteristics outlined in the first Symposium paper. Three such solutions, for different values of $\mathbf{F}_1$, are shown in Fig. 53.

The method of characteristics, in effect, reduces the functional relationship of Eq. 45 to the form:

$$\frac{h}{h_1} = f_2\left(\frac{x}{b_1}, \frac{y}{b_1}, \mathbf{F}_1\right) \quad \ldots\ldots\ldots\ldots\ldots\ldots\ldots\ldots\ldots\ldots (46)$$

by combining the relative coordinate terms x/h_1 and y/h_1 with the initial width-depth ratio, b_1/h_1. This entails the inherent assumption of hydrostatic pressure distribution at all points—that is, the absence of appreciable vertical acceleration. As a matter of fact, at the abrupt end of either channel wall the pressure is far from hydrostatically distributed, as the water surface is practically vertical in such a zone. The extent to which this lack of fulfilment of

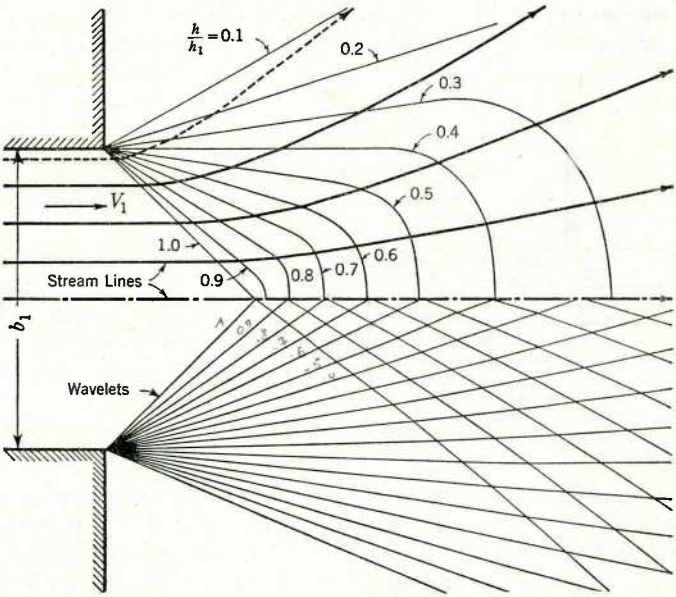

FIG. 52.—EFFECT OF WAVE INTERFERENCE FROM OPPOSITE SIDE OF CHANNEL

the assumption causes the actual surface configuration to differ from the theoretical evidently depends upon the magnitude of the ratio b_1/h_1. In wide, shallow channels the zone of disagreement is of relatively small extent; in narrow, deep channels, on the other hand, the pressure distribution will be markedly nonhydrostatic from wall to wall.

In illustrating the variation to be expected, experimentally measured surface contours for three different width-depth ratios are plotted in Fig. 54 for the same Froude numbers as those in Fig. 53. The deviations with b_1/h_1 are appreciable, but nevertheless secondary to the variation with the Froude number. In other words, using an average system of contours in preliminary design is quite in order. Even for the widest channel, however, it will be found that there is also a discrepancy between the measured contours and those

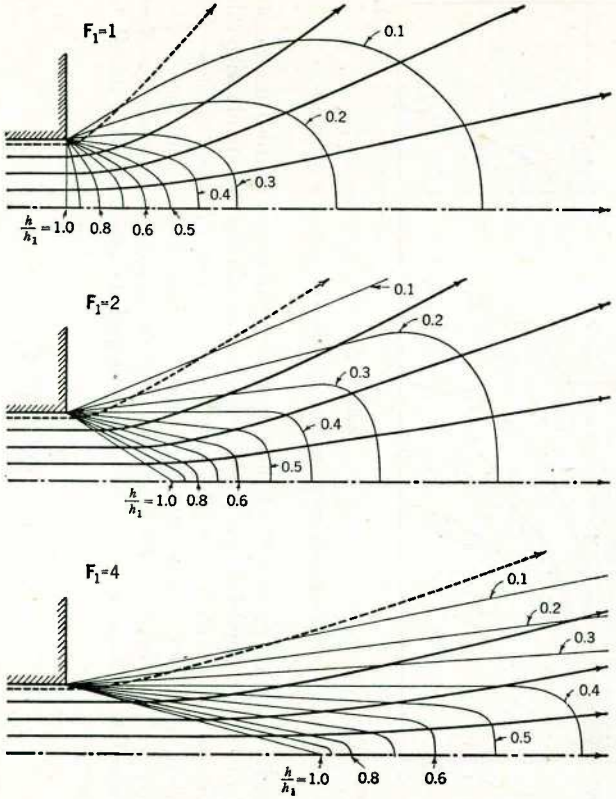

FIG. 53.—VARIATION OF THE FLOW PATTERN WITH THE FROUDE NUMBER

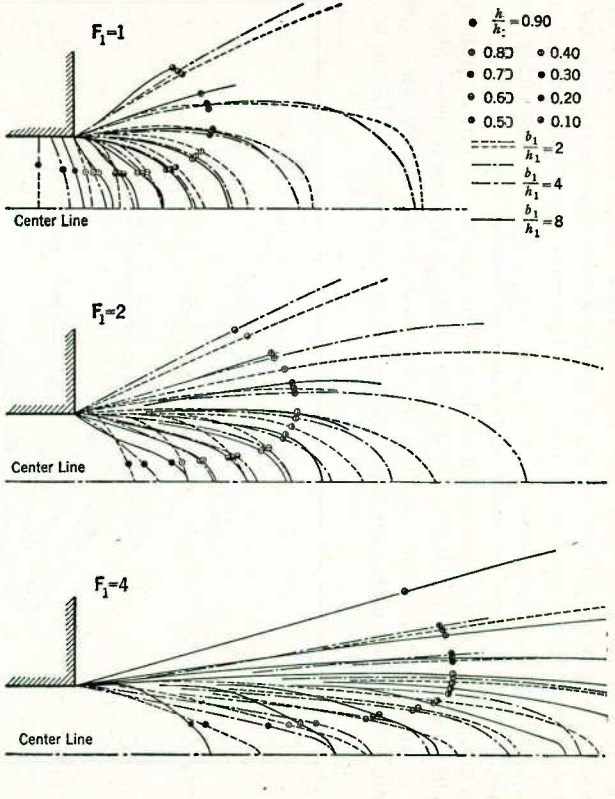

FIG. 54.—EXPERIMENTAL MEASUREMENTS OF SURFACE CONFIGURATION FOR VARIOUS FROUDE NUMBERS AND WIDTH-DEPTH RATIOS

obtained by the graphical method of analysis. This may be attributed to the failure of the analysis to provide for any variation of total head due to boundary resistance, since the analytical contours are invariably displaced upstream. Again, however, the discrepancy is secondary in comparison with either the measured or the predicted variation of the flow pattern with $\mathbf{F}_1$.

For purposes of rapid exploration of the various possible conditions of flow, it would be desirable to combine the Froude number with one or more of the other parameters, just as the method of characteristics effectively eliminates the ratio b_1/h_1 by combining the terms x/h_1 and y/h_1 (compare Eqs. 45 and 46).

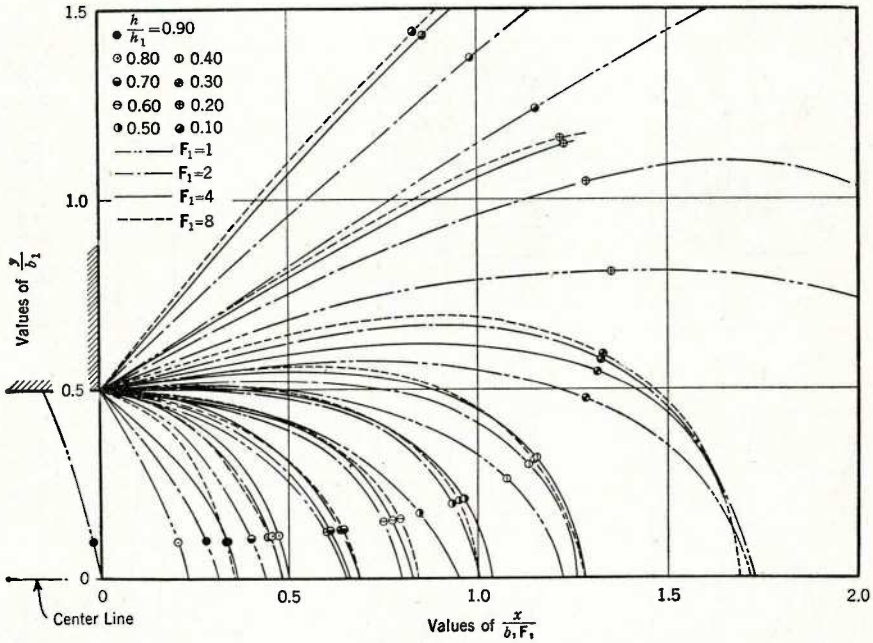

FIG. 55.—GENERALIZATION OF EXPERIMENTAL DATA FOR ABRUPT EXPANSIONS

A logarithmic plot against $\mathbf{F}_1$ of the location of particular contour intercepts along any longitudinal axis (say, the line of each wall in Fig. 54), made with this purpose in mind, indicated that—except at very low Froude numbers—the variation in location was essentially a linear function of $\mathbf{F}_1$. In other words, division of all values of x/b_1 by $\mathbf{F}_1$ should tend to superpose all equivalent surface contours for all Froude numbers. Eqs. 45 and 46 are thereby reduced to the form:

$$\frac{h}{h_1} = f_3\left(\frac{x}{b_1 \mathbf{F}_1}, \frac{y}{b_1}\right) \quad \ldots\ldots\ldots\ldots\ldots\ldots\ldots\ldots\ldots\ldots (47)$$

As may be shown analytically, this is certainly not a rigorous generalization. However, as will be seen from inspection of Fig. 55, when replotted in this manner the deviation of the mean contours taken from Fig. 54 is not great.

Although single average lines on this generalized diagram would evidently represent means of means, their departure from the contours of twenty-one runs at different values of $\mathbf{F}_1$ and b_1/h_1 is considered sufficiently small to permit the use of this diagram for the preliminary analysis of abrupt expansions at practically any value of either parameter.

Efficient Curvature of Expanding Boundaries

There is a rule of thumb for the design of divergent boundaries in high-velocity flow which arbitrarily fixes the angle of divergence at $\theta = \tan^{-1} \frac{1}{6}$ to $\theta = \tan^{-1} = \frac{1}{3}$, regardless of the depth and the velocity of flow. As is apparent from the foregoing discussion of the expansion of flow without lateral constraint, the angle of divergence of any two neighboring streamlines is constant neither with the Froude number at a particular longitudinal distance nor with the longitudinal distance for a particular Froude number. At the abrupt beginning of such a uniformly divergent section the flow itself cannot abruptly change direction, and local separation as well as a concentration of negative wavelets will result; on the other hand, at a distance downstream which varies with the Froude number. the flow would naturally diverge more rapidly than the constant boundary angle will permit, thereby producing positive wavelets. Thus, as indicated by either of the contour maps of Fig. 56, obtained by the method of characteristics, such a divergent section is invariably inefficient at its beginning (and again before its end) unless the Froude number is so high that recovery from the initial zone is not accomplished before the transition ends.

It is obvious from such reasoning that an efficient boundary expansion should display a continuous change in curvature, and should have different proportions for every Froude number. The latter requirement suggests at once that, for purposes of preliminary design, the best form of boundary, as well as the resulting surface configuration, should be reducible to a generalized diagram such as that of Fig. 55. As a matter of fact, Fig. 55 was initially used in the arbitrary selection of a number of boundary curves for experimental and graphical investigation, the curves being formulated algebraically to approximate streamlines of the unconfined flow which enclosed about 90% of the total discharge.

The boundary equation eventually found to be most satisfactory was of the form:

$$\frac{y}{b_1} = \frac{1}{2}\left(\frac{x}{b_1 \mathbf{F}_1}\right)^{\frac{3}{4}} + \frac{1}{2} \qquad (48)$$

which is plotted in Fig. 57, together with surface contours for a mean value of b_1/h_1 and various values of $\mathbf{F}_1$.

As will be noted from this composite plot, the beginning of the transition is sufficiently gradual to reduce effects of nonhydrostatic pressure distribution to a minimum, so that the factor b_1/h_1 is no longer an essential variable. The gradual increase in boundary angle, moreover, is sufficient to prevent the formation of positive waves—yet not so great as to cause an undue change in depth across any normal section. In fact, using circular arcs to approximate

normalcy to the streamlines at successive sections, it will be found that the variation in depth from wall to wall does not exceed 30% of the center-line value.

It is, of course, possible to reduce such depth variation between wall and center line by decreasing the rate of flare—that is, by decreasing the coefficient

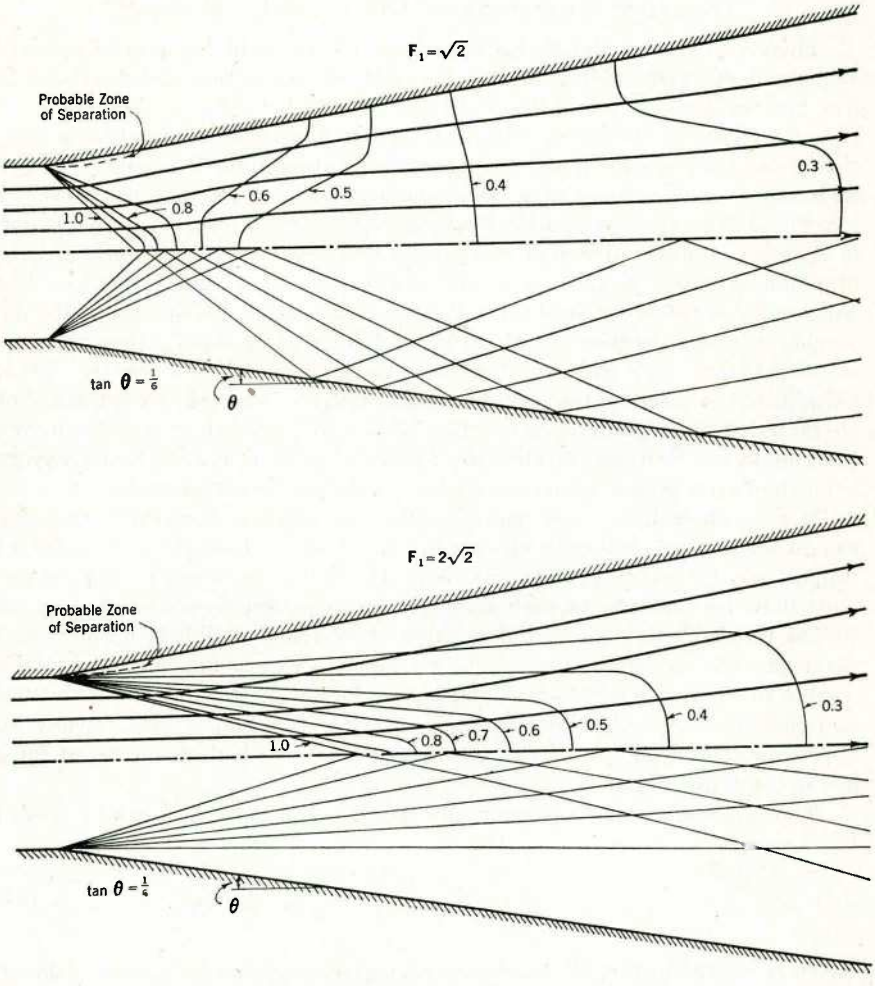

FIG. 56.—PATTERNS OF FLOW IN A UNIFORMLY DIVERGENT CHANNEL AT DIFFERENT FROUDE NUMBERS

of Eq. 48. This reduction, however, will result in a longer (and, hence, more costly) expansion for a given ratio of initial and final widths. Although the decision as to the greatest permissible depth variation is a matter either of judgment or of outlet requirements, it is believed that the curve shown in Fig. 55 will provide a satisfactory average basis for design.

The several curves reproduced in Fig. 55 typify the twenty or more which were determined experimentally for various Froude numbers and width-depth ratios and then checked by the graphical method of characteristics. Although a good general agreement was always obtained, the experimental results invariably yielded contours which were displaced downstream (from 0 to 35%, depending upon the ratio h/h_1). As this was attributed to the failure of the graphical method to take into account the gradual loss in total head due to boundary resistance, the same measurements were repeated on bed slopes varying from 4% to 10%. This, however, resulted in little displacement of the contours longitudinally, but in a considerable displacement laterally—that is, toward the center line, because the maximum bed slope was necessarily in the longitudinal direction rather than in the direction of each individual streamline.

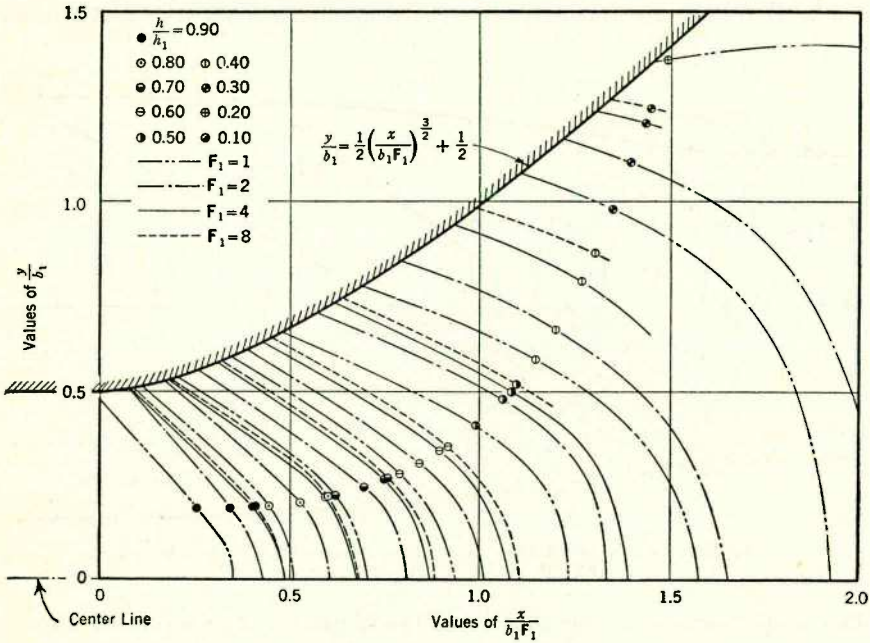

FIG. 57.—GENERALIZATION OF EXPERIMENTAL DATA FOR GRADUAL EXPANSIONS

From these considerations it would appear that the boundary form and surface contours for a level bed, shown in Fig. 57, may also be considered applicable to such moderate slopes as are normally encountered in open-channel design. Great slopes, on the other hand, would require a warped bed to prevent the major part of the flow from tending to follow the direction of maximum slope parallel to the center line. At present, the bottom surface can be warped satisfactorily only by trial and error at model scale. In the latter connection, however, it is to be noted that an effort was made to equalize both the surface elevation and the unit rate of flow across all normal sections by molding the

bottom in conformity with the surface contours of Fig. 57. In other words, the initially horizontal bed was arbitrarily made higher at the center and lower at the walls in exact conformity to the indicated change in surface elevation across each normal section. Although full equalization of flow rate and surface elevation was not attained, conditions were improved perhaps 50%. Since application of this method of partial correction requires no further trial-and-error experimentation, its consideration is recommended where the added expense of bottom contouring is warranted.

Elimination of Disturbances at the End of an Expansion

Just as the analysis of supercritical flow of water is closely related to that of supersonic flow of gases, an open-channel transition for such flow should satisfy essentially the same general requirements as the test section of a supersonic wind tunnel—a variation in cross-sectional area such that the velocity and depth (or pressure intensity) are evenly distributed across the final section.

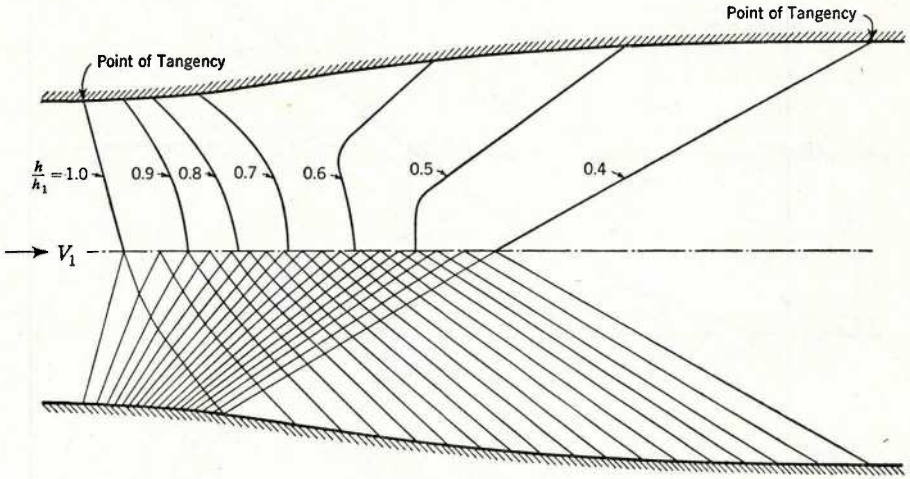

Fig. 58.—Design of an Expansion with Uniform Outflow for $F_1 = 2$, by the Method of Characteristics

The requirements of a supersonic wind tunnel are far more severe than those of an open-channel expansion, to be sure, even though experimental flow conditions are usually subject to arbitrary control; in fact, it is necessary to vary precisely the wall curvature of the tunnel test section from run to run in accordance with particular velocities of operation. Nevertheless, the same basic principles of boundary design could be applied quite generally to the case of open-channel expansions were it not for three practical limitations: First, under many circumstances the Froude number of the flow must be expected to vary over a considerable range; second, the length of transition required for either high Froude numbers or great expansion ratios will frequently be many times that permitted by structural economy; and, third, no method is provided thereby of stabilizing the hydraulic jump.

For the particular condition that an expansion represents merely a desirable increase in the width of a continuously paved channel, however, the same design procedure will yield at least the first approximation to an efficient design for a particular Froude number. As indicated in Fig. 58, the basis of the design technique is the control of wall curvature in such manner that the negative waves formed by successive elements of the outward curve just offset the positive waves formed by successive elements of the subsequent inward curve, so that the flow is restored to complete uniformity at the end of the transition. The procedure is, unfortunately, one of trial and error, and the resulting expansion ratio cannot be accurately foretold. A generalized series of boundary curves for successively greater expansion ratios is therefore presented in Fig. 59, as determined by interpolation from a series of solutions for various Froude numbers and expansion ratios by the method of character-

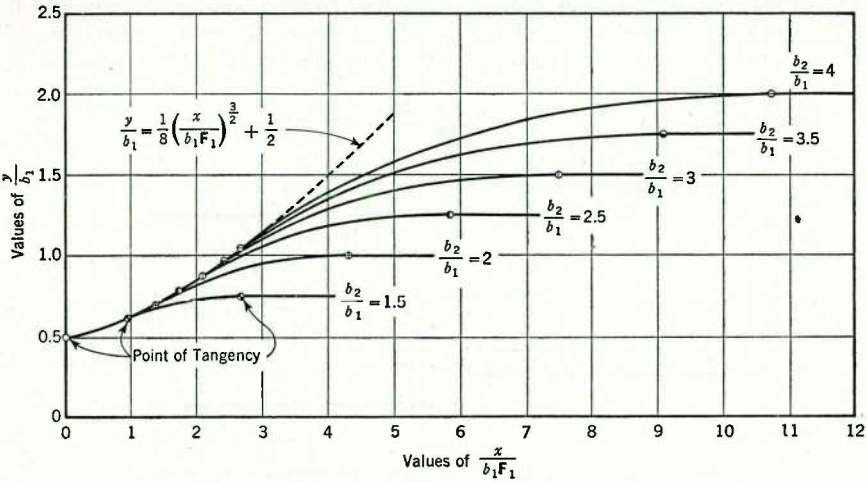

FIG. 59.—GENERALIZATION OF BOUNDARY CURVES DETERMINED BY THE METHOD OF CHARACTERISTICS

istics. These curves must be regarded merely as guides in preliminary design, for the following reasons: (1) Since the primary purpose was the generalization of results, each curve represents the average form of several somewhat different curves for different Froude numbers; (2) since the initial outward curve was chosen to yield without change the greatest practicable expansion range, it is probable that a somewhat shorter expansion curve could be devised for a particular condition; and (3) since the length of any transition is far in excess of that for which the drop in total head could be ignored, the assumption of zero loss in applying the method of characteristics leads to a predicted outlet depth which is considerably smaller than that which will actually prevail. For example, experiments on several expansions constructed in the laboratory on the basis of Fig. 59 resulted in outlet depths as much as from 20% to 40% in excess of that indicated by the simple wave theory, even though the flow was essentially uniform at the exit.

If, on the other hand, the channel expansion is intended to reduce the Froude number of the flow just prior to the formation of the hydraulic jump, it will be possible to hold the expansion to the shorter form of Fig. 57. If the divergent walls are followed by parallel walls with either an abrupt or a gradual transition, a positive wave will be formed at each wall junction and will extend diagonally across the flow at an angle varying with the local Froude number. Such waves would persist a considerable distance down the channel through repeated reflection if no jump were formed. If the toe of the jump lies at or near the end of the expansion, however, the diagonal waves will no longer form. On the other hand, should the jump as a whole advance even slightly into the expanding section, the smaller depth at each side will result in a progressively greater advancement of the jump along the walls, any slight asymmetry of the divergent flow finally giving rise to a deflection of the whole stream along one wall as the jump advances along the other almost to the upstream end of the expansion. The resulting flow will be of an extremely violent nature, and it could conceivably lead to rapid failure of the structure from overtopping of the wall at the juncture or from undercutting beyond the end of the paved floor.

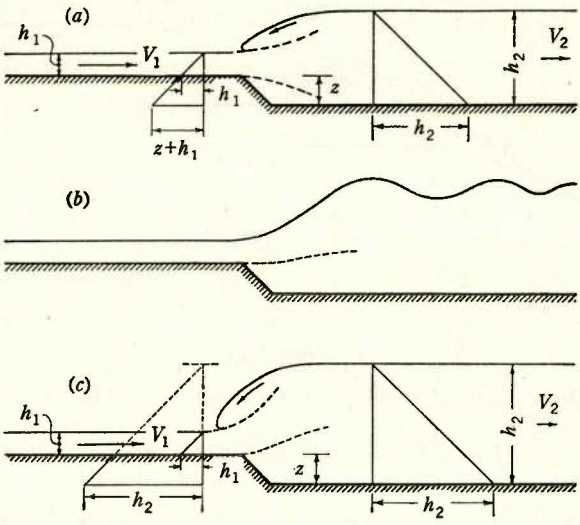

FIG. 60.—ALTERNATE FORMS OF THE HYDRAULIC JUMP AT AN ABRUPT DROP

In order to stabilize the jump at the end of such an expansion it appears necessary to provide a drop in floor level at the beginning of the parallel section. The relative magnitude of the change in elevation should depend primarily upon the Froude number of the flow as it leaves the expanding section. With reference to Fig. 60, it will be seen that the relationship between the Froude number, the relative change in depth, and the relative size of drop may be determined, like the equation of the jump itself, by the momentum and continuity relationships. There are, however, two different types of jump which may form, depending upon whether the downstream depth is below or above that which

produces the standing wave indicated by Fig. 60(*b*). For the condition of Fig. 60(*a*), the pressure on the face of the drop will be determined by the upstream depth; for the condition of Fig. 60(*c*), the downstream depth will govern. The relationships for cases (*a*) and (*c*) are as follows:

$$\mathbf{F}^2_1 = \frac{1}{2}\frac{h_2/h_1}{1 - h_2/h_1}\left[\left(\frac{z}{h_1} + 1\right)^2 - \left(\frac{h_2}{h_1}\right)^2\right] \quad \ldots\ldots\ldots\ldots (49a)$$

and

$$\mathbf{F}^2_1 = \frac{1}{2}\frac{h_2/h_1}{1 - h_2/h_1}\left[1 - \left(\frac{h_2}{h_1} - \frac{z}{h_1}\right)^2\right] \quad \ldots\ldots\ldots\ldots (49c)$$

Curves for Eqs. 49 will be seen in Fig. 61, the right-hand (or lower) series corresponding to Eq. 49*a* and the left-hand series to Eq. 49*c*. The critical zone for the formation of the standing wave—case (*b*)—cannot be foretold therefrom,

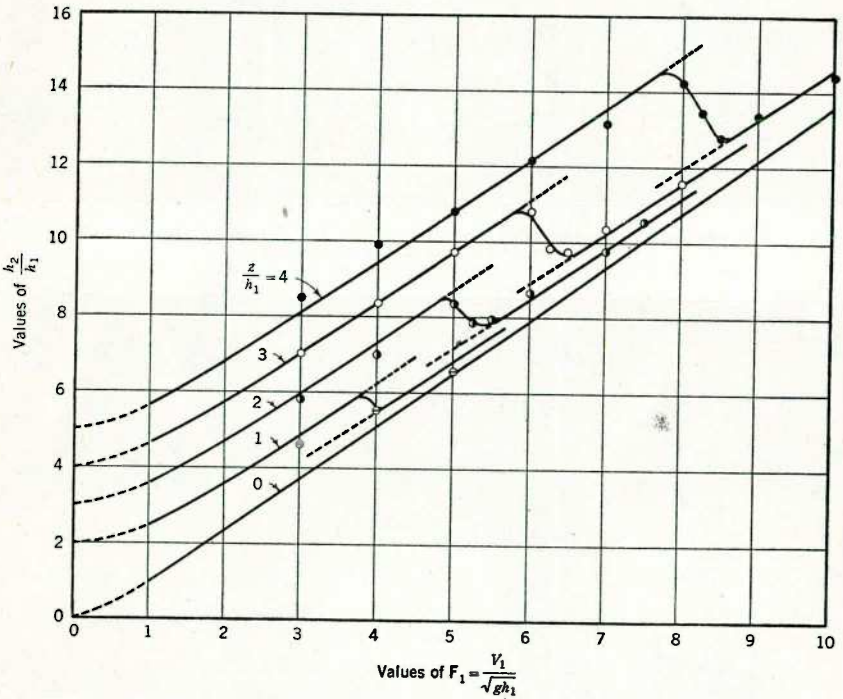

FIG. 61.—ANALYTICAL AND EXPERIMENTAL CHARACTERISTICS OF THE HYDRAULIC JUMP AT AN ABRUPT DROP

however, and recourse must be had to experimental measurement. Tests on both abrupt and sloping drops resulted in the points plotted in the figure, which not only verify the approximate analysis but indicate a systematic trend of the transition between the two regimes of flow.

From this diagram the magnitude of the drop for a given tailwater depth, or vice versa, may be determined once the average depth and the Froude number of the flow at the end of an expansion have been established. For protection of the structure, the design should be such that at the maximum expected Froude number the tailwater depth will be the minimum required to produce a jump. Figs. 62(*a*) and 62(*b*) are photographs of conditions for expansion ratios of 8 and 4, respectively, the details of the expansions following the recommendations presented herewith.

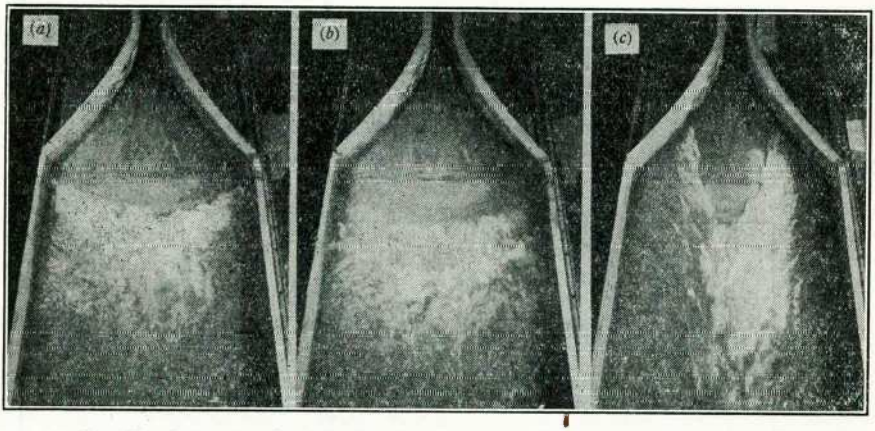

FIG. 62.—CHANGE IN JUMP CHARACTERISTICS AT A 1:8 EXPANSION DURING A 30% INCREASE IN THE TAILWATER DEPTH

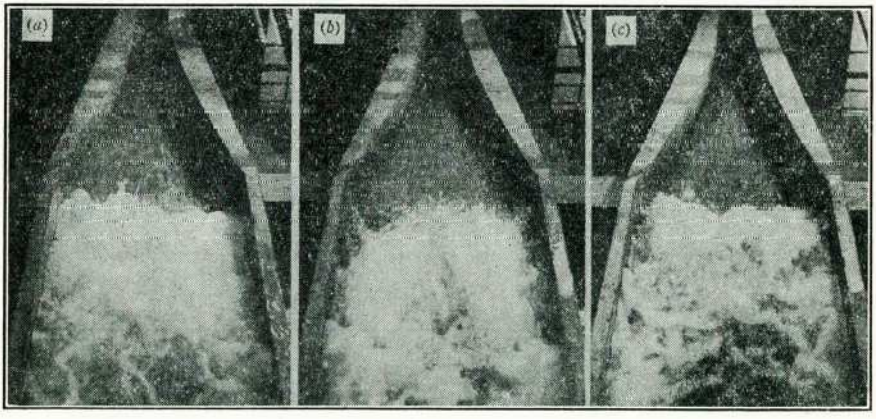

FIG. 63.—CHANGE IN JUMP CHARACTERISTICS AT A 1:4 EXPANSION DURING A 30% DECREASE IN THE RATE OF FLOW

If the tailwater depth is increased beyond the value for minimum jump requirements, the undular regime will first appear (see Fig. 62(*b*)), followed by the second form of the jump and then by an uneven penetration of the expansion (Fig. 62(*c*)). An asymmetric pattern may eventually result, but the presence

of the drop makes this far less likely than would otherwise be the case. On the other hand, if the Froude number increases beyond the design value, or if the tailwater depth decreases, the jump will be carried downstream. This phenomenon again is rendered less sensitive by the drop; the condition shown in Fig. 62(*a*), for example, will prevail during a 10% change in the downstream depth, whereas the three different stages shown in Fig. 62 represent a 30% change. Finally, if the Froude number is decreased, essentially the same sequence will follow as for the increase in tailwater depth (see Figs. 63(*b*) and 63(*c*)). In this event, however, the decrease in discharge will correspond to an equivalent decrease in harmfulness of the flow, and—although asymmetry may eventually develop—the structure planned for higher flows should then be safe.

Conclusions

Application of the elementary wave theory to the analysis of high-velocity flow in open-channel expansions may be expected to yield results in essential agreement with experiment as long as the assumptions involved in the theory are approximately satisfied. For purposes of design, however, it is convenient to reduce all measured data for abrupt expansions to a single generalized plot of surface contours as a function of the initial Froude number and the relative coordinate location. A similar procedure for gradual expansions permits selection of an efficient wall form for any initial Froude number and width-depth ratio. To avoid dangerous asymmetry of the flow at the end of such an expansion, the hydraulic jump should be stabilized by a drop in the channel floor, the proper magnitude of which may be determined by the momentum equation.